

ARIM-1

The Atmospheric Refractive Index Measurements Sounding Rocket Mission



A conceptual design study conducted by students at the
University of Alaska Fairbanks in conjunction with the
NASA Advanced Design Program.

September 1995

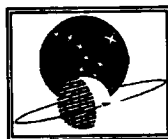
ARIM-1

Atmospheric Refractive Index Measurements - 1

A conceptual Design Study for a sounding rocket mission to measure the refractive index structure constant near the tropopause.

B. Ian Ruiz, Editor
Alaska Student Rocket Program
University of Alaska Fairbanks
Fairbanks, AK. 99775

© September 1995



Alaska Space Grant Program

ARIM-1

Acknowledgments

We would like to thank the many people who provided assistance to our class during this project. In particular we would like to express our gratitude to Kim Aaron from the Jet Propulsion Laboratory for attending our Critical Design Review in Fairbanks in May 1995, Vance Behr from Sandia National Laboratory for traveling to Fairbanks to assist with the design of the ARIM-1 recovery system, and Waren Gurkin from Wallops Island Flight Facility for organizing a design review at Wallops during our visit there.

This work was supported by NASA Grant NAGW-4325 under the NASA Advanced Design Program.

ARIM-1

Student Design Team

B. Ian Ruiz	Program Manager
Jay Baughan	Mechanical Design Team Leader
Steve Bruss	Electrical Design Team Leader
Liz Gao	Power Regulation & Basic Instrumentation
Dirgha Khatri	On-Board Computer Systems
Kelly Krekel	Systems Engineering
Phil Munts	Quality Assurance & Test Engineering
Jonathan Noland	Rocket Performance
Alexei Pudov	RF Communications
Steve Stephens	Principal Instrumentation
Randy Thomas	Recovery Systems
Ed Williams	Configuration
Pete Rogers	Mechanical Systems Teaching Assistant
John Riedman	Electrical Systems Teaching Assistant
Dr. Joseph Hawkins	Faculty Advisor

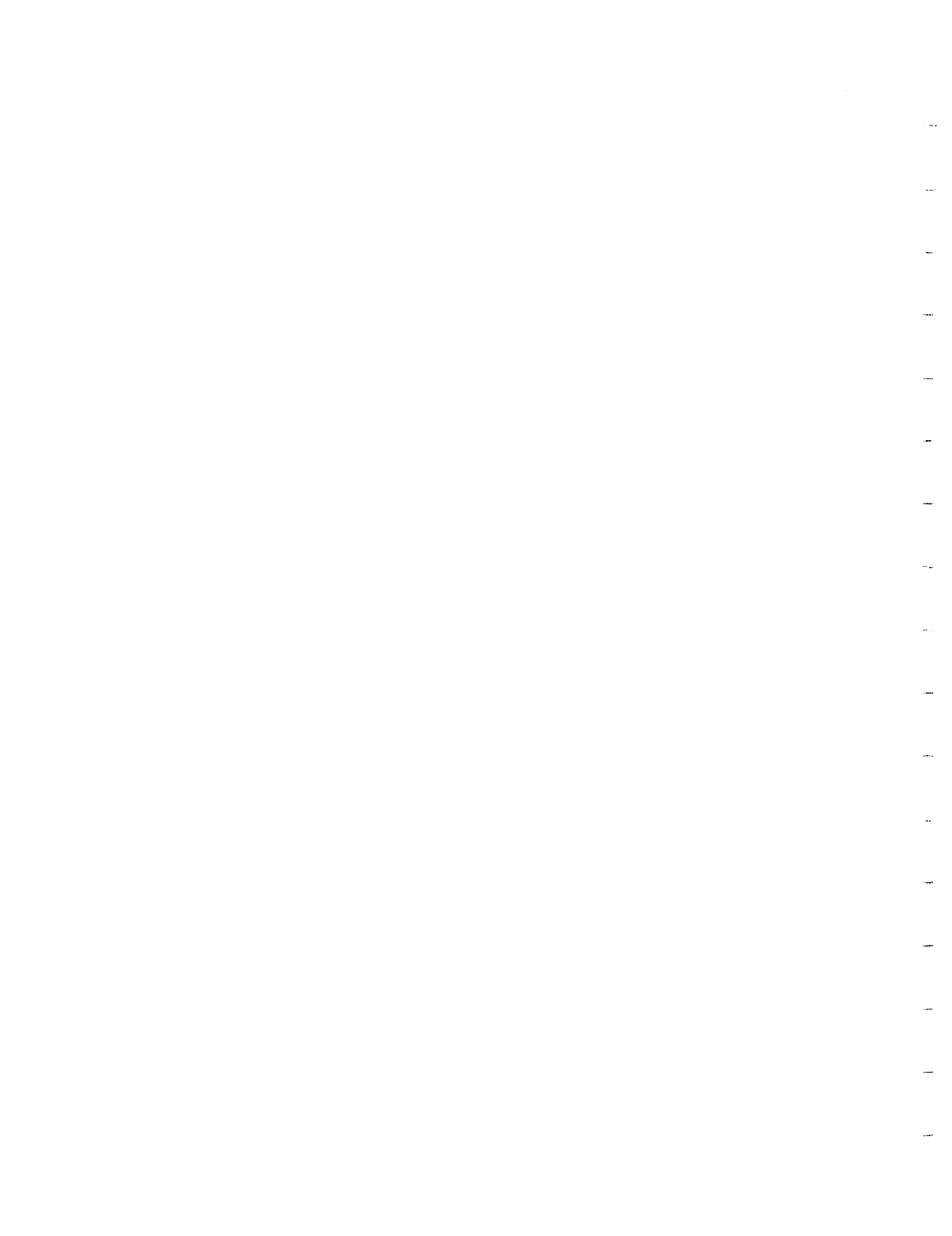


Table of Contents

1. INTRODUCTION	1
2. SCIENCE OBJECTIVES	4
2.1 MAIN OBJECTIVE	4
2.1.1 EFFECTS ON LIGHT TRANSMISSION	4
2.1.2 EFFECTS ON RADIO WAVE PROPAGATION	5
2.2 MEASUREMENT TECHNIQUES FOR ATMOSPHERIC TURBULENCE	5
2.2.1 BACKGROUND	5
2.2.2 ARIM-1 THERMOSONDE	6
2.3 THERMOSONDE EXPERIMENTAL TECHNIQUE	6
2.3.1 THEORY OF OPERATION	6
2.3.2 DIFFERENTIAL TEMPERATURE CIRCUIT	8
2.3.3 OVERVIEW OF THE THERMOSONDE CIRCUIT DESIGNED BY TRI-CON ASSOCIATES	9
2.3.4 PRESSURE, TEMPERATURE AND HUMIDITY	12
2.3.5 PRESSURE, TEMPERATURE AND HUMIDITY SIGNAL CONDITIONING.	13
2.4 SCIENCE MISSION SPECIFICATIONS	13
2.4.1 ROCKET AND PARACHUTE	13
2.4.2 FLIGHT SCHEDULING	13
2.4.3 TRAJECTORY	13
2.4.4 DATA HANDLING	14
2.4.5 PHYSICAL REQUIREMENTS	14
2.4.6 ELECTRICAL	14
3. MISSION ANALYSIS	15
3.1 OBJECTIVE	15
3.2 MOTOR SELECTION	15
3.3 LAUNCH VEHICLE SPECIFICATIONS	16
3.4 MOTOR PERFORMANCE	19
3.5 RECOMMENDATIONS	20
4. PAYLOAD MECHANICAL CONFIGURATION AND STRUCTURAL DESIGN	21
4.1 CONFIGURATION	21
4.2 KEY MECHANICAL EVENTS	22
4.3 STRUCTURAL MATERIALS	22
4.4 OUTER PAYLOAD TUBE AND NOSE CONE ASSEMBLY	23
4.4.1 OUTER NOSE CONE	23
4.4.2 OUTER PAYLOAD TUBE	23
4.5 UMBILICAL SECTION	24
4.5.1 UMBILICAL BLOCK	24
4.5.2 UMBILICAL TUBE	24

4.6 MOTOR/PAYLOAD SEPARATION MECHANISM	26
4.6.1 PYROTECHNICS	26
4.7 SKIN SEPARATION	27
4.8 INNER PAYLOAD DESIGN	29
4.8.1 INNER NOSE CONE	29
4.8.2 BATTERY BOX	29
4.8.3 LONGERON/DECK ASSEMBLY	30
4.8.4 THERMOSONDE BOOMS AND DEPLOYMENT MECHANISM	32
 5. RECOVERY SYSTEM	 34
 5.1 OBJECTIVE	 34
5.2 DESIGN CRITERIA	34
5.3 DROGUE PARACHUTE DESIGN	35
5.4 MAIN PARACHUTE DESIGN	40
5.5 LOCATOR DEVICES	43
5.5.1 RADIO BEACON	43
5.5.2 TRANSPONDER	45
5.6 PARACHUTE RECOVERY SYSTEM	45
5.6.1 PARACHUTE DEPLOYMENT BAGS	47
5.6.2 PARACHUTE CUT KNIVES	48
5.6.3 PYROTECHNIC THRUSTERS	49
5.6.4 PENCIL CUTTERS	50
5.6.5 PACKED PARACHUTES	51
5.7 RECOVERY SYSTEM DEPLOYMENT SEQUENCE	53
5.8 RECOVERY SYSTEM PERFORMANCE	56
5.9 RECOVERY SYSTEM TESTING	59
 6. PAYLOAD ELECTRONICS	 59
 6.1 BATTERY AND POWER SYSTEM	 60
6.1.1 POWER BUDGET	61
6.1.2 POWER REGULATORS	62
6.2 UMBILICAL SYSTEM	62
6.2.1 PYROTECHNICS CONTROL	63
6.3 INSTRUMENTATION SYSTEM	63
6.3.1 REFERENCE VOLTAGE	64
6.3.2 INTERNAL TEMPERATURE	65
6.3.3 PRESSURE	66
6.3.4 BATTERY VOLTAGE	68
6.3.5 ACCELERATION	69
6.3.6 NOSE CONE TEMPERATURE	70
6.3.7 BATTERY TEMPERATURE	71
6.3.8 BOOM ANGLE SENSOR	72
6.3.9 DIGITAL STATUS BITS	73
6.4 FLIGHT COMPUTER	73
6.4.1 SYSTEM CHARACTERISTICS	74
6.4.2 386SX PROCESSOR	74
6.4.3 MEMORY	75

6.4.4 ANALOG TO DIGITAL CONVERTER	75
6.4.5 DATA COLLECTED	76
6.4.6 DATA FORMAT	77
6.4.7 DATA COLLECTION AND TRANSMISSION	77
6.4.8 ARCHITECTURE	78
6.4.9 SERIAL COMMUNICATIONS	79
6.4.10 TELEMETRY FORMAT	80
6.4.11 PC/104 BUS	80
6.4.12 FLIGHT COMPUTER SOFTWARE FLOWCHARTS	80
6.5 ON-BOARD GLOBAL POSITIONING SYSTEM	81
6.6 TELEMETRY SYSTEM	81
6.6.1 TELEMETRY TRANSMITTER	81
6.6.2 LINK BUDGET	82
6.6.3 TRANSMITTING ANTENNA	85
 7. GROUND STATION	 86
7.1 UMBILICAL SYSTEM	86
7.2 TELEMETRY RECEIVER	86
7.3 LOW NOISE AMPLIFIER	86
7.4 GROUND BASED GPS	86
7.5 GROUND BASED COMPUTERS	87
7.5.1 GROUND SUPPORT SOFTWARE	87
7.5.2 SOFTWARE SIZE AND THROUGHPUT	87
7.5.3 DATA ANALYSIS	88
 8. TESTING PLANS	 90
8.1 DESIGN VERIFICATION TESTS	90
8.1.1 BATTERY MODULE TEST.	90
8.1.2 POWER REGULATOR MODULE TEST	90
8.1.3 EED DRIVER MODULE TEST	91
8.1.4 INSTRUMENTATION MODULE TEST	92
8.1.5 FLIGHT COMPUTER MODULE TEST	92
8.1.6 TRANSMITTER MODULE TEST	93
8.1.7 RECEIVER SUBSYSTEM TEST	94
8.2 ENVIRONMENTAL TEST PLAN	95
8.2.1 TEMPERATURE CYCLE TEST	95
8.2.2 RFI SUSCEPTIBILITY TEST	96
8.3 INTEGRATION TEST PLAN	96
 9. MISSION IMPLEMENTATION	 99
9.1 MANAGERIAL OVERVIEW	99
9.2 LOGICAL PROJECT BREAKDOWN	101

9.3 ESTIMATED COST ANALYSIS	102
9.4 MISSION SUCCESS CRITERIA	104
9.4.1 COMPREHENSIVE	104
9.4.2 MINIMUM	104
 References	 105
 Appendix A	 106
References	107
Symbols	110
Ballistic Free Fall Table	111
Guide Surface Drogue Chute	112
33 Ft. Main Cross Parachute Descent Table	113
1976 U.S. Standard Atmosphere Table	114
1976 U.S. Standard Atmosphere Table Continued	115
Parachute Types	116
Parachute Reduction Factor (X_1) and Opening Force Coefficient (C_x) Graphs	117
Parachute Opening Force Factor (X_1) Graph	118
Parachute Performance Parameters Formulas	119
 Appendix B	 122
ARIM-1 Task List	123
Estimated Cost Analysis	125

List of Figures

FIGURE 1-1 : ATMOSPHERIC CHEMICAL REGIMES (AFTER CARPENTER ET AL., 1978)	1
FIGURE 1-2 : ARIM-1 VEHICLE	2
FIGURE 2-1 : WIRE RESISTANCE VERSUS TEMPERATURE FOR A 0.45 CM LENGTH OF 3.45 μ M TUNGSTEN WIRE.	8
FIGURE 2-2 : BLOCK DIAGRAM OF THE DIFFERENTIAL TEMPERATURE PROBE CIRCUIT. THE COMPONENT NUMBERS REFER TO THE CIRCUIT SCHEMATIC IN THE SUCCEEDING FIGURES.	10
FIGURE 2-3 : THE BRIDGE CIRCUIT FOR THE "HOT WIRE" SENSORS IS COMPOSED OF A 1 K Ω VARIABLE RESISTOR, TWO 10 K Ω RESISTORS, AND THE TWO WIRE ELEMENTS (RT-1 AND RT-2) WITH A NOMINAL RESISTANCE OF 27 Ω . THE TWO FET'S AND THE TWO 1.3 K Ω RESISTORS ARE PART OF THE FEEDBACK NETWORK . T1 IS A 20:1 STEP UP TRANSFORMER. THE AMPLIFIER HAS AN ADJUSTABLE GAIN FROM 800 TO 3,000.	11
FIGURE 3-1 : DESIGN SPECIFICATIONS AND DIMENSIONS FOR THE VIPER V SOUNDING ROCKET VEHICLE. NOTE, MOTOR AND NOZZLE CUTAWAY, IN ADDITION TO BASIC FIN GEOMETRY.	17
FIGURE 3-2 : VIPER V SOUNDING ROCKET MOTOR CUTAWAY SHOWING CASING, NOZZLE, HEADCAP, IGNITOR, AND PROPELLANT GRAIN. MOTOR CASING IS MADE OF ALUMINUM TUBING.	19
FIGURE 3-3 : PLOT OF VIPER V ROCKET MOTOR THRUST CURVE IN POUNDS, AS A FUNCTION OF TIME IN SECONDS.	20
FIGURE 4-1 : PAYLOAD CONFIGURATION BEFORE SEPARATION	21
FIGURE 4-2 : INNER PAYLOAD CONFIGURATION SCHEMATIC AFTER SEPARATION	22
FIGURE 4-3 : OUTER NOSE CONE	23
FIGURE 4-4 : OUTER PAYLOAD TUBE WITH STATIC PRESSURE SYSTEM INSTALLED	24
FIGURE 4-5 : UMBILICAL BLOCK	25
FIGURE 4-6 : UMBILICAL SECTION CONFIGURATION	25
FIGURE 4-7 : MOTOR-TO-PAYLOAD COUPLER	26
FIGURE 4-8 : THRUSTER INSTALLATION DETAIL (SIMPLIFIED SCHEMATIC)	27
FIGURE 4-9 : CUTAWAY DETAIL OF CORE-TO-SKIN COUPLER	28
FIGURE 4-10 : PAYLOAD CORE-TO-SKIN COUPLER	28
FIGURE 4-11 : ANTENNA MOUNTING ON INNER NOSE CONE (END VIEW)	29
FIGURE 4-12 : BATTERY BOX CONFIGURATION	30
FIGURE 4-13 : LONGERON	30
FIGURE 4-14 : DECK PLATE	31
FIGURE 4-15 : LONGERON/DECK ASSEMBLY	31
FIGURE 4-16 : BOOMS IN RETRACTED POSITION	32
FIGURE 4-17 : BOOMS EXTENDED	33
FIGURE 5-1 : DESCENT RATE OF 33 FT. CROSS CHUTE AS A FUNCTION OF ALTITUDE. VERTICAL LINE SHOWS DESCENT RATE OF 5 M/SEC FOR PAYLOAD DESCENDING THROUGH 14 KM (46,000 FT).	36
FIGURE 5-2 : RIBLESS GUIDE SURFACE DROGUE PARACHUTE DIMENSIONS	38
FIGURE 5-3 : DROGUE CHUTE GORE DIMENSIONS AND PATTERNS	39
FIGURE 5-4 : MAIN CROSS PARACHUTE DIMENSIONS	42
FIGURE 5-5 : TELONICS RADIO BEACON ON MAIN PARACHUTE BRIDLE.	43
FIGURE 5-6 :RADIO BEACON BATTERIES TACKED INTO POCKET ON KEVLAR MAIN CHUTE BRIDLE WITH CABLE CONNECTED TO RADIO BEACON.	44
FIGURE 5-7 : SIDE VIEW OF RADIO BEACON AND MAGNETIC PULL-PLUG SWITCH. NOTE CONNECTOR PLUG AND WIRE GOING TO LITHIUM BATTERIES LOCATED IN THE 1 INCH WIDE 3,000 POUND KEVLAR BRIDLE.	44
FIGURE 5-8 : CLOSE UP VIEW OF RADIO BEACON TOP SHOWING CONNECTOR PLUG AND WIRE GOING TO LITHIUM BATTERIES. NOTE METAL MOUNTING BRACKET AND METAL SCREWS.	44
FIGURE 5-9 : GENERAL OVERVIEW AND COMPONENTS OF A GENERIC PARACHUTE DEPLOYMENT SYSTEM FOR RECOVERING SOUNDING ROCKET PAYLOADS.	46

FIGURE 5-10 : 4-LEAVE BANANA PEEL BAG USED TO PACK SOUNDING ROCKET PARACHUTE. BAGS ARE LACED UP WITH NYLON CORD THROUGH BRASS GROMMETS.	47
FIGURE 5-11 : CUT KNIFE ATTACHED TO MAIN PARACHUTE SPEED LINK (CONNECTOR LINK) ON THE BRIDLE. PARACHUTE BAG LACING IS THREADED THROUGH CUT KNIVES. WHEN MAIN CHUTE DEPLOYS, TENSION CAUSES CUT KNIVES TO CUT BAG LACING, ALLOWING PARACHUTE TO EXTRACT AND DEPLOY.	48
FIGURE 5-12 : CUT KNIFE DIAGRAM SHOWING TOP AND SIDE VIEWS. THREE HOLES IN CUT KNIFE ARE FOR TACKING CUT KNIFE IN PLACE ON DEPLOYMENT BAGS.	49
FIGURE 5-13 : PHOTOGRAPH OF HOLEX 2900-1 THRUSTER (LINEAR ACTUATOR) USED FOR SEPARATING PAYLOAD FROM EXPENDED ROCKET MOTOR, AND TO BREAK SHEAR PINS ON AFT END OF PARACHUTE CANISTER EXTRACTION PLATES TO DEPLOY DROGUE CHUTE.	49
FIGURE 5-14 : DIAGRAM AND DIMENSIONS OF HOLEX 2900-1 THRUSTER. METAL SPHERE STROKES A DISTANCE OF 1/2 INCH WITH A FORCE OF 225 POUNDS AGAINST DROGUE CHUTE EXTRACTION PLATE TO BREAK SHEAR PINS ON AFT END OF PARACHUTE CANISTER AND EXTRACT DROGUE CHUTE. SEE FIGURE ON LEFT.	50
FIGURE 5-15 : ELECTRICAL FIRING CURVE PLOT OF HOLEX THRUSTER. SEE FIGURE ON RIGHT.	50
FIGURE 5-16 : TECHNICAL ORDNANCE 3,000 LB. PENCIL CUTTER. NOTE MAIN PARACHUTE STAGING BRIDAL THROUGH CUTTER HOLE ON LEFT, AND PULL PIN ON RIGHT SIDE OF CUTTER	51
FIGURE 5-17 : PACKED MAIN AND DROGUE PARACHUTES. NOTE HOW MAIN BAG IS LACED WITH NYLON CORD. NOTE LOOSE KEVLAR CORDS IN FOREGROUND THAT CONNECT TO DROGUE CHUTE EXTRACTION PLATE. ALSO, NOTE NYLON CORD THREADED THROUGH CUT KNIFE ON SET OF UPPER LACES ON MAIN PARACHUTE DEPLOYMENT BAG. BAG HAS TWO CUT KNIVES.	52
FIGURE 5-18 : PACKED PARACHUTE RECOVERY SYSTEM DIMENSIONS (LEFT). PACKED 33 FT CROSS PARACHUTE AND GUIDE SURFACE DROGUE CHUTE PACKED FOR INSTALLATION IN NASA BLACK BRANT XII SOUNDING ROCKET (RIGHT).	52
FIGURE 5-19 : DEPLOYMENT SEQUENCE OF ARIM-1 PARACHUTE RECOVERY SYSTEM. PAYLOAD SEPARATES FROM EXPENDED MOTOR AT APOGEE FOR REENTRY. PAYLOAD IS BALLASTED TO FLAT SPIN IN BALLISTIC FREE FALL FOR MAXIMUM DRAG AND DECELERATION BEFORE DEPLOYING RECOVERY SYSTEM. AT MAIN CROSS CHUTE DEPLOYMENT, FIBERGLASS STAVES AND OUTER PAYLOAD TUBE FALL AWAY TO ACHIEVE RECOVERY WEIGHT OF 31 LBS. FOR DESIRED DESCENT RATE.	55
FIGURE 5-20 : TIME LINE AND PERFORMANCE PARAMETERS OF ROCKET FLIGHT PROFILE AND PAYLOAD RECOVERY SYSTEM EVENTS. NOTE TIME AND ALTITUDE FOR RECOVERY SYSTEM.	58
FIGURE 6-1 : ELECTRICAL BLOCK DIAGRAM	60
FIGURE 6-2 : REFERENCE VOLTAGE CIRCUIT	65
FIGURE 6-3 : TEMPERATURE SENSOR CIRCUIT	66
FIGURE 6-4 : PRESSURE SENSOR	67
FIGURE 6-5 : BATTERY VOLTAGE CIRCUIT	69
FIGURE 6-6 : THREE AXES MONITORED BY THE ACCELEROMETER	69
FIGURE 6-7 : NOSE CONE TEMPERATURE CIRCUIT	70
FIGURE 6-8 : BATTERY TEMPERATURE SENSOR CIRCUIT	71
FIGURE 6-9 : BOOM ANGLE SENSOR CIRCUIT	72
FIGURE 6-10 : DEMONSTRATION OF DIGITAL STATUS BITS	73
FIGURE 6-11 : MECHANICAL INTERRUPT SERVICE ROUTINES	81
FIGURE 7-1 : GROUND BASED COMPUTER CONFIGURATION	89
FIGURE 8-1 : BATTERY TEST SETUP	90
FIGURE 8-2 : EED DRIVER TEST SETUP	92
FIGURE 8-3 : FLIGHT COMPUTER TEST SETUP	93
FIGURE 8-4 : TRANSMITTER TEST SETUP	94

FIGURE 8-5 : RECEIVER SUBSYSTEM TEST SETUP	95
FIGURE 8-6 : COMPONENT FAILURES OVER TIME	95
FIGURE 9-1 : PERSONNEL STRUCTURE	99
FIGURE 9-2 : LOGICAL BLOCK DIAGRAM FOR ARIM-1	102
FIGURE 9-3 : PROJECT COST ANALYSIS.	103

List of Tables

TABLE 2-1 : THE REQUIRED RANGE AND ACCURACY FOR THE TEMPERATURE, PRESSURE AND HUMIDITY MEASUREMENTS.	12
TABLE 4-1 : PROPERTIES OF STRUCTURAL MATERIALS	22
TABLE 6-1 : SPECIFICATIONS FOR LITHIUM BATTERY PACK	61
TABLE 6-2 : POWER BUDGET	61
TABLE 6-3 : FLIGHT COMPUTER POWER BUDGET	62
TABLE 6-4 : DC-DC CONVERTERS	62
TABLE 6-5 : HOUSEKEEPING INSTRUMENTATION SENSORS	63
TABLE 6-6 : HOUSEKEEPING INSTRUMENTATION DIGITAL STATUS BITS	64
TABLE 6-7 : FLIGHT COMPUTER SYSTEM CHARACTERISTICS	74
TABLE 6-8 : FLASH MEMORY CHARACTERISTICS	75
TABLE 6-9 : ANALOG-TO-DIGITAL CONVERTER CHARACTERISTICS	76
TABLE 6-10 : COMPUTER DATA RATES	76
TABLE 6-11 : DATA COLLECTED DURING PHASE ONE	77
TABLE 6-12 : DATA COLLECTED DURING PHASE TWO	78
TABLE 6-13 : ON-BOARD COMPUTER ARCHITECTURE	78
TABLE 6-14 : COM1 AND COM2 CONFIGURATION OPTIONS	79
TABLE 6-15 : COM1 AND COM2 RS-232 PIN-OUT	80
TABLE 6-16 : TELEMETRY PACKET FORMAT	80
TABLE 6-17 : TRANSMITTER CHARACTERISTICS	82
TABLE 6-18 : SIGNAL CHARACTERISTICS	82
TABLE 6-19 : RECEIVING SIGNAL CHARACTERISTICS AT 25 KM FOR CASE1/CASE2	85

1. Introduction

This report presents a conceptual design study of the ARIM-1 sounding rocket mission. The design study was conducted by an interdisciplinary team of students at the University of Alaska Fairbanks who were enrolled in a Space Systems Engineering course. This course was offered during the 1995 spring semester in conjunction with the NASA Advanced Design Program.

The implementation of the ARIM-1 mission will be carried out by students participating in the Alaska Student Rocket Program (ASRP) at the University of Alaska Fairbanks, with a projected launch date of August 1997. This project will be the third payload to be designed and built by students at UAF. The first two student-built payloads were launched in July 1992 and May 1995, respectively.

The scientific goal of the ARIM-1 mission is to study atmospheric turbulence in the tropopause region of the atmosphere. The troposphere is the lowest region of the atmosphere, extending from the surface to approximately 12 km. Solar heating of the earth's surface causes strong convection and turbulence within the troposphere. Overlying the troposphere is a stable region called the stratosphere, which extends from approximately 12 to 38 km, and is separated from the troposphere by the tropopause (see Figure 1-1).

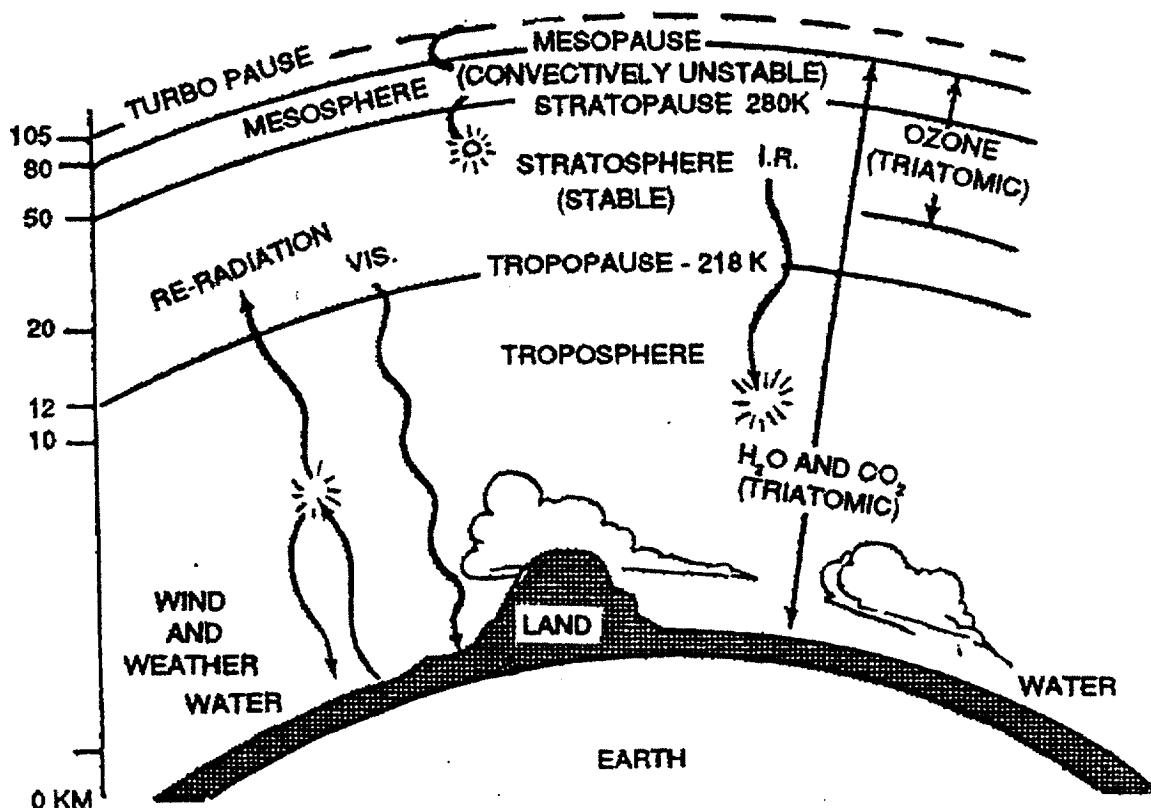


Figure 1-1 : Atmospheric Chemical Regimes (after Carpenter et al., 1978)

The goal of the ARIM-1 payload is to measure the propagation of turbulence from the troposphere, across the tropopause, and into the stratosphere. This measurement will help scientists understand how pollutants in the troposphere are transported into the stratosphere, where they can be distributed by the jet stream. It will also help to understand problems associated with energy balance in the atmosphere. In addition, the measurements will provide a site survey of atmospheric turbulence above the Poker Flat Research Range, which will help scientists at Space Telescope Science Institute (at the Johns Hopkins University) to develop a proposal for a next-generation infrared telescope called the POLar Stratospheric Telescope (POST).

In addition to the scientific goals of the ARIM-1 mission, this project will also help advance the goals of the Alaska Student Rocket Program. The SRP was created to provide opportunities for students to participate in exciting *real-world* design projects in conjunction with their academic programs. The payload proposed for the ARIM-1 mission is intended to provide the next iteration of a standardized payload that can be used by future student-designed sounding rocket missions. The adoption of a standardized payload will allow increased emphasis to be placed on the scientific return from future missions rather than on the engineering development of the payload support subsystems.

Standard mechanical hardware includes the payload structure, separation mechanisms, and the recovery system. Standard electrical support includes a basic instrumentation package, a microprocessor-based flight computer, a power supply and regulation system, a telemetry system, and the necessary logic and firing circuits for the pyrotechnic actuation. In addition, ARIM-1 will also carry a Global Positioning System (GPS) receiver. The coordinates from the on-board GPS receiver will be compared with a ground-based GPS receiver to provide a Differential GPS (DGPS) tracking system. In the future, DGPS may provide an alternative to ground-based radar tracking.

The ARIM-1 vehicle is a single stage sounding rocket with a payload diameter of 8 in., a motor diameter of 7.6 in., and a height of 16.3 feet, which is somewhat larger than the previous two SRP payloads. Figure 1-2 illustrates the configuration of the ARIM-1 vehicle.

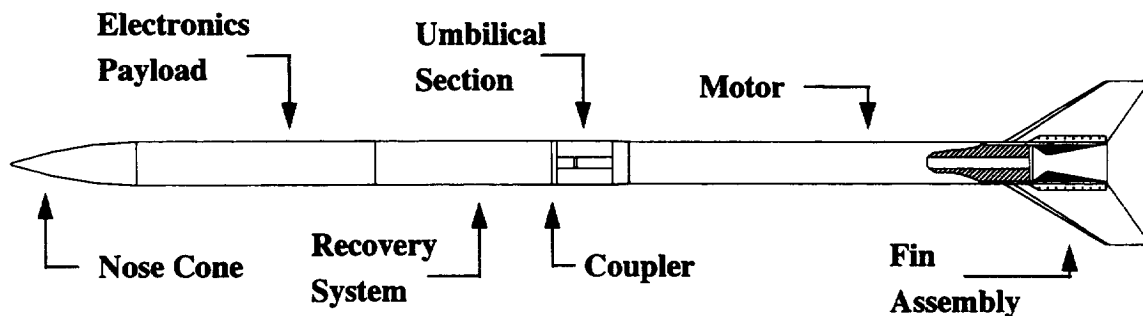


Figure 1-2 : ARIM-1 Vehicle

The nose cone conforms to a 3:1 ogive, has a metal insert in the tip, and is made of a fiberglass epoxy. The metal insert provides a means for ballasting the payload and a

mass to absorb the heat from the high stagnation temperature experienced during the boost phase of the mission. The electronics section houses the vehicle's computer, instrumentation, battery packs, and the main science payload. This portion of the rocket will be recovered for future flights. ARIM-1's recovery system is located below the vehicle's electronics pack and is packaged inside the chute canister which is discarded during chute deployment. The coupler, actuated by an electro-explosive device (EED), separates the payload and recovery section from the spent motor at apogee. The umbilical section is permanently attached to the motor and is discarded at separation to minimize the hanging weight under the parachute. Its purpose is to provide a communications link between the crew in the blockhouse and the rocket up till the moment of launch. The motor and fin assembly is one of the few pieces of ARIM-1 that will not be designed and constructed by students.

The remainder of this document will provide a more detailed description of the science objectives and technical details of the rocket systems and the necessary ground support, followed by testing and implementation plans.

2. Science Objectives

2.1 Main Objective

The mission science objective is to measure the minute changes in atmospheric turbulence versus altitude in a vertical column of the atmosphere. The atmospheric turbulent energy is determined by measuring the difference in temperature between two probes separated by one meter. Information about the refractive index structure constant and the turbulent energy can then be obtained from the differential temperature measurement. The measurements will be made with a vertical resolution of 20 meters from an altitude of 15 km to the surface. Additionally, measurements of the differential temperature will be taken from an altitude of 25 km to 15 km with a resolution greater than 20 meters.

The ability to predict, forecast or detect the level and location of atmospheric turbulence is important to the performance of optical and radio frequency devices. The proposed POLar Stratospheric Telescope (POST) would be located at Poker Flat Research Range and operated at an altitude of approximately 12 km. The objective of the POST project is to place an optical telescope above the turbulent region of the atmosphere to avoid degradation of image resolution. Turbulent air causes small scale changes in the atmospheric density and the corresponding index of refraction which appears as a blurring effect to a telescope.

Small scale changes in the atmospheric density also cause radio waves to disperse causing power fades. This is of importance to satellite communications. Small changes in the refractive index are caused by small scale atmospheric turbulence which causes fluctuations in the received signal power (scintillations) of electromagnetic radiation resulting in temporary loss of signal or signal distortions. Consequently, it is desirable to develop a statistical model of atmospheric turbulence that could be used to determine the required transmission power of various communication links. Such a model would result in more efficient and reliable satellite to ground communications.

2.1.1 Effects on Light Transmission

Localized changes in the atmospheric refractive index causes dispersion and a resultant blurring of distant images. The image blurring is a particular problem for optical telescopes and limits the ultimate obtainable resolution. The POLar Stratospheric Telescope (POST) hopes to avoid most of the problems due to scintillations by using a balloon to lift an optical telescope to an altitude of 12 km. At this altitude POST should be above the majority of the turbulent effects. Data gathered from this mission (particularly that data above 12 km) will help to determine the optimum operating altitude for POST.

2.1.2 Effects on Radio Wave Propagation

Small scale changes in the atmospheric index of refraction have a significant effect on satellite communications links and on radio telescopes operating at frequencies "well above 1 GHz" [1]. The principle effect on satellite communications links is to require a large enough fade margin to accommodate the expected changes in signal amplitude due to scintillations (as well as other effects). The engineer must rely on statistical models and long term observations in order to select the size of the fade margin required to overcome these effects for the degree of reliability required.

2.2 Measurement Techniques for Atmospheric Turbulence

2.2.1 Background

The measurement of atmospheric turbulence is accomplished by measuring the spatial variation of the refractive index, the temperature difference over a known distance [3] or by measuring the change in the wind velocity over a known distance [2]. There are two categories of atmospheric turbulence measurements, direct measurements and remote sensing. Direct measurements involve methods that require the sensors to be in direct contact with the point of measurement. Remote sensing involves determining the refractive turbulence structure coefficient (C_n^2) from the effect it has on the transmission of electro-magnetic radiation [3].

Direct Measurement

Thermal or wind velocity sensors are mounted directly on a vertical tower. This method provides any degree of vertical resolution required but is limited by the physical height of the tower. Tower measurements are also subject to disturbances in the air flow caused by the tower when ever the tower is up-wind or nearly so.

Aircraft have been used to measure the temperature difference over a short distance (usually one meter). Aircraft measurements can reach a maximum altitude of about 10 km and give an altitude resolution of between 10 and 20 meters. These measurements are subject to errors produced by the aircraft's structure and by the required forward airspeed [3]. Thermosondes are differential temperature probes that are suspended from balloons or parachutes. In balloon measurements it is necessary to suspend the probes a considerable distance below the balloon to avoid turbulence caused by the balloon's wake [2,4]. Parachute measurements can be made from directly below the parachute suspension because the wake from the parachute will not interfere with the probes. In this mission a rocket will be used to carry a thermosonde to an altitude of about 80 km. The thermosonde will then free-fall to an altitude of 25 km at which point the a parachute will open and the thermosonde will be activated. The parachute is designed to produce a descent rate of 5 m/s or less below 15 km in order to give the required altitude resolution.

Remote Sensing

Sensitive radar's can be used to measure the radiation that is "back scattered" from refractive index fluctuations caused by atmospheric turbulence. Maximum altitudes for radar are a function of the wavelength and the turbulent scale size. Generally, the turbulent scale size must be equal to half of the wavelength or less. Also, the turbulent scale size increases with altitude [9].

A stellar scintillometer "measures the stellar scintillation pattern through spatial filters passing a narrow band of frequencies" [3]. The altitude resolution of the scintillometer is limited by the ability to adjust the spatial wave length of the filters.

2.2.2 ARIM-1 Thermosonde

The ARIM-1 thermosonde will measure the atmospheric turbulence by direct measurement of the temperature difference over a distance of one meter using two 3.45 μm "hot wire" probes. This information will be gathered from an altitude of 25 km to the ground. The differential temperature will be sampled at a rate of 1,000 times per second and the individual data points will be simultaneously stored in on-board memory and transmitted to the ground.

The mean square variation of the temperature difference data C_T^2 can be calculated over some averaging interval by:

$$C_T^2 = \frac{\sum \Delta T^2}{n}$$

where ΔT^2 is the square of the difference in temperature between the two probes and n is the number of samples. The number of samples, n , is determined by the time interval over which the temperature difference is averaged. The desired vertical resolution of C_n^2 for this project is 20 m with the summation computed over 4,000 samples. The maximum sample rate (based on the response time of the probes) is 1,000 samples per second. At this sampling rate ARIM-1 will require a maximum descent rate of 5 m/s. This information, along with the absolute temperature, absolute pressure and relative humidity, will be used to determine the refractive index structure coefficient, C_n^2 , as explained below.

2.3 Thermosonde Experimental Technique

2.3.1 Theory of Operation

The hot wire system consist of two hot wire sensors mounted on the ends of a one-meter long boom. The most commonly used sensor materials are platinum and tungsten wire that has a diameter of a few micrometers. The wires are usually plated with another metal for additional structural strength and for soldering. Plated wire,

known as Wollaston wire, is commercially available in either silver-coated platinum or platinum-coated tungsten [5]. All types of commercially available Wollaston wire varies in diameter due to manufacturing limitations. Also, the length of the probe wires will be slightly different because of measurement errors. The variation in the diameter and in the length of the probe wires creates difficulties in matching the resistance of two wire sensors. Tungsten wire has the advantage of strength and platinum wire has the advantage of a very smooth surface. The disadvantages associated with tungsten wire are oxidation at high current levels and an irregular (rough) surface [6]. Platinum coated tungsten wire was selected for this project because of the high "g" loads that will be imposed on the probes during the ascent phase of the flight and the high (greater than 10 m/s) winds that may be encountered during the opening of the booms. Also, the probes will be operated at an extremely low current level to reduce the oxidation hazard.

The temperature probes are made from the Wollaston wire by cutting the wire to a specified length (0.45 cm), etching away the platinum coating from the center of the wire and attaching the wire to supports [5,6]. The process of cutting the wire to length will introduce another error in the resistance of the wire because of errors introduced in the length from measurement and cutting. The length and diameter variations of the wire will cause the two probes to vary slightly in their resistance as the background temperature changes. The center of the wire must be etched with acid to expose the tungsten wire inside of the platinum. The residual platinum on the ends of the wire will aide in attaching the wire to the supports and will help to support the exposed tungsten wire. The wires are soldered to the probe supports which provide structural and electrical connections to the balance of the circuit.

The term "hot wire" is generally applied to sensors that are operated at sufficiently high current levels to cause the wire elements to self heat. The principle application for "hot wire" sensors is in the field of anemometry where there is a constant air flow over the sensors. When used for measuring the differential temperature, the sensors are operated in the constant current mode at very low current levels to prevent the sensor wires from self heating. This mode of operation is sometimes referred to as the "cold wire" method, for obvious reasons. The difference in temperature is derived from the change in resistance of the wire elements as their temperature changes. The differential temperature (ΔT) is determined by measuring the difference in the voltage of the two sensors that is produced by a constant current.

The resistance of the tungsten wire elements is given by [7]:

$$R = \frac{\rho L}{A} = \frac{\rho_0(1 + \alpha(T - T_0))L}{A}$$

where R is the wire resistance, L is the wire length, A is the cross sectional area and ρ is the resistivity. The last term on the right shows that the resistivity is a function of the absolute temperature of the wire, where α is the temperature coefficient of resistance, T_0 is the reference temperature (0°C or 273.15 K) and T is the temperature of the wire. The resistance of the wire elements at 0°C (273.15 K) from the equation

above is 26.4757Ω . A plot of the resistance of tungsten wire with the above dimensions for -50 to $+40^\circ\text{C}$ is shown in Figure 2-1.

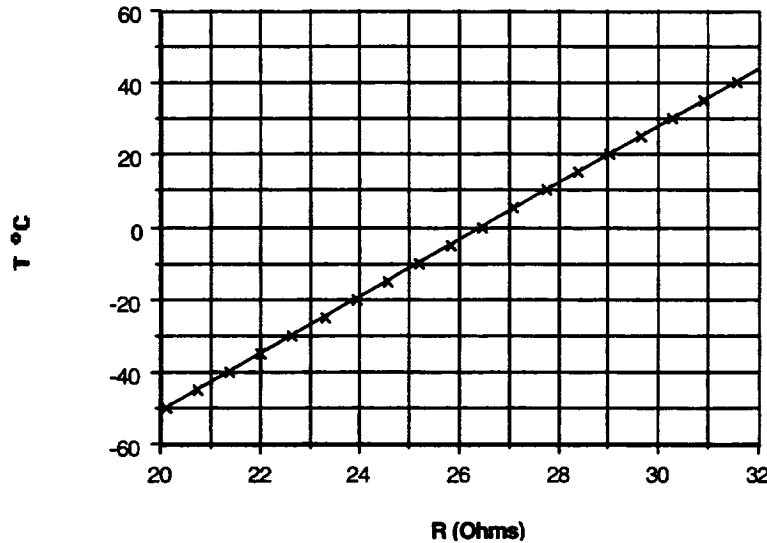


Figure 2-1 : Wire resistance versus temperature for a 0.45 cm length of $3.45 \mu\text{m}$ tungsten wire.

The change in resistance due to a change in the wire temperature of 0.002°C is found by calculating the new wire resistance, R_2 , from the previous equation with T set to 273.152 K . The resulting value for R_2 is 26.4759Ω . The change in the resistance due to a 0.002°C change in temperature is found by subtracting R from R_2 and is equal to $200 \mu\Omega$.

If the mission objectives are to be met then a circuit capable of measuring the very small change in resistance must be found. Also, the current passing through the wire elements must be small to prevent a significant heating of the wire. Another problem associated with the wire resistance is due to the manufacturer's inability to produce wire with a constant diameter. Also, there are small differences in the length of the wire due to measurement errors. The differences in the wire dimensions creates a difference in resistance between the two probes when the probes are at the same temperature giving a false indication of differential temperature. These problems must be considered in designing or selecting a circuit to extract the differential temperature information from the probe resistance.

2.3.2 Differential Temperature Circuit

The extremely small changes in wire resistance coupled with the small current levels (required to prevent self-heating of the wire) results in extremely small differential voltages that must be amplified and measured. The most direct method of amplifying the differential voltage is to pass a dc current through the probes and then use a high

the same order of magnitude as the amplifier noise voltage and the common mode noise from the sensor circuit.

The second problem is the small error voltage due to the slight difference in resistance of the probes caused by differences in the wire dimensions. As the background temperature changes, the resistance of the two probes will change by a slightly different amount. The small resistance change will cause a small differential voltage between the probes that is not caused by the effects of turbulence. If the background temperature were constant then the resistance of each probe could be compensated for by adding an appropriate amount of resistance to the probes with the lower resistance. However, the background temperature will change as the parachute descends through the atmosphere negating any adjustment that was made on the ground at a constant temperature.

A solution to the above problems was found in the thermosonde circuit developed by Tri-Con Associates [4] and the subsequent modifications made by Systems Integration Engineering, Inc. [8]. In this circuit, an oscillator generates an ac signal that is passed through the sensors. The differential voltage is then fed to a transformer that acts as an initial amplification stage. Since the transformer has an essentially infinite common mode rejection ratio and creates little thermal noise of its own, the first problem is solved. The resulting differential voltage signal from the probes can now be thought of as the oscillator signal that is amplitude modulated by the combination of the differential probe voltage plus the error voltage. A filtering process can now be used to feed the error voltage (which is at a much lower frequency than the differential probe voltage) back to the sensor circuit. A disadvantage of this approach is that the on-board oscillator will generate a potentially large amount of noise at the oscillator frequency.

2.3.3 Overview of the Thermosonde Circuit Designed by Tri-Con Associates

A block diagram of the basic circuit is shown in Figure 2-2. The oscillator generates a 3 kHz sine wave with an amplitude of 3 V and a 3 kHz square wave of the same amplitude. The sine wave is fed to the sensors, which are arranged in a bridge circuit, producing a current of about 0.3 μA . The square wave is sent to a demodulator, U2, for use as a carrier signal. The differential voltage from the probes for the smallest change in temperature (a 0.002°C change in temperature results in approximately a 47 nV differential voltage) is picked off by a 20:1 transformer and sent to an instrumentation amplifier, U6. The signal into U6 should be on the order of 0.94 μV . U6 has an adjustable gain of 863 to 3,021 which amplifies the 0.94 μV signal to a maximum of 2.84 mV. From this point the signal is demodulated by U2 which separates the amplitude information from the 3 kHz carrier signal. After demodulation the signal is differentially amplified by a factor of 12 by U9 to about 27 mV.

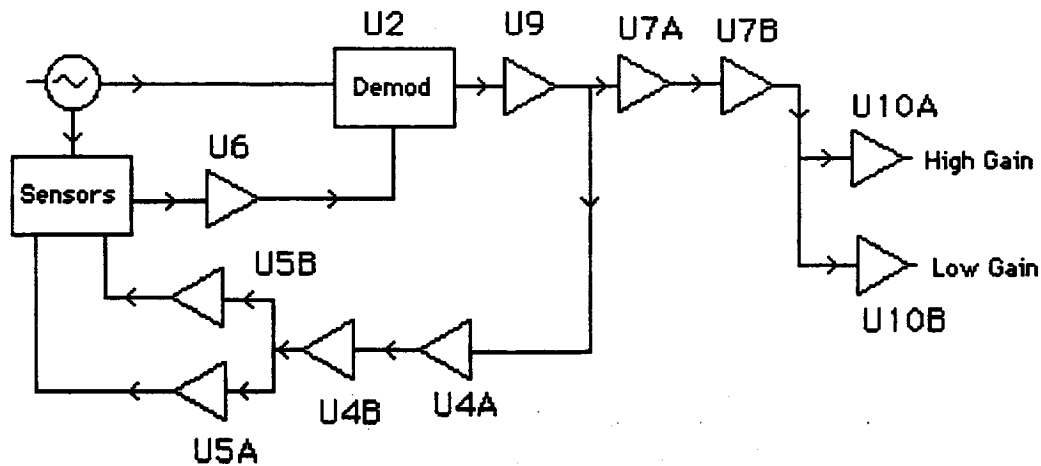


Figure 2-2 : Block diagram of the differential temperature probe circuit. The component numbers refer to the circuit schematic in the succeeding figures.

After the demodulated signal is amplified by U9 it splits into two signals, one of which proceeds to the output circuit and the other to the feedback circuit. The feedback circuit filters out all of the high frequency components and passes only those components that are changing at a rate of 0.05 Hz or less. This component of the signal represents the error signal due to slight differences in the probe resistance's and to common mode heating of the probes. The resulting signal is fed back to the sensor bridge through two FET's that make slight changes in the sensor resistance to compensate for the difference in the probe resistance. The output circuit consist of two two-pole low pass filters, two amplifiers and two RMS-to-DC converters. The signal passes through the low pass filters then splits into a high gain and a low gain path. The high gain path consist of an amplifier with a gain of 1000 followed by an RMS-to-DC converter with an averaging time constant of 3.7 seconds. The low gain path is identical to the high gain path except that the amplifier gain is 2 instead of 1,000.

Bridge Circuit and Amplification

The sensors are configured in a bridge circuit. The bridge output is fed to a 20:1 transformer which acts as a first stage amplifier with a infinite CMRR and a gain of 20. The bridge is compensated for long term dc effects (due to equal heating or cooling of the probes) by a feedback circuit that is fed into the bridge through two 1.3 k Ω resistors and two FET's. The transformer output is sent to U6, a μ A725 Instrumentation Amplifier. The μ A725 has a CMRR of 120 dB and an input noise voltage of about 0.8 μ V at 3 kHz. This is a high gain amplifier with a gain of between 900 and 3000 as used in this circuit. The gain is adjusted by varying the resistance of the resistor to ground shown in Figure 2-3. The signal out of U6, shown in Figure 2-2, should be in the mV range.

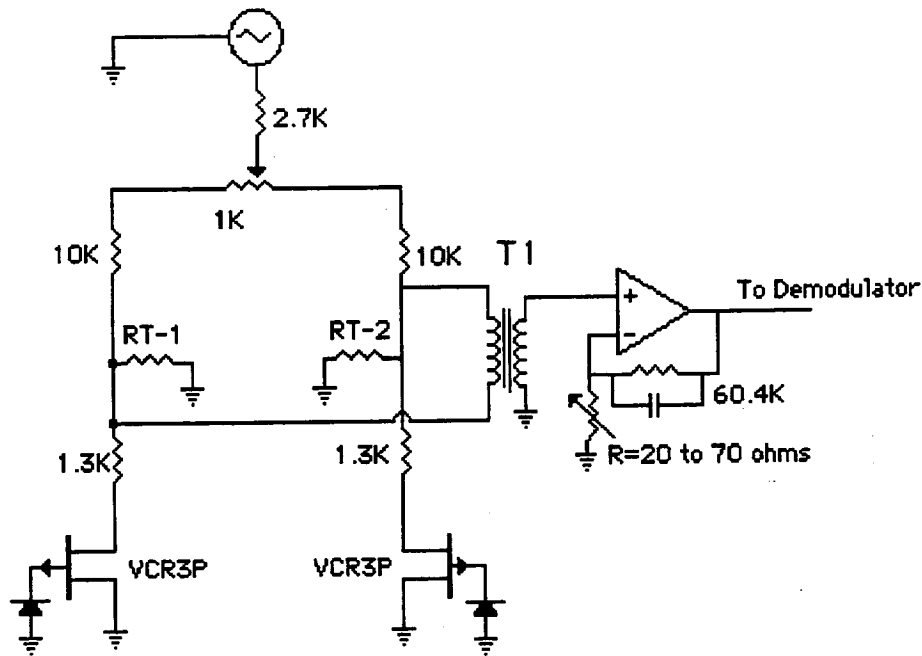


Figure 2-3 : The bridge circuit for the "hot wire" sensors is composed of a 1 k Ω variable resistor, two 10 k Ω resistors, and the two wire elements (RT-1 and RT-2) with a nominal resistance of 27 Ω . The two FET's and the two 1.3 k Ω resistors are part of the feedback network . T1 is a 20:1 step up transformer. The amplifier has an adjustable gain from 800 to 3,000.

Demodulator

The demodulator, U2 , is an MC1596 integrated circuit. The signal from U6 is a 3 kHz signal that is modulated by the differential change in resistance of the probes. U2 uses a carrier from the oscillator to demodulate the signal from U6. The demodulator output is amplified by U9, a CA3240A Operational Amplifier. U9 is used as a differential amplifier and amplifies the demodulated signal by a factor of about 12.

Feedback Network

The purpose of the feedback network is to adjust the current through the sensor bridge to compensate for any effects due to equal heating of the probes. The feedback network consists of the following components:

1. U4A CA3240A Operational Amplifier. This device works like a low pass filter with a cut-off frequency of about 0.2 Hz.
2. U4B CA3240A Operational Amplifier. This is an integrator with a time constant of 20 seconds. The purpose of U4A and U4B is to feedback any long term (or constant) effects to the bridge circuit.
3. U5A and U5B (CA3240A Operational Amplifier). These devices amplify the feedback signal by a factor of ± 2 . The resulting signal is used to drive FET's which are connected to the bridge arms through 1.30 k Ω resistors. Essentially, these

resistors are in parallel with the temperature probes (nominal resistance of about 27 Ω) and make small changes in the leg resistance.

Output Circuit

The output circuit described above consist of the following components:

1. U7A and U7B (CA3240A Operational Amplifier). These two devices are configured as two pole low pass filters. U7A has one pole at 377 Hz and the second pole at 802 Hz. U7B has one pole at 159 Hz and another pole at 5.89 kHz. The purpose of this circuit is to eliminate all signal components with frequencies above about 200 Hz. The oscillator at 3 kHz is probably the chief source of high frequency noise.
2. U10A and U10B (CA3240A Operational Amplifier). U10A provides a gain of about 2 (low gain) and U10B provides a gain of about 1000 (high gain).

2.3.4 Pressure, Temperature and Humidity

The absolute temperature, pressure and humidity are required in order to reduce the raw differential temperature data. The requirements for the pressure, temperature and humidity sensors are outlined in Table 2-1.

Table 2-1 : The required range and accuracy for the temperature, pressure and humidity measurements.

Sensor	Range	Accuracy
Temperature	-50 to 20°C	0.002°C
Pressure	0 to 30 in Hg	0.01 in Hg
Humidity	0 to 100%	± 2.0%

Pressure Sensor

The Syn Sym model SCX15A pressure sensor is an absolute pressure device with a measurement range of 0 to 15 psi (0 to 30.54 in-Hg). The SCX15A is basically a bridge network consisting of four strain gauges that respond to a change in the structure of a diaphragm due to a change in pressure. This sensor has a sensitivity of 6.0 mV/psi (2.947 mV/in-Hg) with a supply voltage of 12 volts dc and a response time of 100 μ s. A twelve bit analog-to-digital converter is used to process the pressure data which results in a resolution of 0.0073 in-Hg per step over the full range (0 to 15 psi). An amplifier with a gain of 55.56 is used to change the output voltage range from 0 to 90 mV to 0 to 5 V with a corresponding resolution of 0.1637 V/in-Hg.

Temperature Sensor

The temperature sensor is a Omegafilm type 100W30 thin film platinum resistance temperature device (PRTD) with a nominal resistance of 100 Ω at 0° C. The PRTD has a temperature range of -70 to 600° C and a coefficient of temperature of 0.00385 $\Omega/^{\circ}$ C.

Humidity Sensor

The relative humidity sensor is a Omega model Hx92V. This device has a range of 0 to 100% relative humidity with a resolution of $\pm 2\%$. The Hx92V produces a 0 to 1 volt output that is proportional to the relative humidity. An amplifier with a gain of 5 is used to change the output voltage range from 0-1 volt to 0-5 volts. An eight bit analog-to-digital converter is used to digitize the humidity data which gives a resolution of 0.39% RH/step, which is more than adequate for the resolution of the humidity sensor (i.e., $\pm 2\%$).

2.3.5 Pressure, Temperature and Humidity Signal Conditioning.

The conversion of the differential temperature and the pressure reading will require a 12 bit analog-to-digital converter to achieve the required resolution. The absolute temperature and humidity will require an 8 bit analog-to-digital converter to obtain the desired resolution. The A/D converters are located on the computer board and will require an input voltage range of 0-5 volts dc.

2.4 Science Mission Specifications

The successful outcome of the science mission requires that the ARIM-1 team provide the following supporting items:

2.4.1 Rocket and Parachute

A rocket capable of boosting the required payload to an altitude of at least 15 km must be provided. Also, a parachute capable of lowering the science payload at a descent rate of 5 m/s or less below 15 km is required to achieve the required vertical resolution in the refractive index structure constant measurements.

2.4.2 Flight Scheduling

The time of the flight is important for two reasons. First, the flight should take place during the hours of darkness to avoid any problems associated with the differential heating of the temperature probes due to solar radiation. Second, the time of the flight should be coordinated with the launch of a weather balloon to obtain a back-up of the temperature, pressure and humidity sensors. The weather balloon data can be used to evaluate the differential temperature data should the on-board systems fail.

2.4.3 Trajectory

At low altitudes the dominant source of atmospheric turbulence is geographic obstacles and ground temperatures. Therefore, a vertical trajectory is desired in order to sample the atmospheric turbulence that exists over a particular area. This can only

be achieved in the absence of all wind. This requirement is obviously not obtainable. However, to minimize the drift caused by surface winds and winds aloft, the flight should be conducted on a relatively calm day.

2.4.4 Data Handling

The science data will be produced at a rate of 16,024 bps. This data must be stored on board and simultaneously transmitted to the ground. The flight computer must be capable of storing two hours of science data (14.4 Megabytes). A transmitter capable of transmitting this data to a ground station must also be provided.

2.4.5 Physical Requirements

The weight of the science package will be approximately one pound and will occupy a space of about 60 cubic inches. Additionally, provisions for supporting the differential temperature probes on booms to provide a one meter horizontal separation must be supplied.

2.4.6 Electrical

The on-board electrical system must be capable of supplying the instrumentation board with ± 15 volts and a +5 volts dc supplies. Finally, the electrical system must be capable of supplying 44 Watts of power for the duration of the mission (2.0 hours).

3. Mission Analysis

3.1 Objective

The ARIM-1 sounding rocket payload, requires a launch vehicle capable of lofting a 50 pound payload to a minimum altitude of 100,000 feet. This is necessary in order to separate the payload from the expended motor at apogee, and deploy the main parachute at the target altitude. The science objective of this mission requires a parachute descent rate of 5 m/sec, at an altitude between 12 to 15 kilometers.

3.2 Motor Selection

The motor criteria required to meet the ARIM-1 mission objective was based on a multi-faceted set of requirements. First, the motor had to be energetic enough to place the payload above 15 km. Secondly, the motor couldn't be too energetic, as this would impose unacceptably high g-loads on the payload components. And finally, the cost of the motor had to be economical enough for purchase by the limited budget of a university student rocket program.

For high altitude sounding rocket payload capability, the most aerodynamically efficient way is to use a long burn, low thrust motor. This strategy prevents the kinetic energy of the rocket motor burn, from being wasted on overcoming the massive drag forces in the most dense layer of the lower atmosphere (Troposphere). Unfortunately, most sounding rocket motors are high thrust with a short duration burn.

The rocket motors considered were those in the 5 to 8 inch diameter class. The use of custom motors was ruled out early in the design process as there is no provision for standardization from one payload to the next. An off-the-shelf motor was desired, which would enable a standard vehicle and payload to be flown without any modification from one mission to the next.

The Viper III and Viper V motors have a proven history of use as launch vehicles for the Super Loki boosted dart, Super Stable Loki boosted dart, and the Viper - Robin boosted dart. These vehicles range in diameter from 4 inches to 7.6 inches. After looking at the performance of these motors, only the Viper V motor had sufficient energetics to place a 50 pound payload to over 100,000 feet. The only drawback to the Viper motor is the high axial acceleration and g-loads.

The final motor selection was the Viper V motor, which is distributed through Industrial Solid Propulsion in Las Vegas, Nevada as part number 920481. This motor was basically designed as a booster for an un-powered dart, when used as a boosted dart vehicle. This motor was engineered by Industrial Solid Propulsion as a sounding rocket booster, capable of carrying a 30 pound payload to an altitude of 328,000 feet (100 km). Cost for this motor was quoted at \$20,000 per motor by Industrial Solid Propulsion. For that price, the basic motor is provided with the igniter.

For the motor to be usable, a fin canister must be fabricated for the aft end of the motor, with fins of appropriate geometry and surface area to allow the rocket to stabilize. At the head cap of the motor, an appropriate coupler mechanism must be machined, for attaching payload to the rocket motor. The motor headcap is threaded, which allows a machined coupler to be thread to the end of the motor.

After the completion of this conceptual design study, Sandia National Laboratories in Albuquerque, New Mexico was reducing their stock of sounding rocket motors. The University of Alaska Fairbanks currently anticipates the procurement of approximately 25 government surplus Thiokol Cajun and Apache rocket motors, which may provide an attractive alternative to the Viper V motor for the ARIM-1 mission.

The Cajun and Apache rocket motors have similar performance to the Viper V motor, and several hundred were flown by NASA in a two-stage configuration known as the Nike-Apache and Nike-Cajun from 1961 to 1978. These motors have a known flight profile and much data on these vehicles is readily available.

This information was made available to the University of Alaska student rocket program after the original engineering design analysis of the ARIM-1 launch vehicle with the Viper V motor. So, the design and performance specifications for the Viper V motor are presented here in this preliminary report. However, all of the information presented here will have to be recalculated if the Cajun and Apache sounding rocket vehicles are employed for lofting the ARIM-1 payload.

3.3 Launch Vehicle Specifications

The Viper V rocket motor is 7.6 inches in diameter, and 86.2 inches from the headcap to the end of the nozzle. The rocket payload is 8.0 inches in diameter, with a 3.0 inch long boat-tail connecting the payload to the motor, with a machined coupler, which screws into the threads on the motor head cap. The top of the payload incorporates a 3:1 ogive nose cone. The umbilical is located between the coupler and the rocket motor head cap. This allows the umbilical to be shed with the expended rocket motor at apogee, for a lighter recovery payload mass during reentry. The rocket also has four one quarter inch thick fins for stabilization with a 70 degree angle at the leading edge, and a 30 degree angle at the trailing edge. The leading edges of the fins are beveled to a biconvex double edge with a one half inch bevel.

Overall rocket length is 206 inches (17.0 feet) with four fins. Each fin has a flat surface (planar) area of 24 in², for a total fin area of 96 in². The frontal area of each fin projected to the relative air stream during flight is 1.4 in², with a total projected frontal fin area for all fins of 8.0 in².

Refer to Figure 3-1 for design dimensions of the Viper V sounding rocket vehicle. Notice the fin geometry, fin canister, motor nozzle, and cutaway view of core burning motor propellant grain. With these design dimensions and vehicle geometry, rocket flight performance parameters can be calculated. Refer to the ARIM-1 flight profile in Figure 5-20, for rocket motor burn out velocity, altitude, and coasting time to apogee altitude.

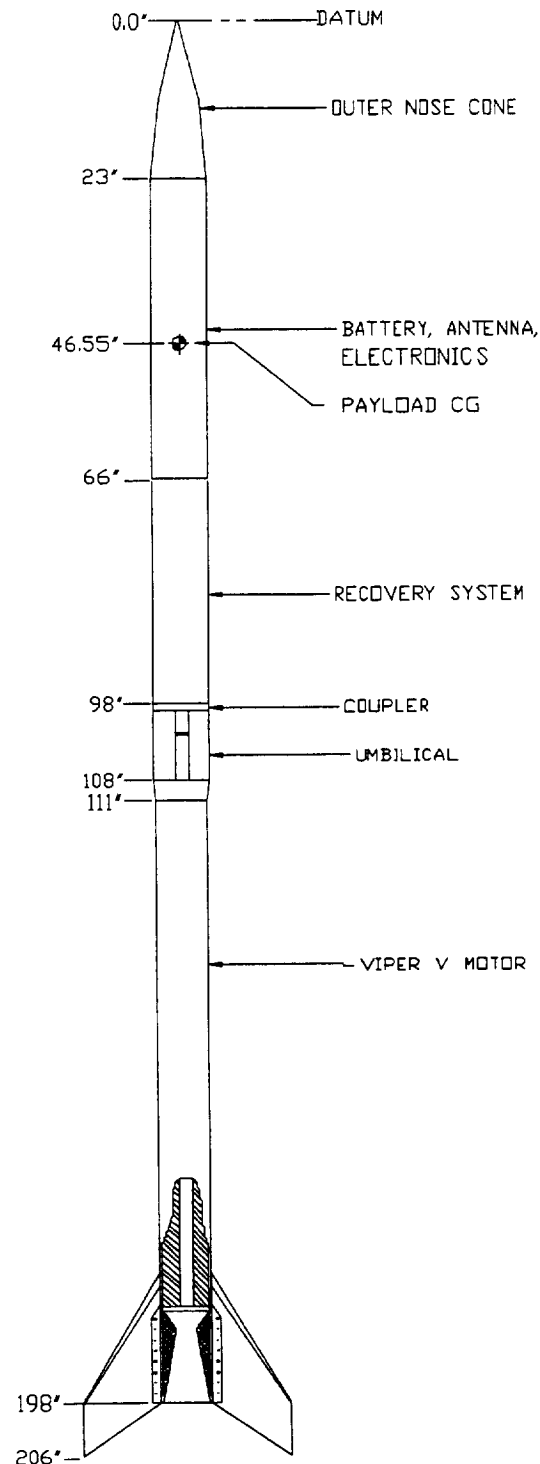


Figure 3-1 : Design specifications and dimensions for the Viper V sounding rocket vehicle. Note, motor and nozzle cutaway, in addition to basic fin geometry.

The rocket flight profile performance parameters are determined using Roger's Aeroscience ALT4 computer program, in addition to NASA's SENSE-5D, 5 degree of freedom rocket trajectory analysis computer program. This is the same program NASA uses to determine flight path trajectory for its sounding rocket launches.

In order for the launch vehicle to be stable and fly along the project flight profile, the vehicle center of gravity (CG) must be properly established. For a rocket to be aerodynamically stable, the center of gravity must always be ahead of the vehicle center of pressure (CP). The center of pressure is the point through which all in-flight aerodynamic forces act on the rocket. For a rocket to be stable, the center of gravity and the center of pressure must be located at least one and a half rocket body tube diameters (calipers) apart as a minimum. This center of pressure and center of gravity relationship is known as static stability. Increasing the distance between the center of pressure and the center of gravity will increase rocket aerodynamic stability. However, a rocket that is too stable is not desirable, as it will have a very strong tendency to fly into the wind (weather cocking) and deviate from the intended ballistic flight profile.

Rocket fins are very important for providing in-flight vehicle stability. Fins provide a strong restoring force (normal force) to aerodynamic disturbances during flight. Such disturbances can result from horizontal wind gusts and dispersion of the rocket from its intended flight path due to thrust misalignment through the nozzle during motor burn. Thus, it becomes important to ensure the fins are properly located on the launch vehicle, have an appropriate geometry for low drag, and provide sufficient surface area for stability. If the fins are too small the rocket will be unstable. If the fins are too large, they will induce excessive parasitic drag, resulting in a corresponding degradation of apogee and vehicle performance.

To achieve these design criteria for a stable launch vehicle, the center of gravity location for the rocket motor must be known. Since the motor manufacturer did not provide a motor center of gravity location, this will have to be calculated for the Viper V motor. This information will provide an aerodynamically stable launch vehicle to place the sounding rocket payload to the intended mission apogee altitude.

The rocket payload must be in the proper attitude for reentry. The payload reentry attitude is controlled by regulating the center of gravity position to make it statically unstable. This is done by separating the center of gravity and center of pressure by less than one body tube diameter (calipers) from each other. This payload instability ensures it will reenter from apogee in a horizontal flat spin or tumbling attitude. This provides maximum payload projected frontal surface area during the ballistic free fall portion of reentry, for maximum drag and aerodynamic deceleration prior to deploying the parachute recovery system.

This payload reentry attitude is accomplished by using what is known as the *Sandia '45% to 55% rule'*. This means the payload center of gravity is located between 45% to 55% of the payload distance as measured from the tip of the nose cone. This rule will always place the payload center of gravity at less than one caliper from the center of pressure position to ensure aerodynamic static instability for reentry during ballistic free fall.

The parachute recovery system is located at the aft end of the payload, and comprises approximately one third of the total payload weight. To achieve payload reentry instability with the least amount of ballast, the payload should be statically balanced at

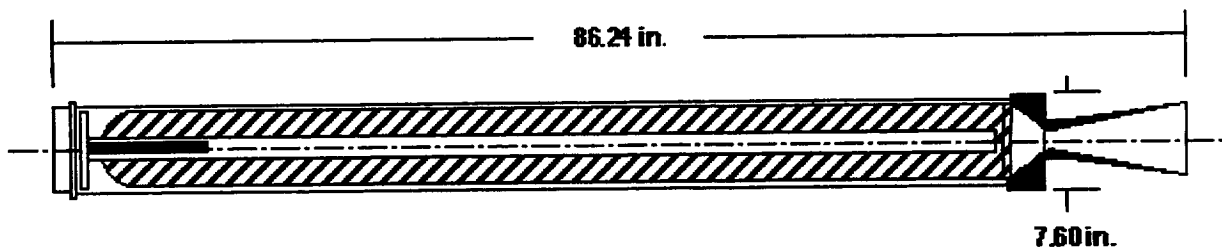
55 percent of the payload distance as measured from the nose cone tip. This is necessary to keep the total payload weight to a minimum.

3.4 Motor Performance

The Viper V motor is a slotted tube, composite solid propellant sounding rocket motor. The propellant is composed of hydroxyl terminated polybutadiene - ammonium perchlorate (*HTPB-AP*) and aluminum (*Al*). Ammonium perchlorate is the oxidizer, while polybutadiene is the binder, and aluminum is an inhibitor which slows the propellant burn rate. This propellant formulation has a density of 0.0650 lb./in³ (0.901 cm/sec), with a theoretical specific impulse (I_{sp}) of 263.0 lb.-sec/lb. (2,579 m/sec), and a specific heat ratio of 1.13. The nozzle exhaust temperature is 5,926 degrees Fahrenheit (3,548 degrees Kelvin).

Motor dimensions are 7.6 inches in diameter (193 mm), and 86.24 inches in length (2,190 mm). The motor mass is 152.2 lb. (73.57 kg), with a propellant mass of 30.2 lb. (59.06 kg), and an igniter mass of 0.64 lb. (0.29 kg). The nozzle throat area is 2.573 in² (16.60 cm²) with an associated nozzle expansion ratio of 12.01.

The Viper V motor has a thrust duration of 6.25 seconds, with an average thrust of 5,473 lbs. (24,344 N), and a maximum thrust of 7,150 lbs. (31,800 N). Motor performance provides a total specific impulse of 34,207 lb.-sec (152,150 N-sec), with an average chamber pressure of 1,327 psi (9,149 kPa), and a maximum chamber pressure of 1,703 psi (11,741 kPa). The normal operational limit or storage temperature for the Viper V rocket motor is (50°-125° F) or (10°-52° C). Maximum nose tip stagnation temperature during flight is 1,600 degrees Centigrade (2,912 degrees Fahrenheit) for a duration of a few seconds, so no special ablative coating is needed.



Viper V (Block - II Version) Sounding Rocket Motor

Figure 3-2 : Viper V Sounding Rocket Motor cutaway showing casing, nozzle, headcap, ignitor, and propellant grain. Motor casing is made of aluminum tubing.

The total vehicle weight of the Viper V Vehicle at lift off is approximately 230 pounds. The rocket motor will accelerate the vehicle to a maximum velocity of Mach 5 at an altitude of 6,972 feet at 6.3 seconds when the motor burns out. The maximum axial acceleration is +35 g's at max q, and the maximum axial deceleration is -22 g's just after motor burn out. The rocket will then coast for 77 seconds to an apogee altitude of 127, 751 feet at 83 seconds after lift off. Please refer to Figure 5-20 in the recovery section for the rocket performance flight profile.

Viper V Sounding Rocket Motor Thrust Curve

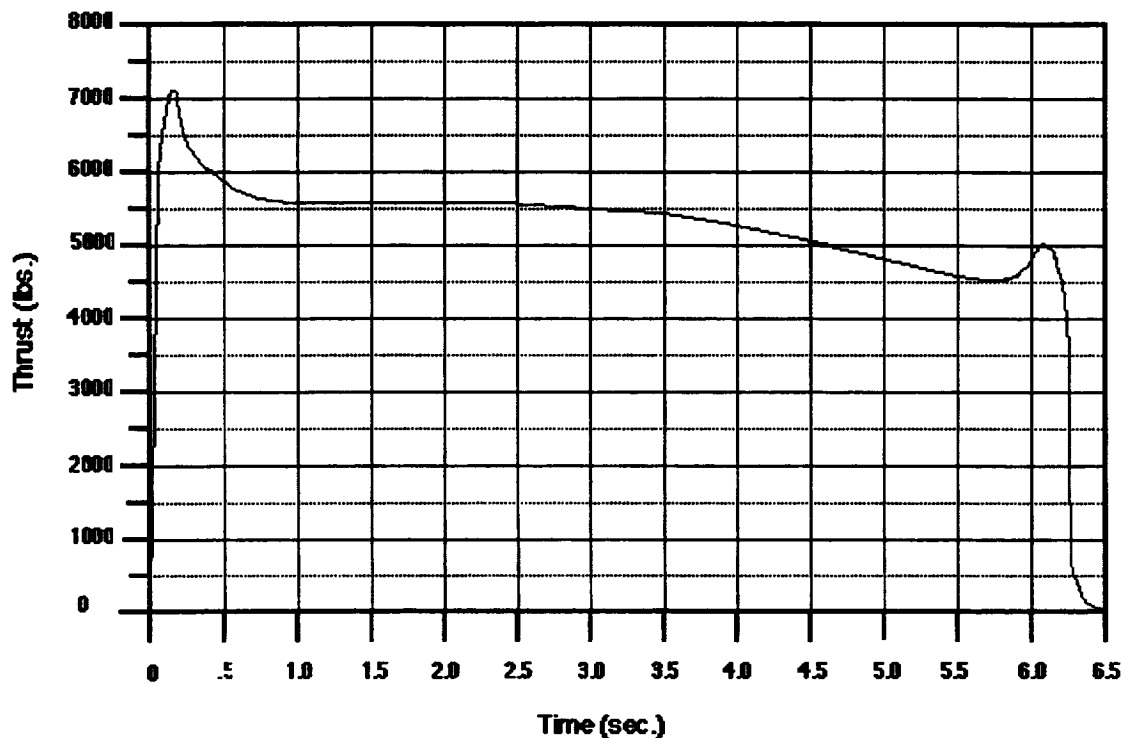


Figure 3-3 : Plot of Viper V rocket motor thrust curve in pounds, as a function of time in seconds.

3.5 Recommendations

If the Apache rocket motors become available it is recommended that this information be modified for a complete performance analysis of the ARIM-1 sounding rocket vehicle based on the specifications of the Apache rocket motors. The Apache motors have known centers of gravity and centers of pressure, which makes stability calculations easier to determine. Also, the known flight parameters of these vehicles is an added assurance for successful missions. The preliminary performance analysis based on the Viper V rocket motor provided a baseline flight profile, which can now be refined to reflect the vehicle geometry of the new launch vehicles. This new vehicle analysis should include complete calculations for pitch and roll moments of inertia, to establish the degree of rocket vehicle stability.

4. Payload Mechanical Configuration and Structural Design

4.1 Configuration

The main objective in configuring the payload is to ensure that the booms may be deployed without difficulty. The following layout meets this criterion, while maintaining the center of gravity of the payload between the battery box and the recovery section until the parachute is deployed, as these two portions of the payload contain the majority of the mass. This CG location creates aerodynamic instability (after motor separation) that imparts the tumble or flat spin required to limit the terminal velocity during free-fall.

There are two main components to the payload. The first is an outer, aerodynamic shell used to protect the internal components during the ascent of the rocket. This assembly consists of the outer nose cone and payload tube. This outer skin is ejected immediately after deployment of the main parachute. Jettisoning the outer payload tube achieves a large weight reduction. This helps to accomplish the science objective of this mission, which depends upon a very low descent rate under parachute. The inner "core" section contains all of the electronics and the hardware necessary to operate them.

Schematics of the payload configuration before and after motor and skin separation are shown in Figure 4-1 and Figure 4-2. The inner payload structure is composed of four main parts: the inner nose cone, the battery box, the longeron/deck assembly, and the parachute section. The telemetry transmitter and antenna are located in the inner nose cone, situated on top of the battery box. Beneath the battery box are the deployment booms and the longeron/deck assembly. This section houses the computer, GPS, instrumentation boards, and science electronics. At the bottom of the longeron/deck assembly is the outer shell separation coupler, and below this is the parachute section.

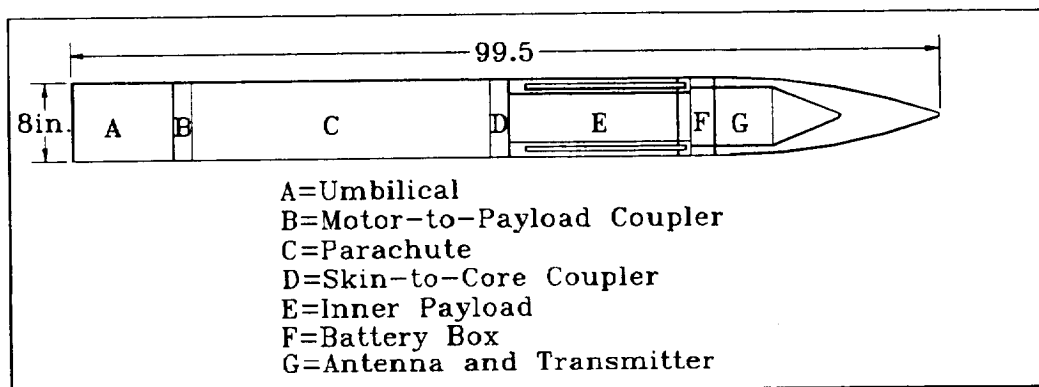


Figure 4-1 : Payload Configuration Before Separation

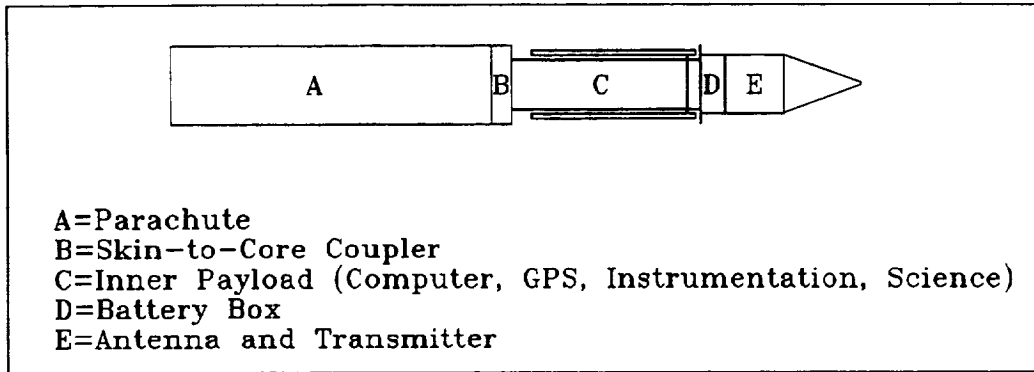


Figure 4-2 : Inner Payload Configuration Schematic After Separation

4.2 Key Mechanical Events

Motor/payload separation occurs as near as practicable to apogee. This is accomplished by the coupler described in section 4.6.

Parachute deployment takes place after a free-fall period as the payload approaches the altitude of interest for the taking of data. For details, see the *Recovery System* section.

The main payload tube and nose cone are jettisoned immediately after main chute deployment (see section 4.7). Six seconds later, when the payload has slowed sufficiently, the booms containing the thermosondes are deployed, as described in section 4.8.4.

4.3 Structural Materials

The materials selected for the structural components are 6061-T6 aluminum alloy, and glass-reinforced epoxy (GRE) composite. These materials were selected for their availability, low cost, ease of machining, and structural properties.

Table 4-1 : Properties of structural materials

Material	Density lb./in ³	E (Msi)	UTS (ksi)	YS (ksi)
filament-wound GRE composite	≈0.05-0.1 depending on G/E ratio	30 (typical)	65-200 depending on direction of fibers	65-200
aluminum alloy 6061-T6	0.098	10.1	38	35

4.4 Outer Payload Tube and Nose Cone Assembly

4.4.1 Outer Nose Cone

The outer nose cone assembly is constructed of filament-wound, glass-reinforced epoxy composite, with a steel tip added for heat resistance (see figure 4-3). The basic shape is a 4:1 ogive. The ogive portion is 32 inches long, and the straight portion for mounting to the payload tube is 4 inches. The steel tip is 4.5 inches long, with 3.5 inches exposed, and has a 0.1875-inch radius on the tip to create a detached shock wave, thereby reducing the stagnation temperature at the tip.

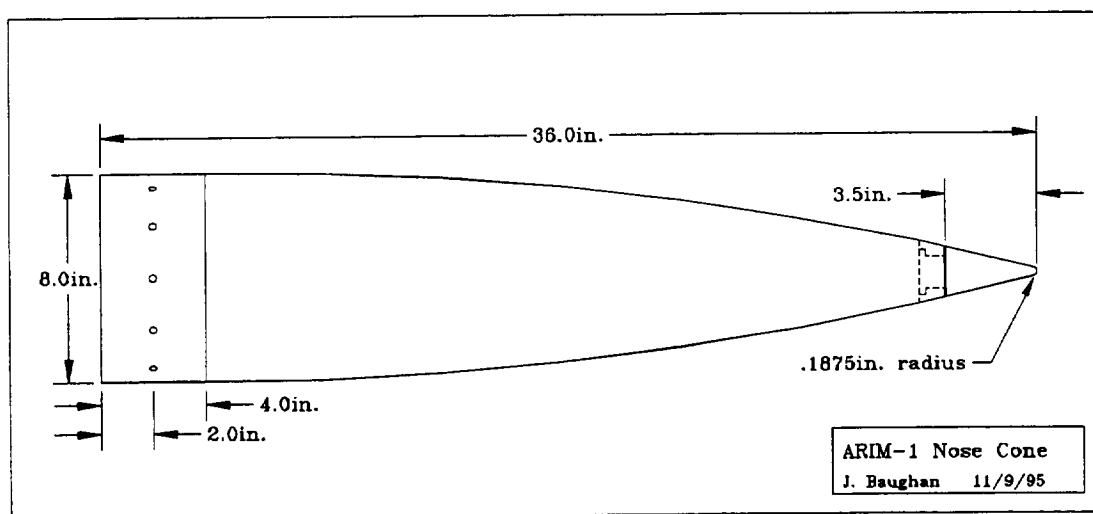


Figure 4-3 : Outer Nose Cone

4.4.2 Outer Payload Tube

The outer payload tube, shown in Figure 4-4, is made from 8-inch OD, 6061-T6 seamless aluminum alloy tubing, with a wall thickness of 0.25 inch. The OD of the first four inches is reduced by 0.140 inch to fit inside the outer nose cone. The tube is drilled and tapped two inches from the forward end to mount the outer nose cone. Four static ports are located radially one inch aft of the nose cone. These ports are connected by Nylon tubes to a pressure plenum. Atmospheric pressure is directed to the altitude switch (see *Recovery System*) through an o-ring interface on top of the battery box. Three bronze bushings are threaded into the payload tube to accept the tapered, steel pins of the core separation coupler. Two radial grooves are machined into the aft end to mate with the motor separation coupler.

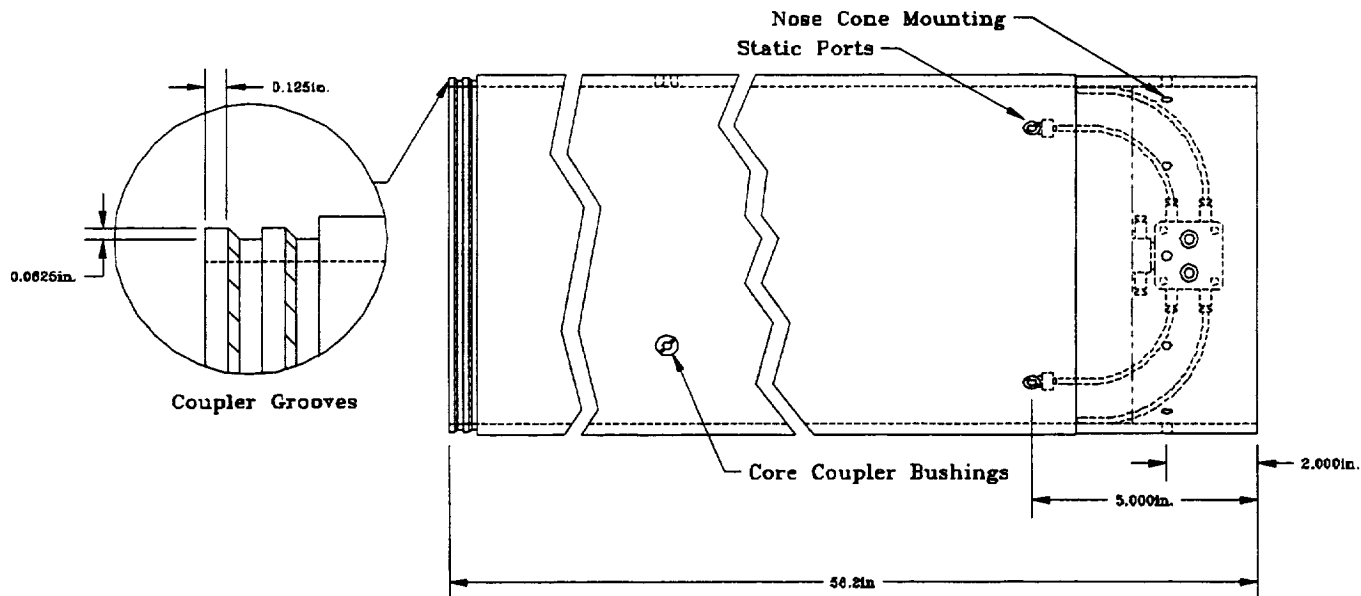


Figure 4-4 : Outer Payload Tube with Static Pressure System installed

4.5 Umbilical Section

The umbilical section contains the components required for powering and communicating with the payload while it is staged on the launcher. The main components are the umbilical tube and block. The payload-to-motor coupler is installed in the umbilical section, which will be discarded, along with the motor, at apogee.

4.5.1 Umbilical Block

The umbilical block (Figure 4-5) is an aluminum alloy casting, produced in the School of Engineering machine shop's foundry. The casting pattern is hand-made from aircraft-grade, birch plywood. This design will accommodate a wide range of payload tube diameters with a minimum of custom milling. The block is 9.75 inches long, and fits an opening 1.5 inches wide. Space has been provided for an umbilical connector up to one inch wide, as well as a separate lanyard switch. Connectors are set at a 10° angle to the direction of rocket travel, to assure a clean breakaway without damage to the connectors.

4.5.2 Umbilical Tube

The umbilical tube section is made from the same material as the outer payload tube (8-inch OD, 6061-T6 aluminum alloy). It is bolted to a steel boat-tail adapter, which is, in turn, bolted to the motor (see detail in Figure 4-6), and is discarded along with the motor at separation. The top of the tube is grooved for the payload-to-motor coupler bands. The coupler platform is bolted into the top of the umbilical section. Besides

housing the umbilical block, the umbilical tube also houses the spring assembly used for positive separation of the payload from the motor, when the bands are released.

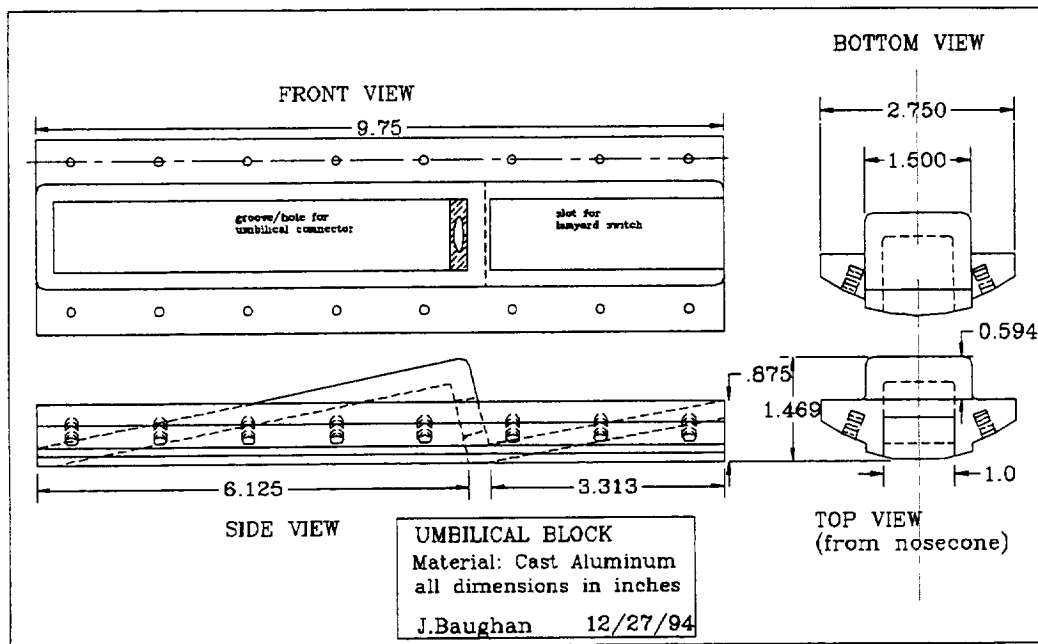


Figure 4-5 : Umbilical Block

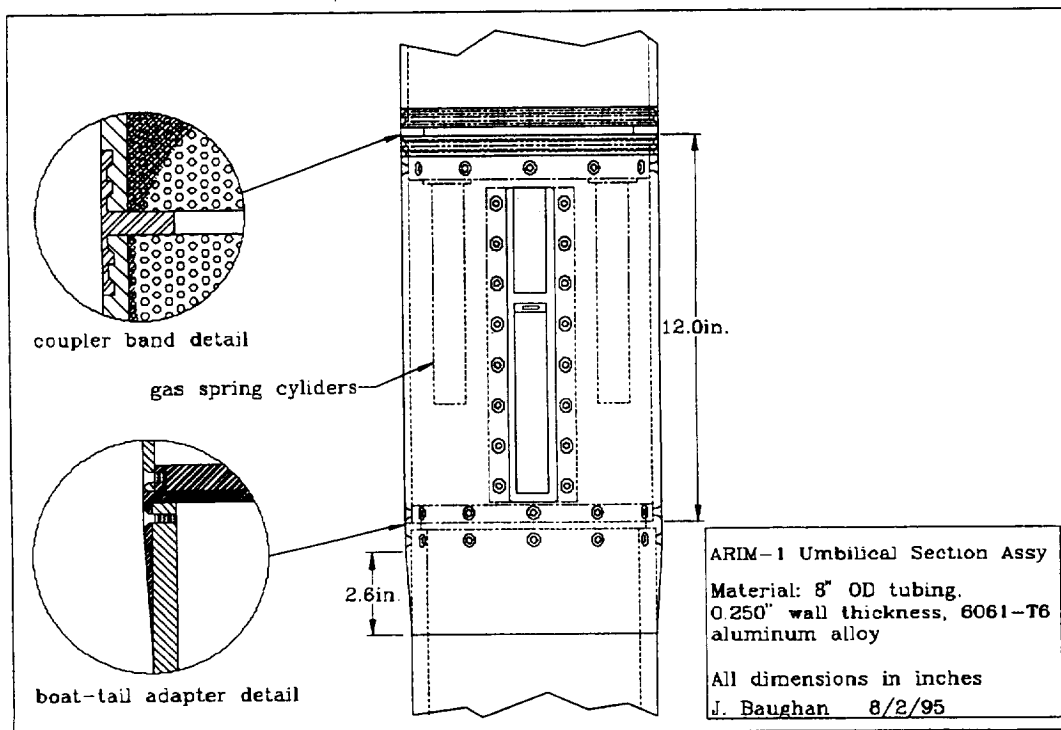


Figure 4-6 : Umbilical section configuration

4.6 Motor/Payload Separation Mechanism

The motor and payload are held together by a multi-rib Vee-band coupler. A pair of grooves, machined into the outer surface of the payload tube (see detail, Figure 4-4), interlocks with ridges in the coupler band sections (Figure 4-6). The umbilical section is mated to the coupler bands in exactly the same way.

The coupler band (Figure 4-7) is divided into three sections, retained at the ends by spring-loaded clips, which also serve as wedges to drive the sections apart when released. The clips/wedges are attached to spring-loaded rods, latched into a central hub. The latch is released by a Hoxlex ZD426 EED thruster, as shown in figure 4-8.

One of the goals of the student rocket project is to build upon the work of previous student engineers. This is the reason for the choice of this design. This type of coupler mechanism was designed by Victor Mimken for use on SRP-2. The style of the Vee-band has been changed, and a positive separation mechanism has been added. Positive separation is assured by three gas-pressure springs housed in the umbilical section.

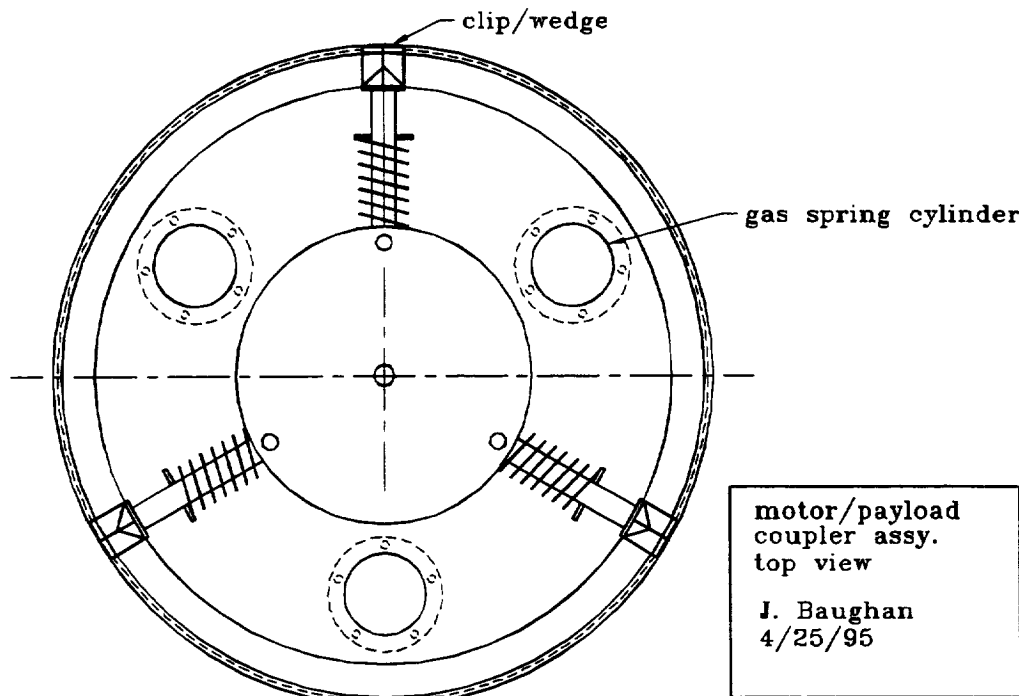


Figure 4-7 : Motor-to-Payload Coupler

4.6.1 Pyrotechnics

The pyrotechnic selected for both the motor and skin separation is the Hoxlex ZD426 thruster. It produces a 0.5-inch stroke against a 225-lb. load. The "business end" is a #10-32 stud, which is threaded into the actuating mechanism of the motor coupler, and into a button that actuates the core coupler.

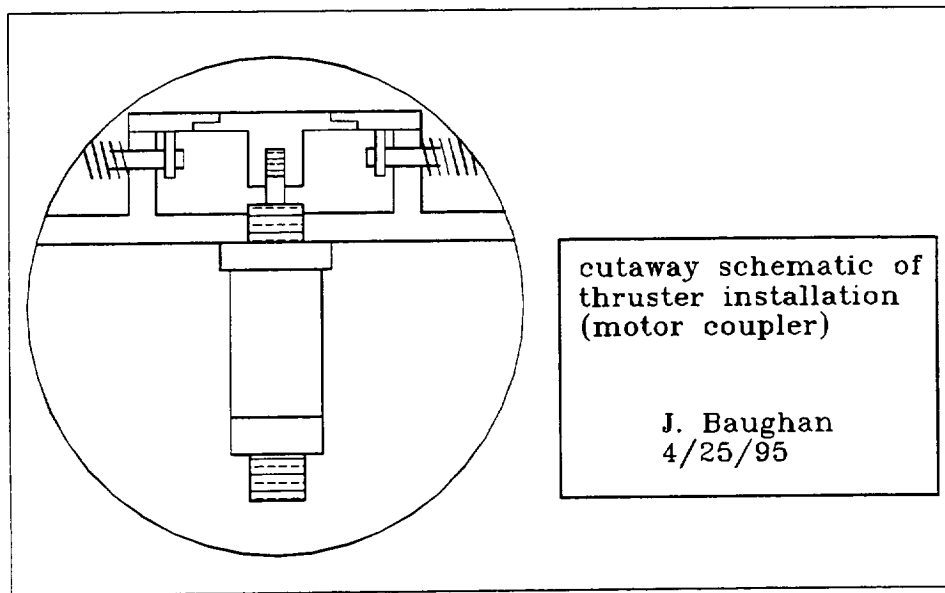


Figure 4-8 : Thruster installation detail (simplified schematic)

4.7 Skin Separation

Separation of the outer payload tube (skin) from the core payload is accomplished by withdrawing a set of pins that lock the two sections together. These steel pins are spring-loaded and held in the locked position by a disc, which abuts the inboard ends of the pins. The disc is pushed out of the way by a Hoxlex ZD426 EED thruster. This allows the springs to drive the pins inward into the hub, thus releasing the core payload from the skin, as shown in Figure 4-9 and Figure 4-10. A bondable, 1/32-in. thick Teflon[®] sheet material is cemented to the outer surface of this coupler, as well as the battery box flange, to ensure that the core payload slides freely out of the skin. The bulkhead provides a terminus for the longerons and a mounting surface for the parachute attachment yokes. The hub housing also provides a platform for a puck-type GPS antenna.

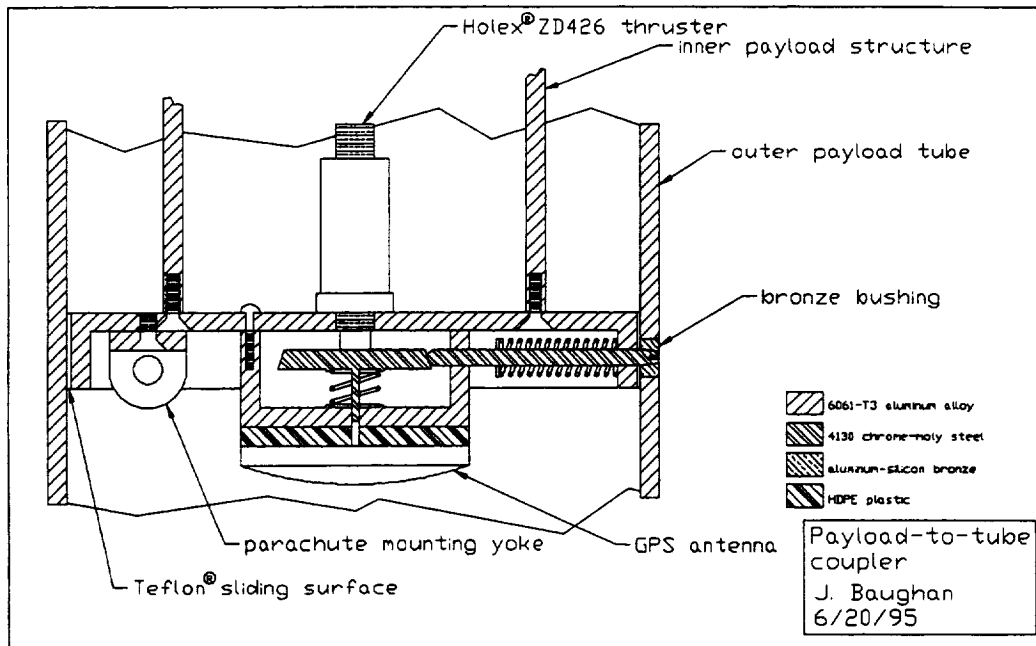


Figure 4-9 : Cutaway Detail of Core-to-Skin Coupler

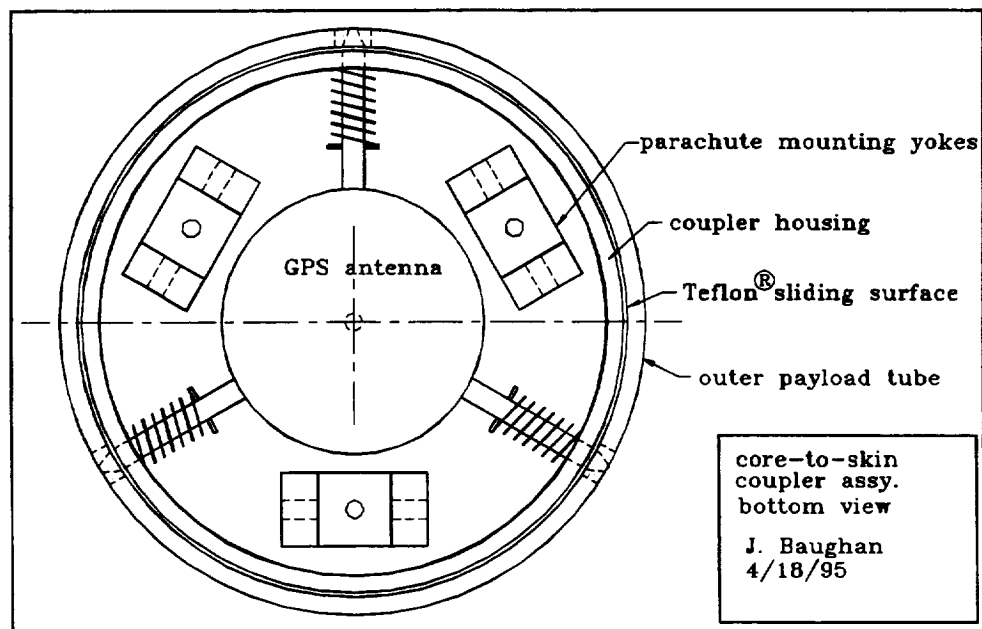


Figure 4-10 : Payload Core-to-Skin Coupler

4.8 Inner Payload Design

4.8.1 Inner Nose Cone

The on-board transmitter and antenna are located in the inner nose cone section. The transmitting antenna is wrapped around the outside of the cylindrical portion, and fastened with screws. The transmitter is mounted concentrically, on top of the battery box. The conical portion of the inner nose cone serves to smooth the airflow around the payload on descent. This prevents induced turbulence that would interfere with thermosonde operation. It also provides some protection on impact. The inner and outer nose cones are the only structural components made from GRE composite. This material is used because it can be molded into the required shapes, and it will allow the antenna to transmit to the ground station with minimal interference. Figure 4-11 depicts the antenna mounting and transmitter position.

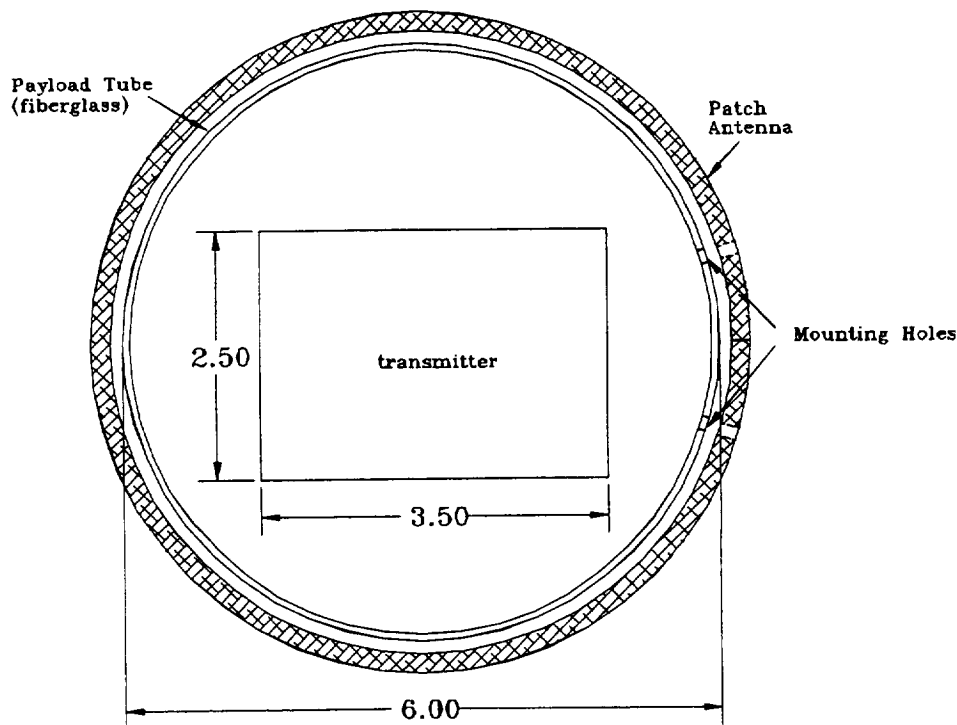


Figure 4-11 : Antenna Mounting on Inner Nose Cone (end view)

4.8.2 Battery Box

The battery box contains forty-eight AA-size lithium cells that will power the onboard systems of the payload. They are potted in place with Loctite® 598 RTV silicone. The battery box is machined from solid, round 6061-T6 aluminum alloy. The battery layout is shown in Figure 4-12.

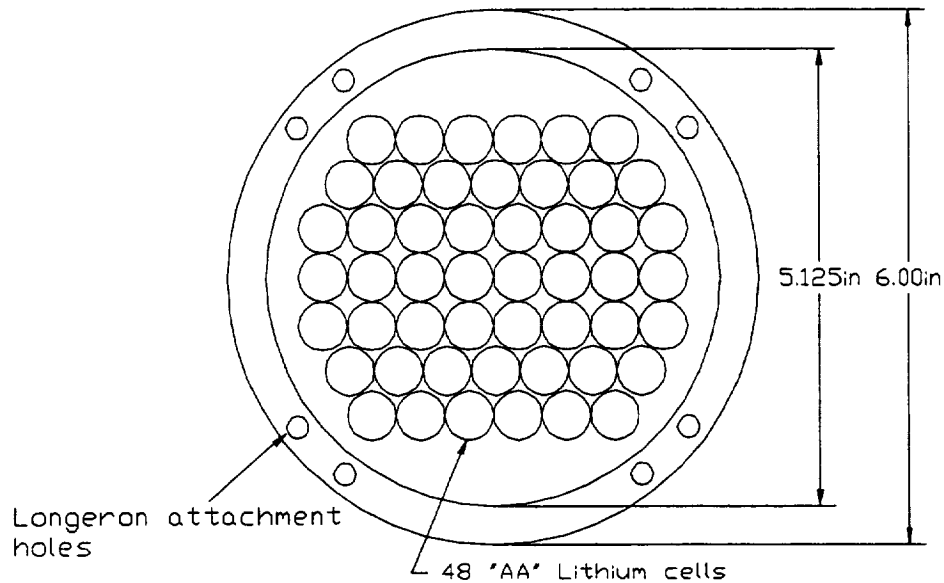


Figure 4-12 : Battery Box Configuration

4.8.3 Longeron/Deck Assembly

Most of the payload electronics are located in the longeron/deck assembly (Figure 4-15). This assembly is constructed by bolting four rectangular bars (longerons, Figure 4-13) into notches in the perimeter of circular deck plates (Figure 4-14). The longerons are the most stress-critical part of the structure. Each one will experience a peak stress of 2.2 ksi, assuming the payload will undergo a 50g acceleration force. This is well below the tensile yield stress of 35 ksi for 6061-T6 aluminum alloy.

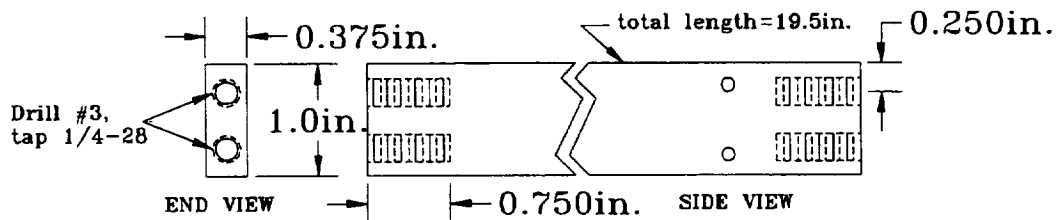


Figure 4-13 : Longeron

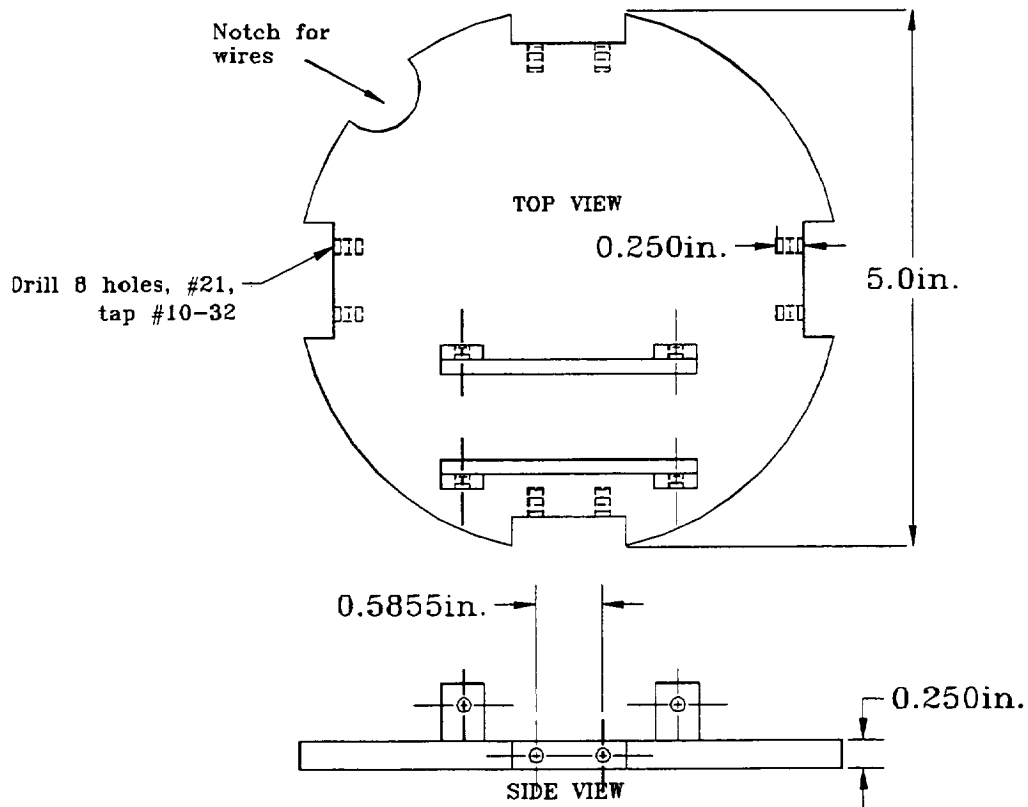


Figure 4-14 : Deck Plate

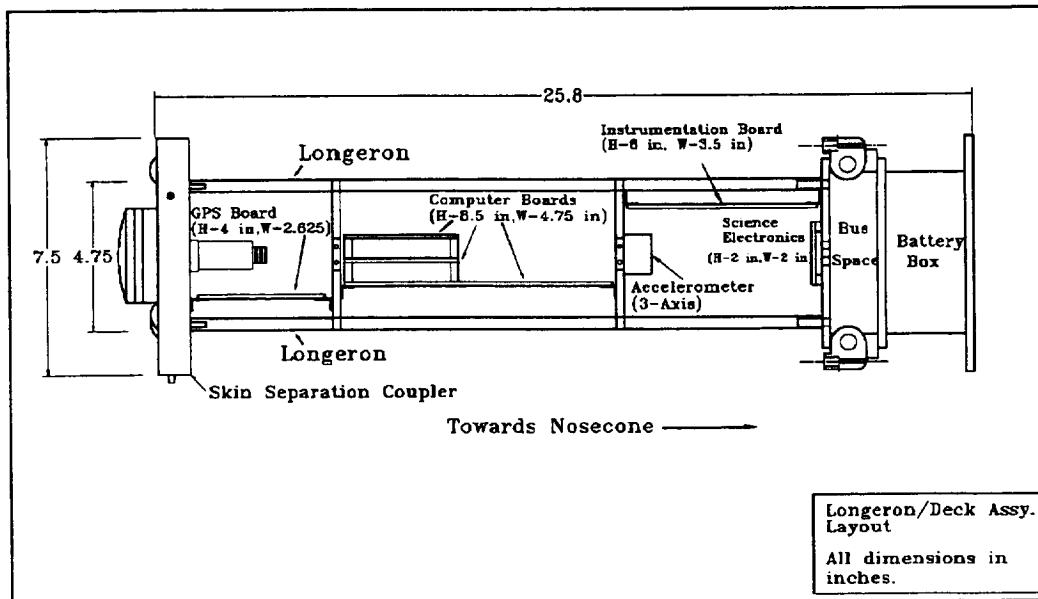


Figure 4-15 : Longeron/deck assembly

4.8.4 Thermosonde Booms and Deployment Mechanism

The thermosondes are mounted at the outboard ends of a pair of booms. When deployed, they will position the sensors one meter apart. The boom hinges are mounted to the bottom of the battery box. This end of the payload is pointed downward, with the booms trailing, upon descent. The booms are held in the retracted position by protective covers (doors), hinged vertically on one side. These covers are retained in the closed position by a length of cord running through the payload (Figure 4-16). Six seconds after the main chute inflates, this cord is cut by a mechanically activated, pencil-type pyrotechnic cutter with an internal timer. The spring-loaded booms then push open the covers and deploy outward into the air stream (Figure 4-17). A detent in each hinge locks the booms in place.

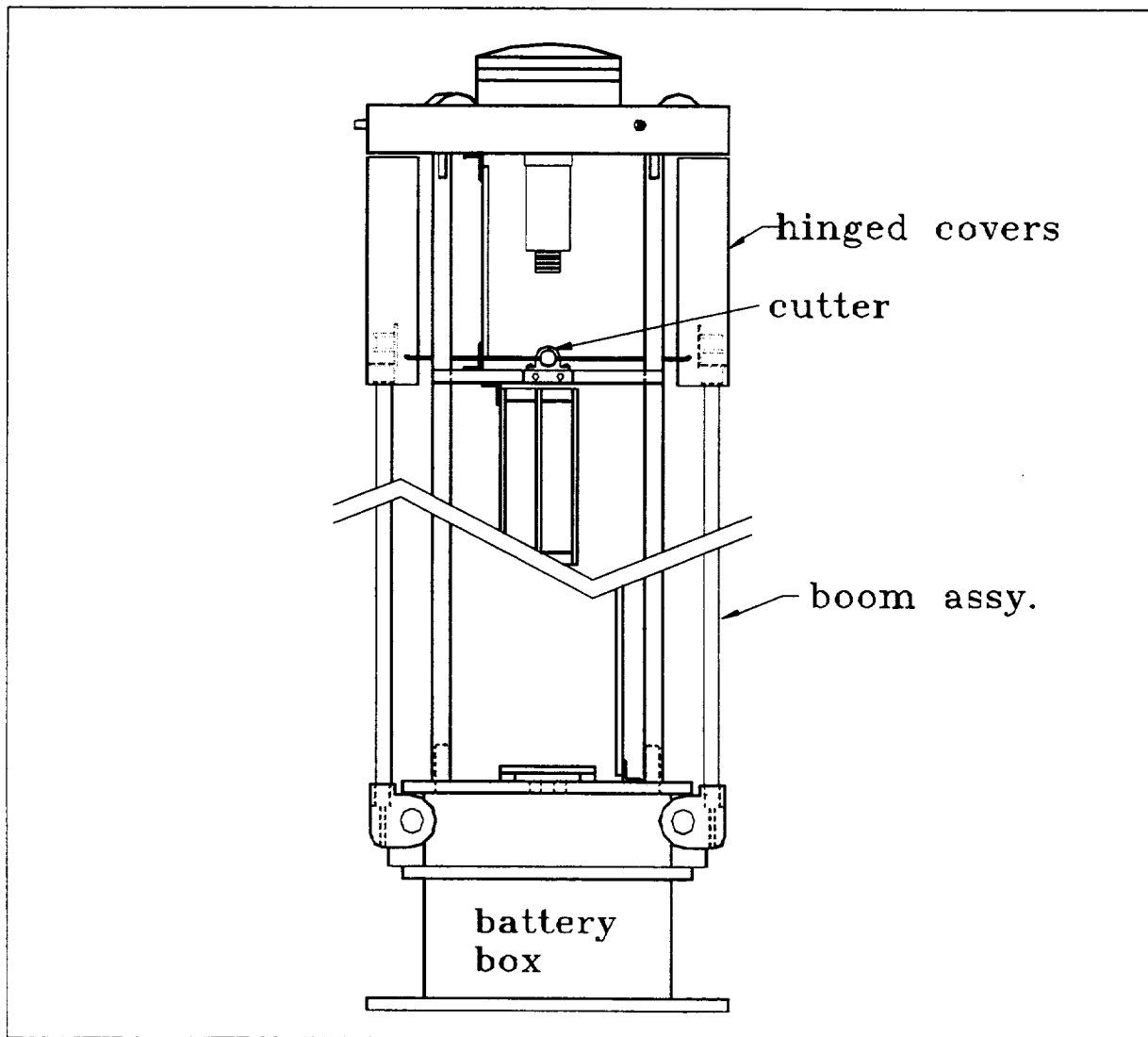


Figure 4-16 : Booms in Retracted Position

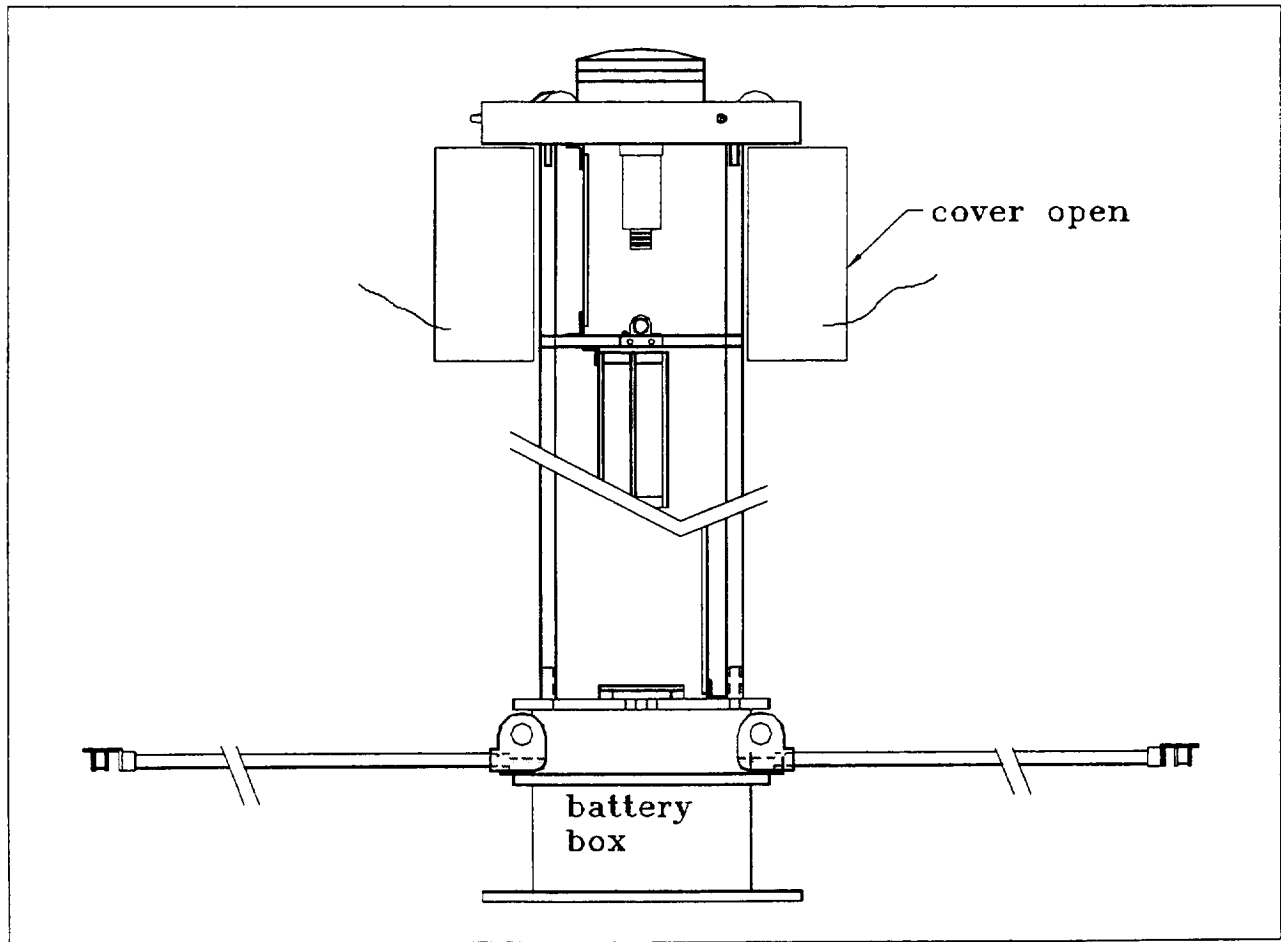


Figure 4-17 : Booms Extended

5. Recovery System

5.1 Objective

The science objective of the ARIM-1 mission dictates a parachute recovery system to provide a stable and slow descent rate of 5 meters per second, for a sounding rocket meteorological payload descending through an altitude of 15 kilometers. So, the engineering and design challenge was to produce a high altitude sounding rocket parachute recovery system; to meet the science objective of the mission, and be able to be packed into the allocated payload recovery system space. The recovery system consists of a 6 feet diameter ribless guide surface drogue chute, and a 33 feet diameter main cross parachute to recover a payload of 31 pounds.

5.2 Design Criteria

To meet the science mission objective, the parachute recovery system must be light in weight, able to be packed into a small volume, and sustain the parachute deployment opening loads. The high altitude parachute recovery system consists of a drogue parachute and a main parachute. The drogue chute must be able to quickly stabilize and decelerate a payload from a flat spin in ballistic free fall during reentry. The drogue chute must also be very stable at high airspeed deployments, for an orderly deployment of the main parachute. The main descent parachute must also be stable and have a high drag coefficient for a slow rate of descent.

To achieve these design criteria, the parachutes must be made of lightweight ripstop nylon fabric, tapes, webbing and cord. By using light weight materials and construction, the largest possible size parachute can be packed into the relatively small space allocated for the recovery system. Materials used for parachute fabrication consists of nylon, dacron and kevlar.

The cross parachute and guide surface drogue chute were chosen as aerodynamic decelerators for the ARIM-1 sounding rocket payload. These parachute types are currently used by NASA in all Black Brant and Orion class sounding rocket payloads. The rationale for these design choices is specified in sections 4.3.4 and 4.3.5, for the drogue and main parachutes.

Determining the appropriate diameter for the parachutes is accomplished by calculating the parachute descent rates based on payload recovery weight. The objective was to achieve a terminal descent rate for the main cross parachute of 5 meters per second descending through 15 kilometers. Terminal descent rate of a parachute is calculated by the following formula.¹

¹ The equation uses air mass density values from the standard atmosphere table (appendix D1), and parachute drag coefficient values (appendix E). In addition, a list of the symbols found in this chapter and their definitions is given in appendix B.

$$V_e = [(C_p) (W) / (C_p) (\rho) (S_o)]^{1/2}$$

Where:

- V_e = Equilibrium velocity (descent rate in ft/sec)
- W = Weight of payload and parachute
- C_p = Parachute drag coefficient
- ρ = Mass density of atmosphere at given altitude (slugs/ft³)
- S_o = Parachute surface area in ft² = ($\pi * DO^2 / 4$)

A point of diminishing return for parachute weight and diameter is reached at 14 km (46,000 feet). The mission objective of a 5 meter per second main parachute descent rate at 15 km (49,000 feet), can be achieved with a 33 feet diameter main cross parachute, for a recovery weight of 31 pounds at 14 km Refer to Figure 5-1 for a plot of the descent rate of the 33 feet diameter main cross parachute as a function of altitude.

5.3 Drogue Parachute Design

The rate of descent of the reentering payload at 86,000 feet, for the drogue parachute at full line stretch is 398 ft/sec, or 271 mph, for a payload weight of 49 lbs., after jettisoning the drogue chute extraction mass (see Table C2 in the appendix). This is the deployment altitude and velocity of the drogue parachute. The equivalent descent rate at sea level is:

$$V_{\infty} = V_e (\rho/\rho_o)^{1/2} = 398.23 \text{ ft/sec } (\sigma)^{1/2} = 65.5 \text{ ft/sec}$$

Where $(\sigma)^{1/2}$ at 86,000 feet is 0.1645 (*See standard atmosphere table in appendix A*); Therefore, the required drag area for the drogue parachute $(CD_s)_p$, can be calculated from the dynamic pressure by:

$$(CD_s)_p = \text{payload weight } (W_p) / \text{dynamic pressure } (q)$$

Where the dynamic pressure is:

$$q = (\rho / 2) v^2 = v^2 / x \quad (\text{Where: } x = v/x = [(\text{ft/sec}) / 841.40])$$

$$q = (65.50)^2 / 841.4 = (4,290.25 / 841.40) = 5.10 \text{ lb./ft}^2$$

The parachute drag area then is:

$$(CD_s)_o = (49 \text{ lb.} / 5.10) = 9.61 \text{ ft}^2 = 1,758.24 \text{ in}^2$$

Using this drag area, the parachute surface area (S_o) is:

$$S_o = (CD_s)_o / CD_o$$

For a circular parachute with a ratio of suspension line length to constructed diameter (l_e / D_o) of at least 1.00, the drag coefficient is 0.34. From this, the parachute area, S_o is:

$$S_o = (CD_s)_p / CD_o$$

$$S_0 = (9.61 \text{ ft}^2 / 0.34)$$

$$S_0 = 28.27 \text{ ft}^2 (4,070.88 \text{ in}^2) = 2.63 \text{ m}^2$$

Descent Rate of 33 Ft. Diameter Main Cross Parachute Versus Altitude

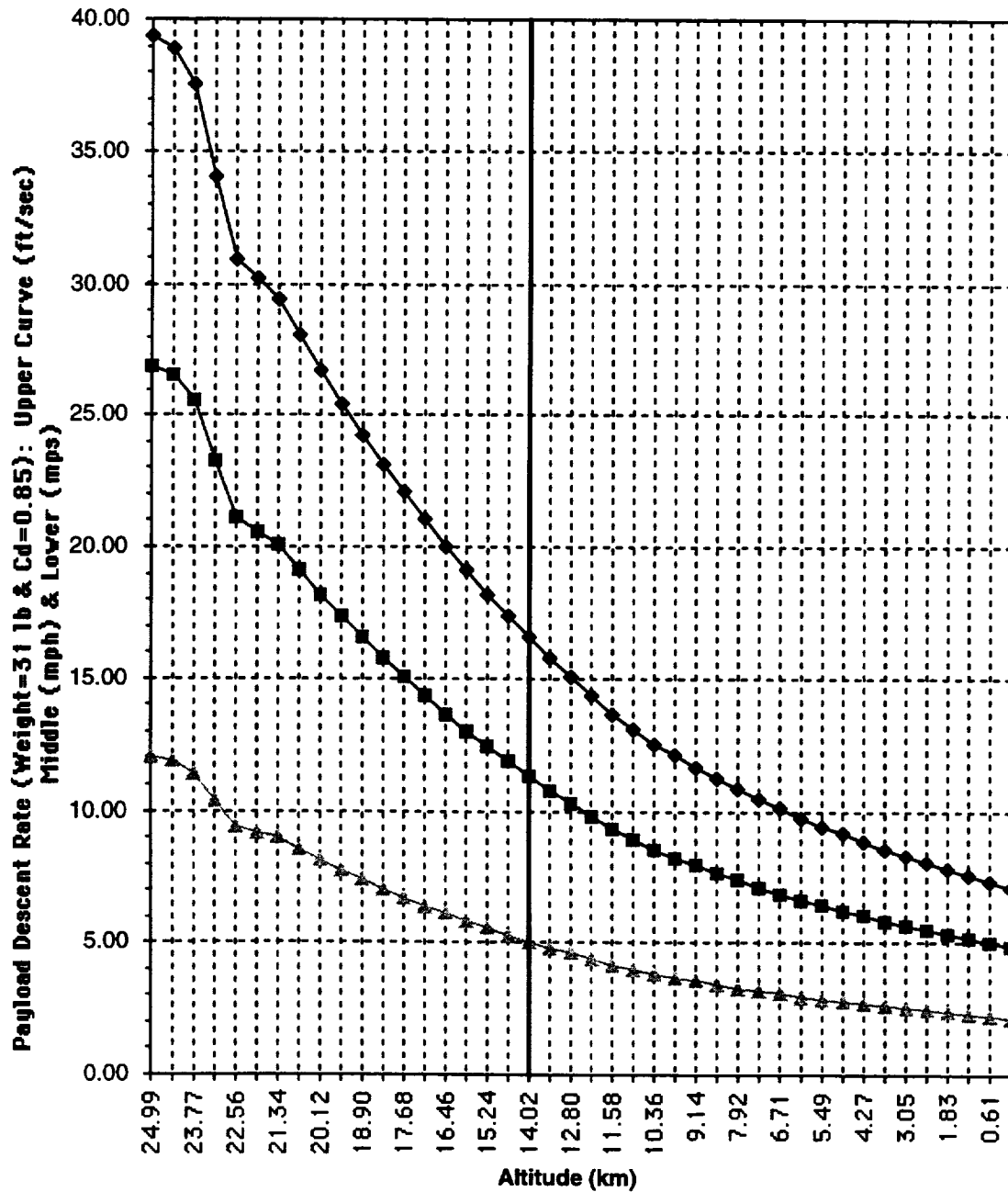


Figure 5-1 : Descent rate of 33 ft. cross chute as a function of altitude. Vertical line shows descent rate of 5 m/sec for payload descending through 14 km (46,000 ft).

And finally, the nominal drogue parachute diameter (D_o) is:

$$D_o = (4 (S_o) / \rho)^{1/2} = 1.1284 (S_o)^{1/2}$$

$$D_o = 1.1284 (28.27)^{1/2}$$

$$D_o = 1.1284 (5.32 \text{ ft}^2)$$

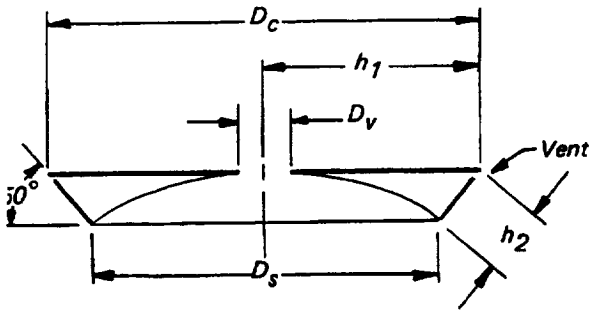
$$D_o = 6.00 \text{ ft. (72.00 in.)} = 1.83 \text{ m}$$

The constructed (manufactured) drogue parachute will be a 6.0 ft. (72.0 in.) diameter ribless guide surface parachute. Normal suspension line ratio for guide surface parachutes is (1.0 to 2.0). A suspension line ratio of at least 1.0 is needed to maintain the drag coefficient value of the canopy. A suspension line ratio of 1.33 (96.0 in. / 8.0 ft.) is chosen to maintain the 0.34 drag coefficient of the parachute.

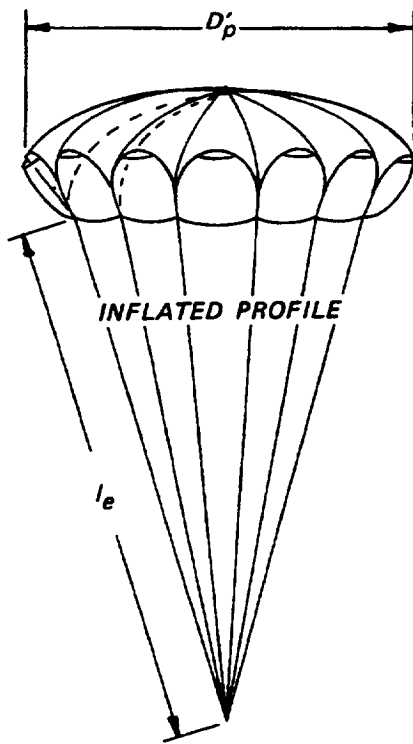
A ribless guide surface drogue parachute is the most stable design for deployment envelopes from low airspeed up to mach 1.5, and is routinely used in suborbital sounding rocket applications by NASA/Wallops Flight Facility at Wallops Island, Virginia, and by the parachute systems division of Sandia National Laboratories in Albuquerque, New Mexico. NASA uses ribless guide surface drogue chutes for recovering payloads of up to 750 pounds in the Black Brant XII series of sounding rockets. This stable drogue chute design produces an angle of oscillation of less than three degrees. Strong restoring forces are produced by uniform flow separation around the oncoming air at the canopy skirt, when displaced from the zero angle of attack position. This condition makes a guide surface drogue chute ideally suited for sounding rocket payload deceleration, stabilization and recovery. Low porosity material is used to obtain fast and uniform canopy inflation. A guide surface drogue chute decelerates and stabilizes a reentry body from a flat spin in ballistic free fall because it opens quickly. This places the payload body to be recovered in a nose down attitude for an orderly linear deployment of the main parachute. The drogue chute function is critical, in that it prepares the main descent parachute for an orderly lines-first deployment. Even the best constructed parachute will not operate reliably if not properly deployed. So, the drogue functions to place the payload to be recovered in the proper position and attitude for an orderly and reliable deployment of the main descent parachute.

This parachute is difficult to construct. The gore pattern dimensions for this particular guide surface drogue chute are obtained from a table of values listed in Figure 5-3. These table values are used to mark and cut the precise and tedious gore patterns for canopy fabrication.

Figure 5-2 shows the general layout and measured dimensions of the constructed guide surface drogue chute. Figure 5-3 shows the gore pattern geometry, and dimension specifications for fabrication. Note, actual drogue chute bottom view showing suspension lines and canopy skirt.



CONSTRUCTION SCHEMATIC



SO	= 28.3 Ft 2 (2.6 m 2)
CD	= 0.34
CX	= 1.4
Osc	= +/- 3 degrees
DC	= 6.0 Ft (1.8 m)
DP	= 5.7 Ft (1.7 m)
DS	= 4.2 Ft (1.3 m)
h1	= 3.0 Ft (0.9 m)
h2	= 1.4 Ft (0.4 m)
DV	= 0.8 Ft (0.2 m)
le	= 8.0 Ft (2.4 m)
NG	= 12
Lines	= 12

Figure 5-2 : Ribless Guide Surface Drogue Parachute Dimensions

Roof Pattern

Panels	12 Gores
X / h_1	Y / X
.10	.394
.15	.394
.20	.394
.30	.407
.40	.410
.50	.416
.60	.428
.70	.441
.80	.492
.832	
.866	
.875	.696
.882	
.888	
.896	
.90	.527
.95	.261
.975	.1625
1.0	0

Guide Surface Pattern

Panels	12 Gores
X / h_2	Y / X
.05	4.33
.10	3.21
.15	2.58
.20	2.13
.30	1.58
.40	1.25
.50	1.03
.60	.86
.70	.722
.80	.61
.885	
.90	.515
.919	
.922	
.93	.491
	.000
.937	
.944	
.95	.472
	.226
.954	
1.0	.430

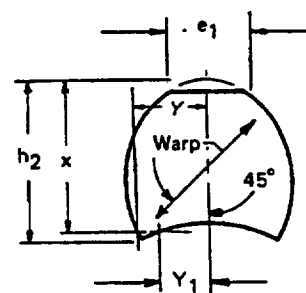
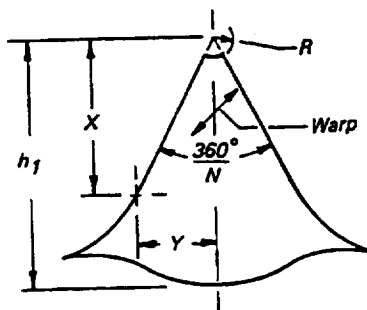


Figure 5-3 : Drogue Chute Gore Dimensions and Patterns

5.4 Main Parachute Design

Rate of descent at the deployment altitude of 82,000 feet (24.99 km) for the main parachute was selected to be 39.36 ft/sec, or 26.84 mph, for a payload recovery weight of 31 pounds (see appendix A). The equivalent descent rate for the main canopy at sea level is:

$$V_{\infty} = V_c (\rho / \rho_0)^{1/2} = 39.36 \text{ ft/sec } (\sigma)^{1/2} = 7.12 \text{ ft/sec}$$

where $(\sigma)^{1/2}$ at 82,000 feet is 0.1810 (see standard atmosphere table in appendix A)

The required drag area for the main parachute $(CD_s)_p$, can be calculated from the dynamic pressure by:

$$(CD_s)_o = \text{payload weight } (W_p) / \text{dynamic pressure } (q)$$

Where the dynamic pressure is given by:

$$q = (\rho / 2) v^2 = v^2 / x \text{ (Where: } x = 841.40 \text{ for [ft/sec] conversion)}$$

$$q = (7.12)^2 / 841.40 = (50.7 / 841.40) = 0.0603 \text{ lb./ft}^2$$

The main parachute drag area is:

$$(CD_s)_o = (31 \text{ lb.} / 0.0603) = 514.10 \text{ ft}^2 = 74,029.85 \text{ in}^2$$

Using this drag area, the parachute surface area, (S_o) is:

$$S_o = (CD_s)_o / CD_o$$

For a cross parachute with a suspension line ratio of $(l_e / D_o) = 1.00$, the drag coefficient (CD_o) is 0.85 for a descent rate of less than 15 ft/sec, and the parachute surface area, (S_o) is:

$$S_o = (CD_s)_p / CD_o$$

$$S_o = (514.10 \text{ ft}^2 / 0.85)$$

$$S_o = 604.8 \text{ ft}^2 \text{ (} 87,094.59 \text{ in}^2 \text{)} = 56.19 \text{ m}^2$$

And finally, the nominal parachute diameter (D_o) is:

$$D_o = (4 (S_o) / \rho)^{1/2} = 1.1284 (S_o)^{1/2}$$

$$D_o = 1.1284 (604.8)^{1/2}$$

$$D_o = 1.1284 (24.59 \text{ ft}^2)$$

$$D_o = 27.75 \text{ ft (333.00 in)} = 8.46 \text{ m}$$

The constructed (manufactured) main parachute will be based on a 28 feet (336 inch) diameter circular parachute. The actual cross parachute diameter will be 33 feet in diameter, but have the same surface area as the 28 feet diameter flat circular parachute. The area of the cross parachute will be calculated, to determine appropriate constructed diameter, and the arm width. Drag, stability, and opening force are effected by ratio of the arm width to length for a cross parachute. A lower ratio (thinner arm) provides better stability and lower opening forces, as more air is channeled through the parachute due to its greater geometric porosity. However, the

canopy surface area will be smaller with a corresponding higher descent rate for the cross parachute. A higher canopy arm ratio (wider arm) produces higher parachute opening loads and slightly less stability, but the increased surface area provides a more desirable lower descent rate. The width-to-length ratio for the arm of a cross parachute (W/L) ranges from 0.264 to 0.333. Because the maximum parachute descent rate is desired, an arm-to-width ratio for the arms of the cross parachute was chosen to be 0.333.

Cross parachute surface area can also be determined from the formula for this parachute.

$$S_{o1} = 2D_c (eS) - e_s^2$$

$$S_{o1} = [2(33 \text{ ft}) (11 \text{ ft})] - (11 \text{ ft})^2$$

$$S_{o1} = (66 \text{ ft}) (11 \text{ ft}) - 121 \text{ ft}^2$$

$$S_{o1} = 726 \text{ ft}^2 - 121 \text{ ft}^2$$

$$S_{o1} = 605 \text{ ft}^2$$

$$S_{o2} = 2D_c (e_s) - e_s^2$$

$$S_{o2} = [2(33 \text{ ft}) (8.7 \text{ ft})] - (8.7 \text{ ft})^2$$

$$S_{o2} = (66 \text{ ft}) (8.7 \text{ ft}) - 76 \text{ ft}^2$$

$$S_{o2} = 575 \text{ ft}^2 - 76 \text{ ft}^2$$

$$S_{o2} = 499 \text{ ft}^2$$

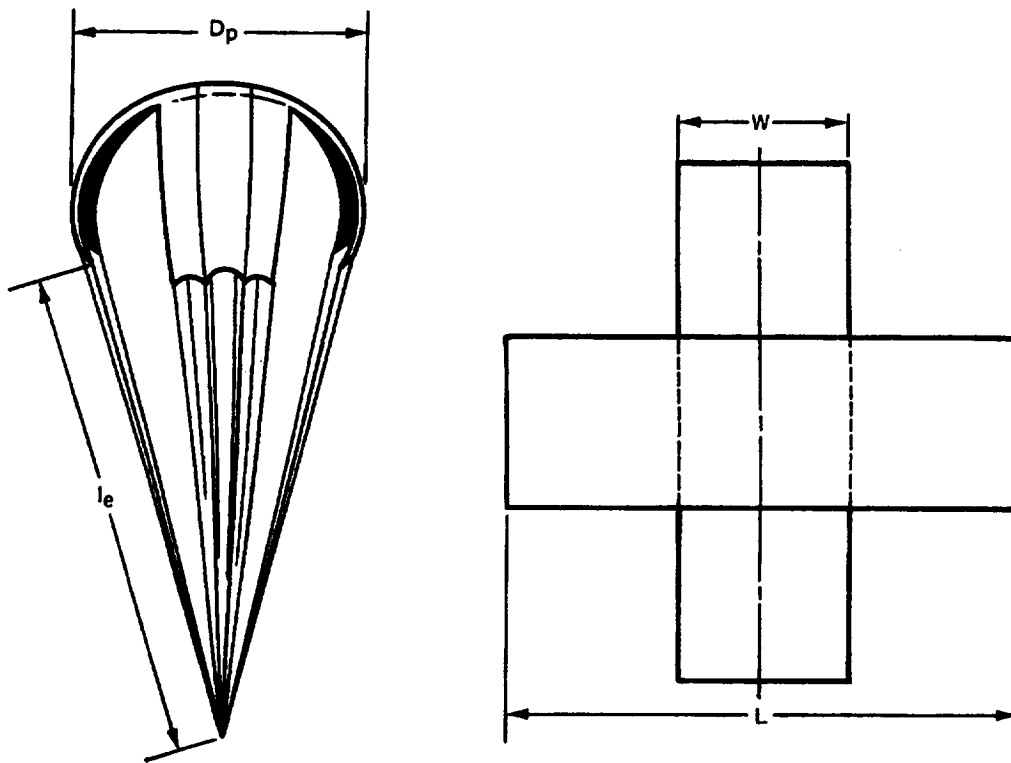
Difference in canopy surface areas based on the arm width to length ratios, is:

$$S_{o1} - S_{o2} = 605 \text{ ft}^2 - 499 \text{ ft}^2 = 106 \text{ ft}^2$$

An arm-to-width ratio of (0.264) results in a canopy surface area of 499 ft², compared to 605 ft² for an arm-to-width ratio of 0.333. The canopy surface area difference of 106 ft² increases the canopy descent rate by ten percent. The higher arm-to-width ratio is chosen to achieve a lower parachute descent rate based on the increased canopy surface area.

Normal suspension line ratio range for cross parachutes is (1.0 to 2.0). A suspension line ratio of at least 1.0 is needed to maintain the drag coefficient value of the canopy. A suspension line ratio of (1.0) is chosen, for a canopy suspension line length of 33 feet, to keep parachute weight and bulk to a minimum. This ensures the minimum payload recovery weight of 31 pounds can be achieved, for the desired parachute descent rate. Minimum parachute bulk also allows easier packing of the parachutes with less bulk and displacement.

The cross parachute design was chosen due to its high drag coefficient range of 0.60 to 0.85 (see appendix A), ease of construction, low cost, and stability. For cross parachutes with low canopy loading at low descent rates, the drag coefficient is 0.85. Also, the cross parachute is currently used by the NASA/Wallops Flight facility for all Black Brant XII and Orion class suborbital sounding rockets. The objective is to keep the design and fabrication of the final descent parachute as simple as possible, yet retain a high drag coefficient and slow rate of descent.



S_o	$= 604.8 \text{ Ft}^2 (56.2 \text{ m}^2)$	e_s	$= (e_s/D_c) = (0.263 \text{ to } 0.333)$
CD	$= 0.60 \text{ to } 0.85$	l_e	$= 33.0 \text{ Ft. } (10.1 \text{ m})$
C_x	$= 1.1 \text{ to } 1.2$	L	$= 33.0 \text{ Ft. } (10.1 \text{ m})$
Osc	$= +/- 3 \text{ degrees}$	W	$= 11.0 \text{ Ft. } (3.4 \text{ m})$
D_c/D_o	$= 1.15 \text{ to } 1.19$	N_G	$= 24$
D_p/D_o	$= 0.66 \text{ to } 0.72$	Lines	$= 24$
D_p	$= 23.1 \text{ Ft. } (7.0 \text{ m})$		

Figure 5-4 : Main Cross Parachute Dimensions

These preliminary calculations verify that the drogue and main parachute will provide the required descent rates for the payload recovery weight of approximately 31 pounds. The values of dynamic pressure, drag area, surface area and diameter of the drogue and main parachutes are for standard day conditions at sea level. These values are basic guidelines for design criteria and performance parameters. Actual descent rates will be higher or lower, depending on the atmospheric variables of air pressure and temperature. This basically means, that the parachute descent rates will be lower during cold winter weather, and of course higher during hot summer weather.

This preliminary information is then used to design parachute gore dimensions, and fabricating a template. This template is used to cut out the gores from parachute nylon for canopy construction. These fabric gores are then sewn together, to fabricate the drogue and main parachute canopies. Refer to Figure 5-4 for general layout and dimensions of the main cross parachute and canopy gores.

5.5 *Locator Devices*

The radio beacon mounted on the main parachute, used to physically locate and retrieve the recovered payload after touch down. Without such an active location device, the recovered payload would not be able to be physically located and retrieved from its impact site. Other passive measures used to aid location of the recovered payload included brightly colored parachute fabric which can be easily spotted from the air by search aircraft. The ARIM series of main descent parachutes will be constructed of either international orange, or red ballistic parachute nylon.

5.5.1 *Radio Beacon*

A Telonics radio beacon will be used as a direction finding device for post flight payload location and retrieval. This small and light weight transmitter is currently used by the Department of Fish and Game in Alaska to track wildlife. These transmitters are also currently used by NASA as radio beacons on suborbital sounding rocket flights. The Telonics transmitter weighs 4 ounces, and uses two small 1/2 AA size Tadiran lithium batteries as a power source. This beacon can operate for up to a year on a set of lithium batteries at temperatures well below 0° F. The beacon was tested for a period of two weeks at 0° F in a refrigerator on the parachute recovery system for the second sounding rocket project (SRP-2) at the University of Alaska Fairbanks. After two weeks, the beacon continued to put out a strong signal, and the smaller size batteries were deemed as flight-worthy hardware. The Telonics radio beacon is also cold tested by NASA/Wallops Sounding Rocket Flight Facility to -40° F. This is necessary, as many Black Brant XII and Orion sounding rockets launched from Poker Flat Research Range in Alaska are done so at temperatures around -40° F. So, these lithium batteries function well in the subzero temperatures of Alaska.

This radio beacon was adopted for the second student rocket project (SRP-2) parachute recovery system at the University of Alaska Fairbanks. Since this is an already proven design used by NASA, it has been adopted for use on the ARIM-1 parachute recovery system. This beacon transmits a pulsed tone on a frequency of 146.x megahertz (MHz). The radio beacon is activated by main parachute deployment. A magnetic pull-plug switch activates the beacon. When the parachute comes to full line stretch the radio beacon sends out a pulsed carrier signal which can be acquired by a hand held receiver on the ground, or from an aircraft carrying this receiver.



Figure 5-5 : Telonics Radio Beacon On Main Parachute Bridle.



Figure 5-6 :Radio beacon batteries tacked into pocket on kevlar main chute bridle with cable connected to radio beacon.

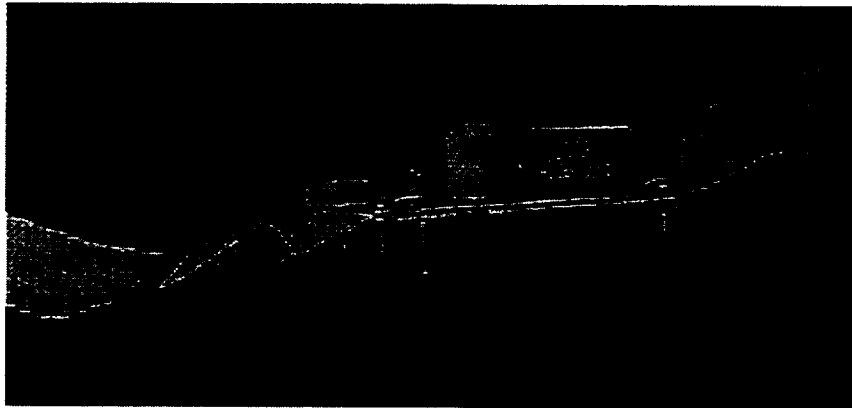


Figure 5-7 : Side view of radio beacon and magnetic pull-plug switch. Note connector plug and wire going to lithium batteries located in the 1 inch wide 3,000 pound kevlar bridle.

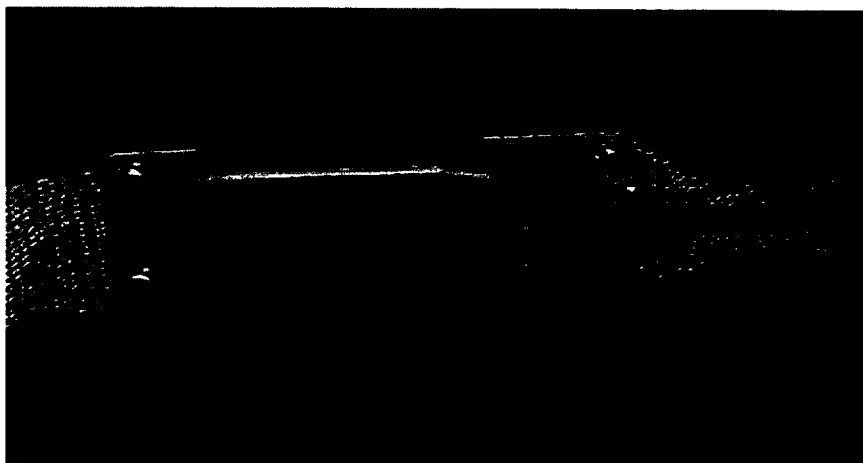


Figure 5-8 : Close up view of radio beacon top showing connector plug and wire going to lithium batteries. Note metal mounting bracket and metal screws.

5.5.2 Transponder

Radar transponders are frequently flown on a sounding rocket. When the main parachute deployment is above 20,000 feet MSL (mean sea level). This is an FAA requirement for air traffic control at Poker Flat Research Range. The transponder emits a coded reply when interrogated by the air traffic controller radar. A main parachute descending at high altitude is a foreign object hazard to jets flying beneath the descending payload and the possibility exists for a parachute to be ingested into a jet aircraft engine

Normally, a transponder is also a range safety requirement in addition to a requirement by the Federal Aviation Administration (FAA) for sounding rocket parachutes deployed at high altitudes. Upon checking with Poker Flat Research Range where the ARIM-1 rocket will be launched, it has been tentatively verified that a transponder will not be required on this payload due to the small rocket size. Also, the decision not to fly a transponder helps to reduce the payload recovery weight, thereby helping to achieve the desired terminal descent rate of the main parachute to support the science mission objectives. However, the decision not to fly a transponder requires coordination with Poker Flat to obtain the necessary altitude waiver from the FAA.

5.6 Parachute Recovery System

This section provides a general overview of the design, construction, and deployment sequence of the parachute recovery system for the ARIM-1 series of sounding rocket payloads. A generic deployment system overview is provided in Figure 5-9 as a model. Then, the actual mechanical hardware components of the recovery system in relation to their function are described. The procedure for packing the parachutes, rigging the pyrotechnic initiating devices, and integrating the system into the rocket payload are addressed, to show how all of the pieces fit together to make a complete parachute recovery system.

The recovery system for this sounding rocket payload is a two-stage, lines-first parachute recovery system. This system consists of a drogue chute and a main parachute packed in deployment bags. The main parachute is packed in a 4-leave banana peel bag, which is laced up with eviscerated 375 pound nylon cord. The drogue chute bag is packed in a stuff bag. Both deployment bags are lined with Teflon material to eliminate friction between the parachute and deployment bag. Each bag has brass grommets on each side of the bag leaves to facilitate lacing up the deployment bags. Parachutes are packed by hand in small diameter banana peel bags, attain pack densities of 24 pounds per square foot. This high pack density provides maximum mass compaction of the recovery system into the limited space of a sounding rocket payload. This high packing density also ensures there will be no shifting of components of the recovery system during the high positive and negative g forces during and immediately after rocket motor burn.

The challenge of a recovery system is to be able to pack a very large diameter main descent parachute into a small 8 inch diameter payload. Total recovery system weight had to be low, yet constructed of light weight materials, able to withstand and sustain

high parachute snatch forces and opening loads. The idea is to be able to deploy the parachutes without using skirt reefing, as this adds another level of complexity. This process entails using aerodynamic deceleration of the payload in ballistic free fall to slow it down before deploying the drogue chute. The deployed drogue chute acts to further slow and stabilize the payload to a low enough velocity, for the main parachute to sustain the opening forces, without being damaged or using skirt reefing.

The diagram in Figure 5-9 shows a generic model for the deployment of a parachute recovery system from a rocket payload. Figure 5-10 shows a generic banana peel bag used to pack parachutes for sounding rocket recovery systems. These deployment bags are key components for successfully deploying parachutes from high altitude reentering sounding rocket payloads.

The parachute deployment system components are then integrated into the packed parachute recovery system, and installed into the sounding rocket payload (see Figure 5-17 and Figure 5-18). To gain a final understanding of how this all works, the parachute recovery system deployment sequence is presented graphically in Figure 5-9.

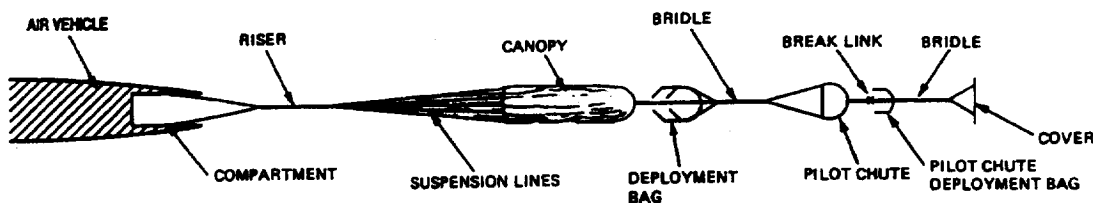


Figure 5-9 : General overview and components of a generic parachute deployment system for recovering sounding rocket payloads.

Depicted above is the generic deployment scheme for a sounding rocket parachute recovery system. The air vehicle in this case is the rocket payload, and is often referred to as the forebody. Note that a multiple leg bridial is attached to the main parachute riser. This attachment method provides enhanced stability for the decelerating payload to be recovered during deployment of the recovery system. The suspended payload provides a more stable platform while descending under the main parachute. This is especially important for the ARIM-1 payload, as a steady platform will provide better quality science data collection during the main parachute descent to touch down.

Note that the main parachute is attached to the main chute deployment bag with a break cord. The main chute is also attached to the drogue chute by way of a bridial line. The drogue chute is attached to its deployment bag with a break line. Finally the drogue chute deployment bag is attached to the drogue chute extraction plate or plates by way of a multi-leg bridial. Refer to Figure 5-9 above for how the components of the recovery system are connected to each other. The sequence of events for deployment of the ARIM-1 parachute recovery system are presented at the end of this section along with a graphic overview of these events.

When the recovery system is initiated by expulsion of the parachute canister extraction plate, its drag withdraws the drogue chute deployment bag from the parachute canister. The drag force opens the deployment bag, breaking the break line, allowing the drogue

chute to inflate. This increased drag area serves to decelerate the payload mass before deploying the main parachute. At reduced velocity, the main parachute will open with a more desirable reduced opening load. The drogue chute drag then extracts the main parachute from its deployment bag, breaking the break line, allowing the main chute to inflate. All components of the recovery system are stripped away at deployment, in the process of deploying the main parachute. The purpose of a parachute recovery system is to provide an orderly process for parachute deployment. This orderly process puts the parachutes in the proper attitude for successful and reliable deployment. This process is the critical to successfully recovering a sounding rocket payload with parachutes.

5.6.1 Parachute Deployment Bags

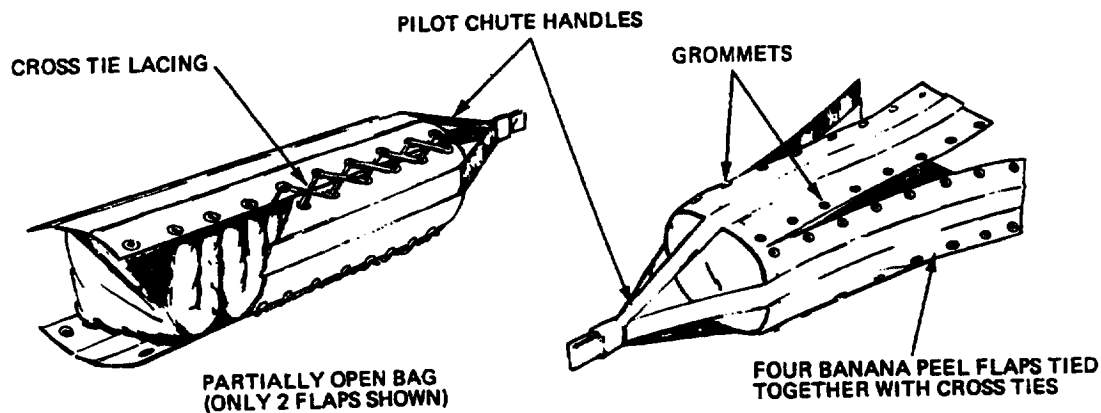


Figure 5-10 : 4-leave banana peel bag used to pack sounding rocket parachute.
Bags are laced up with nylon cord through brass grommets.

Parachutes are deployed using deployment bags. For sounding rockets, parachutes are deployed from "banana-peel" bags as depicted in Figure 5-10 above. The deployment bags can be made of two or four leaves. Each leave of the deployment bag has brass grommets along each side. These grommets are used for lacing nylon cord. Lacing up the deployment bag is part of the parachute packing process. Packing the parachutes into their deployment bags, with all associated hardware to initiate and deploy the parachutes from their deployment bags, is what constitutes a sounding rocket parachute recovery system.

A multi-leg bridle at the top of the deployment bag allows it to be attached to the drogue chute bridle for the main parachute, and to the drogue chute extraction plate for the drogue chute. These bridles are constructed of kevlar, because of its light weight and high strength. Kevlar is also resistant to abrasion and has good heat resistant characteristics. Kevlar is also employed in construction of small deployment bags for drogue chutes which deploy at high speeds and high altitudes, where aerodynamic heating is a factor. Otherwise, drogue chute deployment bags are constructed of nylon duct material used for constructing parachute containers used in the sport parachuting industry.

Main parachute deployment bags are constructed of lengths of horizontal nylon webbing sewn to an underlying piece of nylon pack cloth. This allows for a stiff container to form the packed parachute into the desired cylindrical packed dimensions. Deployment bags are lined with Teflon cloth. Teflon provides a low friction interface between the packed parachute fabric and the deployment bag. Otherwise, the parachutes could experience friction burns and fabric melting as the parachute extracts from the bag, due to friction from high speed extraction during deployment.

5.6.2 Parachute Cut Knives

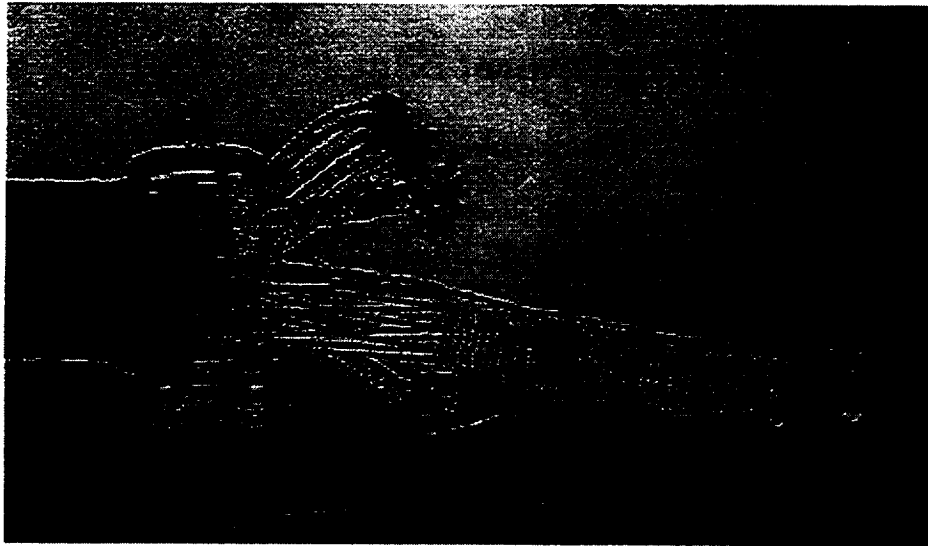


Figure 5-11 : Cut knife attached to main parachute speed link (connector link) on the bridle. Parachute bag lacing is threaded through cut knives. When main chute deploys, tension causes cut knives to cut bag lacing, allowing parachute to extract and deploy.

The parachute cut knife initiates deployment of the parachute from the deployment bag. When the drogue chute extraction plates are blown from the parachute canister, this tension pulls on the cut knives, which cut the bag lacing to de-lace the drogue chute bag, allowing it to be extracted and deployed. When the main parachute is staged, drogue chute drag pulls on the cut knives, which de-lace the main bag, allowing it to be extracted and deployed. Notice how the cut knives are attached to the riser speed link on the main chute as in Figure 5-11 above. For the drogue chute, the cut knives are attached to the drogue chute bridle. These cut knives take about 16 pounds of force to cut through the eviscerated 375 pound nylon cord used to lace up the parachute deployment bags.

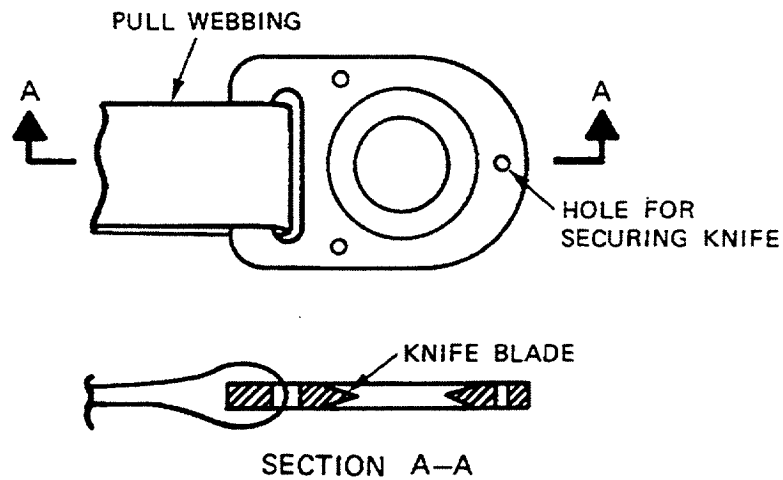


Figure 5-12 : Cut knife diagram showing top and side views. Three holes in cut knife are for tacking cut knife in place on deployment bags.

5.6.3 Pyrotechnic Thrusters

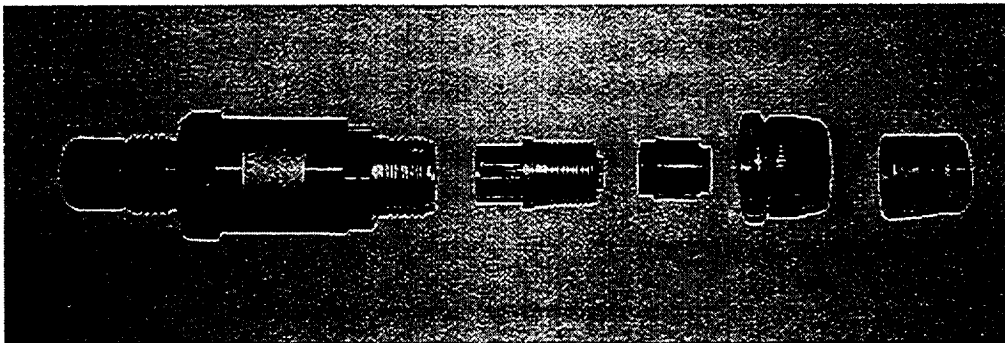


Figure 5-13 : Photograph of Halex 2900-1 thruster (linear actuator) used for separating payload from expended rocket motor, and to break shear pins on aft end of parachute canister extraction plates to deploy drogue chute.

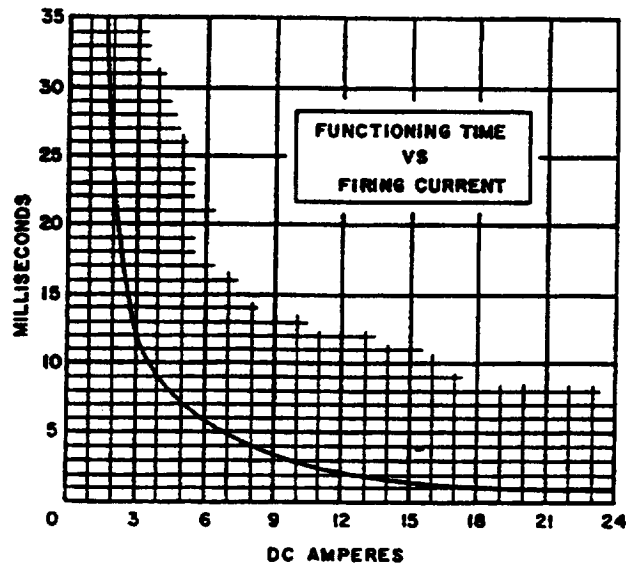
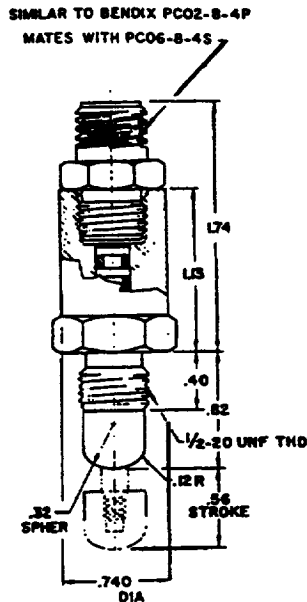


Figure 5-14 : Diagram and dimensions of Hox 2900-1 thruster. Metal sphere strokes a distance of 1/2 inch with a force of 225 pounds against drogue chute extraction plate to break shear pins on aft end of parachute canister and extract drogue chute. See figure on left.

Figure 5-15 : Electrical firing curve plot of Hox thruster. See figure on right.

5.6.4 Pencil Cutters

Technical Ordnance (Pencil Cutters)

Part No. 215810 = 3,000 lb. Cutter	Part No. 215813 = 750 lb. Cutter
Time Delay = 10 sec.	Time Delay = 6 sec.
Weight = 1.5 oz.	Weight = 1.0 oz.
Length = 4.14 in.	Length = 3.82 in.
(To Stage Main Chute Deployment)	(To Deploy Payload Booms)

Depicted above are the details of the pencil cutters used in the parachute recovery system. Note, the cutter mounting bracket and pull pin ring in Figure 5-16. Also, note the details of the pull pin ring, pull cord attached to the ring, and the nylon staging bridal passing through the hole at the head of the cutter. The cutter is tacked in place to the nylon staging bridal attaching the main parachute to the anchor bolt of the payload. The pull cord is attached to the drogue chute bag. Deployment of the drogue chute pulls the pin on the cutter to start the 10 second time delay. The drogue chute flies for 10 seconds allowing its drag to further decelerate the payload. At 10 seconds, the cutter fires, severing the parachute nylon staging bridal. This releases the main parachute, and drogue chute drag extracts the main parachute from the banana peel bag for deployment. The main parachute then inflates at a lower velocity, with a much

lower opening load and shock to the payload. The pencil cutter are used to control the opening loads on the parachutes, so they can be constructed of lighter weight materials, for slower descent rates.



Figure 5-16 : Technical Ordnance 3,000 lb. Pencil cutter. Note main parachute staging bridle through cutter hole on left, and pull pin on right side of cutter

5.6.5 Packed Parachutes

Depicted in Figure 5-17, is a packed 33 feet diameter cross parachute system with a 4 feet diameter ribless guide surface drogue chute. The photograph was taken at the recovery section of the NASA/Wallops Sounding Rocket Flight Facility at Wallops Island, Virginia. This is the current parachute recovery system used by NASA in all its sounding rockets. The ARIM-1 sounding rocket parachute recovery system will look very similar to this, but be 4 inches smaller in diameter, and two and a half times as long.

Total weight of the parachute recovery system will be 18 pounds. Breakdown of this weight includes both parachutes, deployment bags, pyrotechnics, the radio beacon, batteries, the drogue chute extraction lids, and fiberglass parachute canister tube liner.

The packed parachutes will occupy a volume of 1,192 cubic inches (0.69 cubic feet). The length of the packed parachutes will be 26.5 inches for the main parachute, and 2.5 inches for the drogue parachute. The diameter of these packed parachute bags are 7.2 inches. A split fiberglass tube consisting of two staves, will fill the remaining space of the 7.5 inch diameter of the payload tube. See Figure 5-18 for dimensions and details of the packed parachute recovery system, rigged with pyrotechnic initiation devices, and integrated into the rocket payload. And finally, see Figure 5-19 for a graphic depiction of the recovery system deployment sequence.

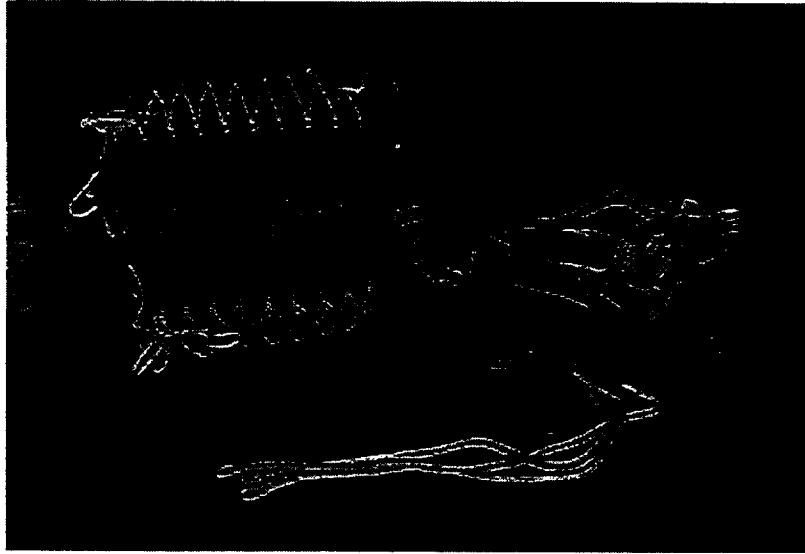


Figure 5-17 : Packed main and drogue parachutes. Note how main bag is laced with nylon cord. Note loose kevlar cords in foreground that connect to drogue chute extraction plate. Also, note nylon cord threaded through cut knife on set of upper laces on main parachute deployment bag. Bag has two cut knives.

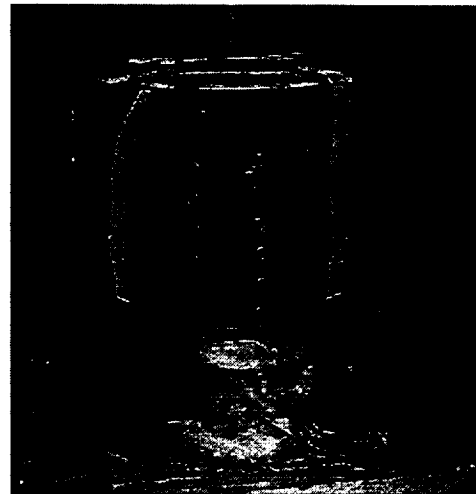
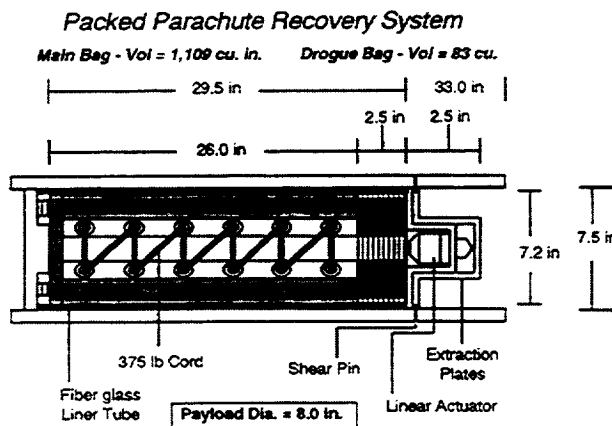


Figure 5-18 : Packed parachute recovery system dimensions (left). Packed 33 ft cross parachute and guide surface drogue chute packed for installation in NASA Black Brant XII sounding rocket (right).

5.7 Recovery System Deployment Sequence

An overview of the deployment system scheme, components, and initiation hardware has been presented. The final portion of this section provides a description of the parachute recovery system deployment. For a graphical depiction of this process, refer to Figure 5-19, and the recovery system flight profile in Figure 5-20.

Initiation of the parachute recovery system begins at an apogee of approximately 127,000 feet, where the rocket motor is separated from the payload by a pyrotechnic charge (EED). This event is triggered by an electronic timer. The pyrotechnic thruster fires to release the V-band clamp which connects the payload to the rocket motor. A spring loaded plate attached to the expended rocket motor pushes against the payload to assure positive separation.

The payload will then flat spin in ballistic free fall, for maximum aerodynamic deceleration prior to deploying the parachute recovery system. The payload center of gravity is located according to the 45 to 55 percent rule developed and used by Sandia National Laboratories in all of their sounding rocket payloads. This design rule places the payload center of gravity at a distance of 45 to 55 percent of payload, as measured from the nose cone tip. This places the center of gravity within one caliper (body tube diameter) of the payload center of pressure. When the center of gravity is one caliper or less from the center of pressure, the payload is statically unstable. Such static instability ensures the payload will flat spin or tumble in ballistic free fall during reentry. This is a desirable condition, to obtain maximum aerodynamic drag and deceleration of the payload during free fall, prior to deploying the parachute recovery system. If the payload reenters in a nose down attitude during reentry, the velocity would be excessive, and the drogue chute would strip from the payload at deployment. It is critical to successful recovery that the payload reenter in a horizontal flat spin attitude for the maximum passive aerodynamic deceleration of the payload during reentry.

It will be necessary to add steel shot ballast to the payload to obtain the desired static instability. The correct center of gravity and center of pressure relationship is obtained by statically balancing the payload with all components installed. The payload is suspended by cord to determine the balance point. This balance point is marked on the payload tube, as is the center of pressure point. The 45 and 55 percent distance points from the payload nose cone are also marked on the tube. Then, weight is suspended from the payload tube nose or tail until the center of gravity is moved the desired distance, to obtain the correct static instability. This lead shot ballast is then secured in place within the payload tube or nose cone. This ensures the completely assembled payload tube, will fly with the same weight as will be flown on the rocket should be balance.

The payload tube should be statically balanced with a slightly nose down attitude, to avoid aerodynamic heating of the extraction plate on the aft end of the parachute canister. The extraction plate and bridal lines connected to the extraction plates will be coated with rubber silicone (RTV), as an ablative material, which can be burned off

during reentry. This technique is employed by NASA in its sounding rocket parachute recovery systems.

At approximately 86,000 feet descending, the drogue parachute will be extracted by a pyrotechnic device triggered by an electronic timer. This thruster (linear actuator) will fire to shear aluminum pins holding the extraction plate to the aft end of the payload. 1/16 inch diameter aircraft quality aluminum TIG welding rod is used for the parachute canister shear pins. The shear strength of these aluminum rods is approximately 29 pounds. Three of these shear pins are used to secure the drogue chute extraction plate to the aft end of the parachute canister until deployment of the recovery system. The thruster that initiates the recovery system thrusts against the drogue chute extraction plate to break these shear pins, and still has approximately 110 pounds left to extract and deploy the drogue chute from its deployment bag. It is important to ensure the g-forces produced by the flat spinning, or tumbling, payload won't exceed the strength of the shear pins. If this should occur, the recovery system would deploy prematurely.

Initiation of the recovery system will extract and deploy the 6 feet diameter ribless guide surface drogue chute to stabilize and decelerate the payload in a nose down attitude. This places the payload in the proper attitude for main parachute deployment. Drogue chute deployment pulls the pull pins on the pencil cutters as the drogue chute bag strips away. The drogue chute inflates and is staged for 10 seconds by two 3,000 pound Technical Ordnance reefing cutters (pencil-cutters). At the end of the 10-second time delay at approximately 83,000 feet descending, the reefing cutters will fire to sever the main parachute staging bridle. Drogue chute extraction force will then extract and deploy the 33 feet diameter main cross parachute.

As the main parachute deploys, it pulls out the two fiberglass staves inside the parachute canister. These are discarded as shown in Figure 5-19. Deployment of the main parachute also releases the outer payload tube and nose cone to reduce payload recovery weight in order to be able to achieve desired parachute descent rate.

Main parachute deployment also pulls the pull pin on a 750 pound Technical Ordnance pencil cutter with a 6 second time delay. At the end of 6 seconds, the pencil cutter fires to sever a small wire cable restraining the temperature sensing booms in their stowed and retracted position. When this is cut, the spring loaded booms gradually extend to the forward deployed position against the oncoming relative airstrip. This allows for gradual boom deployment into the extended position, where they lock into place against stop détentes.

This allows the main parachute to be stabilized and fully inflated at the target altitude of 82,000 feet. The recovery system is able to decelerate the payload from 12 meters per second at the deployment altitude of 82,000 feet, (25 kilometers), to 5 meters per second at 14 kilometers descending in support of the payload science mission objectives. Impact velocity of the payload will be approximately 5 miles per hour (2 meters per second). For an overview of the sequence of events for deploying the parachute recovery system, refer to the flight profile diagram in Figure 5-20. In this figure, note the time, weight, and altitude associated with each event of the deployment sequence of the parachute recovery system.

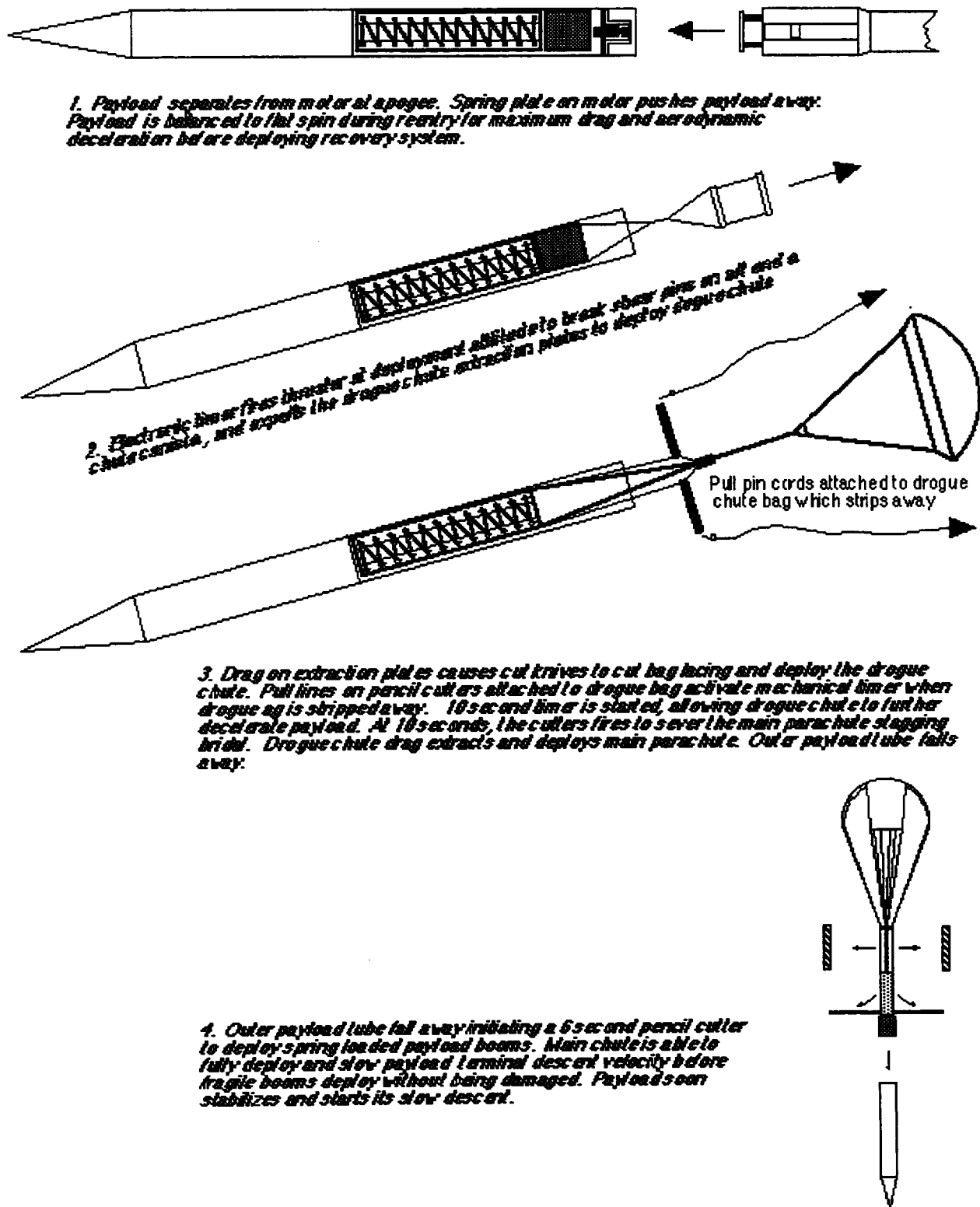


Figure 5-19 : Deployment sequence of ARIM-1 parachute recovery system. Payload separates from expended motor at apogee for reentry. Payload is ballasted to flat spin in ballistic free fall for maximum drag and deceleration before deploying recovery system. At main cross chute deployment, fiberglass staves and outer payload tube fall away to achieve recovery weight of 31 lbs. for desired descent rate.

5.8 Recovery System Performance

The parachute recovery system time line of events and performance parameters for the mission flight profile are graphically depicted in Figure 5-20. The Viper V rocket motor will propel the launch vehicle and payload to an apogee of approximately 128,000 feet at 83 seconds after lift off. This flight profile and time line is based on flying the mission with the Viper V rocket motor. However, the actual ARIM-1 sounding rocket missions will be flown with government surplus Thiokol Cajun and Apache motors, obtained from Sandia National Laboratories in Albuquerque, New Mexico. This means all the parachute recovery system performance parameters presented here will change, and must be recalculated for the new launch vehicle performance geometry.

Reentry mass of the payload at apogee will be approximately 52 pounds. At drogue chute deployment, the payload mass will be 49 pounds. At main parachute deployment, the payload recovery mass will be down to 31 pounds. The reentering payload has an approximate surface area of 5 square feet with a drag coefficient of 0.83 for a reentering body in a horizontal flat spin. The amount of ballast to statically balance the payload cannot be determined at this point, and is deferred until the hardware fabrication phase of the project. This extra weight will increase the payload reentry weight and velocity. These increased parameters will decrease the payload free fall time during reentry, while increasing the opening loads on the drogue and main parachute.

The parachute recovery system operation will commence at apogee at 83 seconds after lift off at an approximate altitude of 128,000 feet. Here the first pyrotechnic thruster will be activated by a mechanical timer to fire, releasing the v-band clamp securing the payload to the expended rocket motor. The payload will separate from the motor and begin the reentry phase of the flight profile. The static instability of the payload will cause it to enter a horizontal flat spin, or tumbling attitude in ballistic free fall for maximum drag and aerodynamic deceleration during reentry, prior to deployment of the recovery system. This attitude will slow the reentering payload from a velocity of Mach 1.6 (1,360 ft/sec / 1,112 mph) to Mach 0.6 (623 ft/sec / 424 mph - see appendix A) at 86,000 feet where recovery system initiation begins.

Dynamic pressure on the drogue chute will be 12.5 lb/ft² (psf) at the deployment altitude of 85,000 feet at Mach 0.6. The drogue chute will open in 0.1 second, while falling a distance of 63 feet. Velocity decay for the drogue chute during inflation is 5.4 ft/sec (3.7 mph for a change in velocity from 622.5 ft/sec to 617.1 ft/sec), while exerting an extraction force of approximately 120 pounds. Drogue chute deployment will activate the two 10-second delay pencil cutters on the main parachute staging bridal. The drogue chute will inflate to stabilize and decelerate the payload from its horizontal flat spin attitude, while placing it in a nose down attitude in preparation for main parachute deployment. At the end of the 10 second time delay, the pencil cutters will fire, severing the main parachute nylon webbing staging bridal. This releases the main parachute deployment bag, so drogue chute drag can extract the main parachute bag for deployment of the cross parachute. The payload is then properly positioned for an orderly lines-first deployment of the main parachute at a distance of ten payload

tube body diameters (80 inches) behind the payload (forebody) by the drogue bridal line in good airflow. This is important so payload forebody drag doesn't reduce the effective drag coefficient of the drogue chute, or disrupt the airflow for good drogue chute inflation.

The cross parachute is then deployed at an altitude of approximately 83,000 feet (25.3 km) at a velocity of Mach 0.36 (371 ft/sec / 253 mph). Inflation time for this large cross parachute with its very low canopy loading at this high altitude, is approximately 22 seconds. Average velocity decay of the main chute during inflation will be 46 ft/sec, while falling 1,000 feet to reach the full open condition by the target altitude of 82,000 feet (25 km). During this time the canopy, will open and partially collapse several times before coming to the full open condition for steady state terminal descent.

The drogue chute is medium weight construction with 1.6 ounce Mil-C-7030 ballistic cloth, and 500 pound (9/16 inch) herring bone webbing radials and suspension lines. With 12 suspension lines, the drogue chute is designed for a 6,000 pound opening load.

The main cross parachute will be constructed of Mil-C-7020 1.1 ounce ballistic parachute nylon. The parachute will have 24 suspension lines made of 250 pound nylon cord, with 250 pound nylon tape reinforcements on the canopy radials. This parachute uses light weight construction with a design strength of 6,000 pounds.

Time from rocket lift off to apogee is 83 seconds (0:01:23). The payload free fall time from apogee is approximately 43 seconds (0:00:43). Free fall time of the inflated drogue chute, to include opening time is 10.1 seconds (0:00:10). Descent time of the main cross parachute is (1:39:46) for terminal descent from parachute deployment to touch down. Total time from apogee to touch down is (1:40:56). Time from lift off to apogee is (1:42:02), with the total mission time being (1:40:02). Refer to Figure 5-20 for the graphic depiction of the ARIM-1 launch vehicle and parachute recovery system performance based on the energetics of the Viper V motor.

Both parachutes have design safety factors greater than 2.0, and are conservatively designed, so parachute reefing isn't required to control the opening loads, thereby eliminating another level of complexity to the design and testing process. Parachute recovery system fabrication and construction will be done according to parachute industry standards, employing conventional materials.

It is very important to remember that these are only numeric projections of parachute performance. Simulations are not the real world, they only provide a ball park or baseline for design and planning purposes. Since the Thiokol Cajun and Apache rocket motors will be used for the ARIM-1 sounding rocket payload, the Viper V motor was only a preliminary design option which will not be used in the final design analysis for motor performance.

All of the performance parameters presented here for the parachute recovery system will have to be recalculated, based on these new motor choices, and launch vehicle geometry. However, the preliminary engineering design analysis of the Viper V rocket motor flight performance provided a close approximation of what the Cajun and Apache flight profiles will be like. The motor energetics are very similar for total

specific impulse and motor burn times. The only difference is that the Cajun and Apache motors will provide apogee around 100,000 feet, which means that the reentry velocity and parachute opening loads will be somewhat lower, due to the lower altitudes.

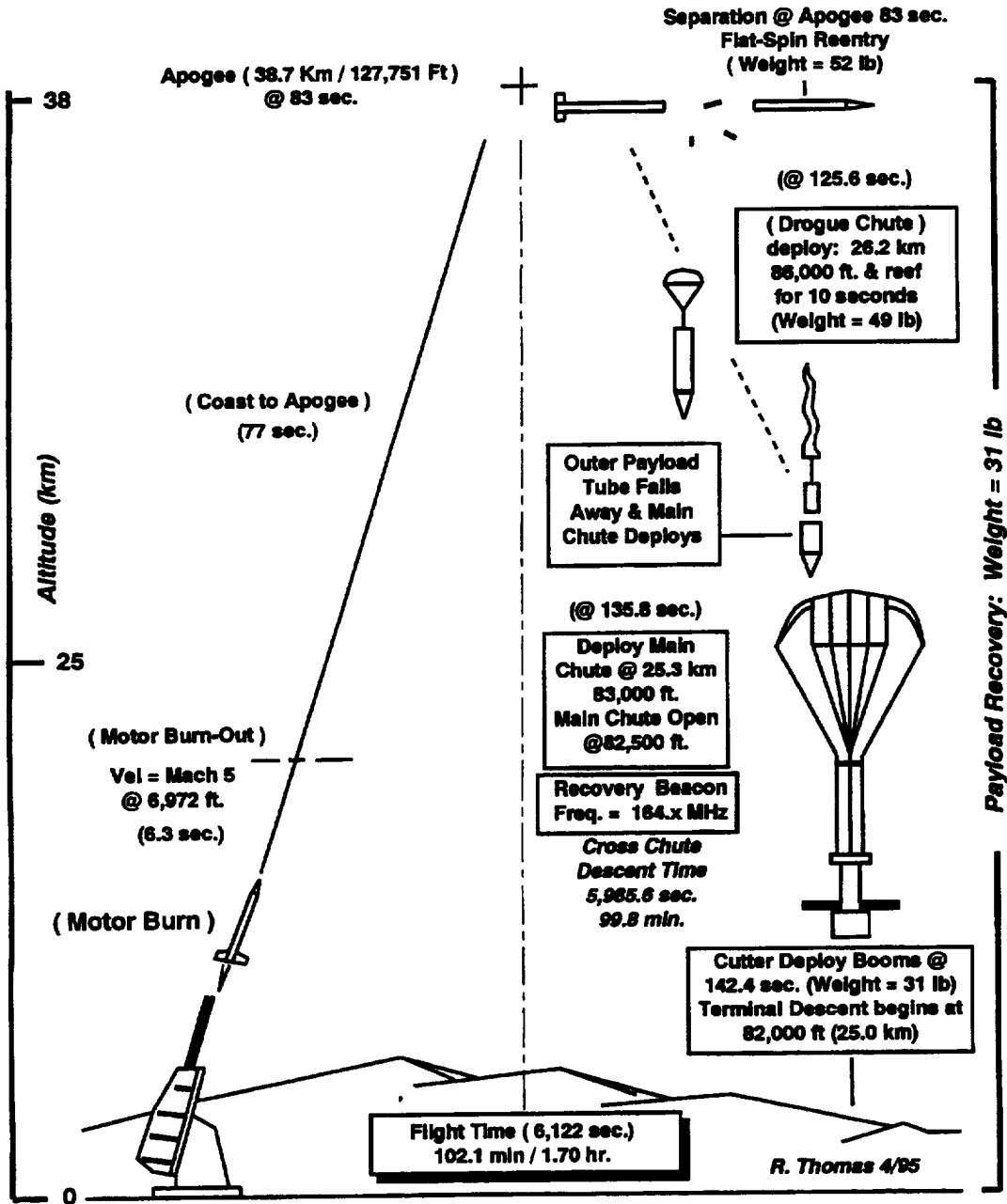


Figure 5-20 : Time line and performance parameters of rocket flight profile and payload recovery system events. Note time and altitude for recovery system.

5.9 Recovery System Testing

Preflight testing of the recovery system is necessary to produce reliable and flight worthy hardware. Such testing is prerequisite to being able to successfully recover any sounding rocket payload. The rationale being that a parachute recovery system wouldn't be flown in a sounding rocket until it has been statically tested on the ground to ensure that all the mechanical mechanism responsible for activating deployment of the recovery system are proven to function. Also, the recovery system must be dynamically tested by performing a functional deployment of the recovery system in flight under conditions as closely matched to the actual rocket flight conditions as possible.

First the parachutes and deployment bags are constructed. Then, the parachutes are physically packed into the deployment bags to ensure that the parachutes can be packed, and will fit in the payload space allowed for the recovery system. This also allows a functional test of integrating all the component hardware into the packed parachute recovery system. Where will the components be located, and how will they be packed with the parachute? This process is partly trial and error to determine the best possible way to integrate the component hardware into the packed and rigged recovery system. Along with this process, each component is weighed so an accurate mass budget can be determined from which to calculate performance parameters for the recovery system including canopy filling time, filling distance, opening force, velocity decay during canopy inflation, free fall distance during staging with pyrotechnic cutters, and descent rate of the parachute.

Next, the payload is assembled with all component hardware that will fly in the rocket and weighed for an accurate actual weight. The payload is then statically balanced to determine proper center of pressure and center of gravity relationship for payload to enter a horizontal spin or tumble during reentry. Ballast is added to the payload as needed, to obtain this relationship.

All pyrotechnic devices will be static fired on the ground to ensure that the initiating mechanisms for the parachute recovery system are functional. This means actually test firing the pyrotechnic thruster which blows apart the V-band clamp. The pyrotechnic thruster, which breaks the shear pins to extract the drogue chute and initiate recovery operations, must also be test fired.

The recovery system must be dynamically deployed to ensure the parachutes will deploy and inflate. At a minimum, the packed recovery system would be drop tested by static line from a balloon or aircraft to ensure the recovery system will function to deploy the parachutes.

Finally, the parachute recovery system would be flown in a test rocket with a dummy payload. This would allow testing of the recovery system under actual flight conditions of the mission, to experience the same parachute opening loads, and payload forces as an actual mission. A successful payload recovery of a test rocket, would ensure the highest confidence, in the preflight worthiness of the parachute deployment and recovery system.

6. Payload Electronics

The electrical system for the ARIM-1 mission includes the following components:

1. Power System
2. Umbilical System
3. Instrumentation System
4. Flight Computer
5. Global Positioning System (GPS)
6. Telemetry System

A block diagram of the rocket's electrical system is shown in Figure 6-1.

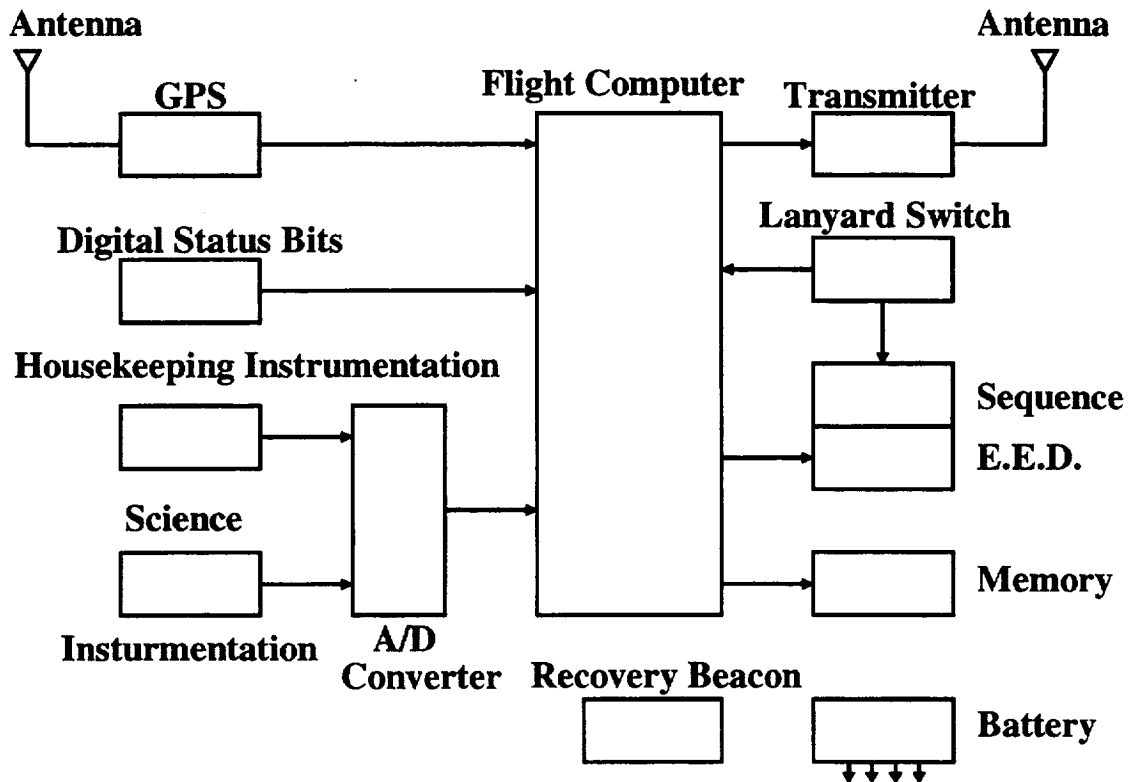


Figure 6-1 : Electrical Block Diagram

6.1 Battery and Power System

The power requirement for ARIM-1 is approximately 45 W at a bus voltage of 28 V. The total flight time is about two hours, thereby yielding a total energy requirement of 90 W-h.

A lithium battery pack has been chosen for this mission to minimize payload weight, thereby reducing the size of the parachute. The current capacity for lithium batteries is higher than Nickel Cadmium rechargeable batteries. However, the disadvantage is

that lithium batteries are not rechargeable, so they can only be used once. Please refer to Table 6-1 for specifications on the lithium battery pack proposed for ARIM-1.

Table 6-1 : Specifications for lithium battery pack

Total power requirement	90 W-h
Normal voltage per cell	1.5 V
Typical capacity per cell	2.6 A-h
Size	AA
Unit weight	15 g
Power per cell	3.9 W-h
Total number cells to use	48 (8 cells for flight computer, 40 cells for other use)
Total weight	720 g
Total voltage	30 V
Storage temperature range	60° C to - 20° C

6.1.1 Power Budget

The power requirements for the ARIM-1 mission are summarized in Table 6-2. The transmitter requires the greatest power and the microprocessor requires the highest current.

Table 6-2 : Power Budget

Used by	Power (w)	Voltage (V)	Current (A)
Thermosonde	4.0	15 and -15	0.30
Transmitter	28.0	28	1.00
Microprocessor	7.7	5	1.54
Instrumentation	1.5	5, 15 and -15	0.30
GPS	1.1	5	0.22
Umbilical Board	2.5	5	0.50
Total	44.8		3.86

The total current requirement is quite high for ARIM-1. Therefore, the flight computer will use a separate battery pack. The ARIM-1 power system outlined in Table 6-2 is implemented with 48 cells. Among these batteries, 8 are used solely for the flight computer and 40 are used for the rest of the payload systems. The remaining 40 cells are configured as two parallel banks of 20 cells each to yield a bus voltage of 30 V. Twenty cells will satisfy the voltage requirements, but the current requirements necessitate the two packs in parallel. Table 6-3 outlines the power budget for the flight computer.

Table 6-3 : Flight Computer Power Budget

Total power requirement	15.4 W-h
Normal voltage per cell	1.5 V
Typical capacity per cell	2.6 A-h
Size	AA
Unit weight	15 g
Power per cell	3.9 W-h
Total number cells to use	8 (4 cells parallel with 4 cells)
Total weight	120 g
Total voltage	6 V

By separating the power supply for the flight computer from the rest of the electrical design, the total current as shown in table 6-2 is reduced to 2.32 A, which will reduce the burden on the regulators. Two banks of 4 cells each will be connected in parallel to satisfy the high current requirement for the flight computer.

6.1.2 Power Regulators

Power will be distributed to most of the payload subsystems by means of DC-DC converters. Table 6-4 shows the voltage and current requirements for the payload subsystems, hence the voltage requirements for the converters. Note, the current level for the 5 volt regulator is reduced substantially because the flight computer uses its own bank of cells. DC-DC converters in this range are readily available, therefore no specific manufacturer has been specified.

Table 6-4 : DC-DC Converters

5	0.82	4.1	GPS Instrumentation Umbilical Board
15	0.25	2.5	Instrumentation Thermosonde
-15	0.25	2.5	Thermosonde
Total	1.32	9.1	

* The displayed currents are for their respective voltages, not the battery currents.

6.2 Umbilical System

The umbilical system will be used to communicate with the rocket while it is on the launch pad. An umbilical cable will be used to transmit data between the rocket's umbilical connector and the umbilical box that is located in the block house at PFRR. The rocket's battery voltage will be monitored with this system as well as the operation of the flight computer. The rocket's sequence board program will be down

loaded from a computer in the blockhouse via this system in order to compensate for temperature differences that will change the flight time to apogee.

6.2.1 Pyrotechnics Control

The pyrotechnics will be discharged by an EED firing circuit. This system is being designed to fire a total of four pyrotechnics. However, ARIM-1 will only utilize two of the four available circuits, one to activate the separation mechanism and another to deploy the parachute. This design was chosen in order to accommodate future missions that may require a more complex firing systems. Now, Each pyrotechnic has 2 firing squibs, only one of which must be blown in order to actuate the device. Therefore, each pyrotechnic will have two firing inputs, one from the flight computer and another from an R-C timing circuit (Sequencer board). The flight computer will be the primary system for firing the EED's and will use acceleration data gathered from the on-board accelerometer in order to predict apogee, which is where separation should take place. The Sequencer board is a backup system that simply times out and fires the EED in the event of a failure.

6.3 Instrumentation System

The purpose of the housekeeping instrumentation is to provide a basic knowledge of how the payload performs during flight. The housekeeping measurements include internal temperature, internal pressure, battery voltage, acceleration (three- axes), GPS, nose cone temperature, battery box temperature, and boom angle, as outlined in Table 6-5. With the exception of the GPS, which sends 128-bit packets straight to the flight computer, the above instrument data is sent through an 8-bit A/D (analog-to-digital) converter prior to reaching the flight computer. In addition, digital status bits are provided to indicate the status of the lanyard switch, parachute deployment, motor separation, boom deployment, and payload tube separation, as shown in

Table 6-6.

Table 6-5 : Housekeeping Instrumentation Sensors

Data Collected	Sensor
Internal Temperature	Analog Device's - AD590JH
Internal Pressure	Motorola's - MPX2100AP
Battery Voltage	Voltage Divider
Acceleration (three-axes)	AMP's - ACH-04-08
GPS	Motorola's - VP-8
Nose Cone Temperature	Thermocouple
Battery Box Temperature	Analog Device's - AD590JH
Boom Angle	Variable Resistor

Table 6-6 : Housekeeping Instrumentation Digital Status Bits

Digital Status Bits
lanyard switch
chute deployment status
motor separation status
boom deployment status
payload tube separation

In this section, the implementation for each sensor is discussed. Note that most of the output signals from the instrumentation board contains a 2 k Ω output resistor, and some of them also have germanium diodes in series with the output signal to protect the A/D's input terminals from excessive fault currents. Since the input terminals have high input impedance, the voltage drop across these output resistors will be negligible during proper operation.

6.3.1 Reference Voltage

It is not a good idea to rely upon the accuracy of the power supply voltages as a standard by which to reference the outputs of sensors' circuits. Therefore, a reference voltage circuit is used. The power supplies may have drift, noise and ripple from a variety of sources, with voltage tolerances up to $\pm 10\%$. The reference voltage circuit in Figure 6-2 will allow instrumentation measurements independent from errors and variations in power supply voltage.

The LM 185A-1.2 is a micro-power voltage references diode with a stable 1.23 V reverse breakdown voltage, which provides the low reference voltage.

The high reference voltage utilizes the LM124, which is a low power quad operational amplifier. It consists of four independent, high gain, internally frequency compensated operational amplifiers that operate from a single power supply over a wide range of voltages. The operating temperature range is -55°C to $+150^{\circ}\text{C}$.

The noise suppression capacitors, C_1 and C_2 , are chosen to be 100 nF. The resistor R1 must be small enough to sink the load current as well as the reference current. Therefore, the value of R1 was selected to be 15 k Ω , which limits the current drain to under 1 mA. Thus allowing for the current consumption of the other sensors.

Since the LM185 is tied to the amplifiers negative terminal, it must be noted that the case will be at -1.23 V rather than ground potential. Hence, the required gain of the LM124 is given by:

$$A_v = -\frac{R_4}{R_2} = -4.2$$

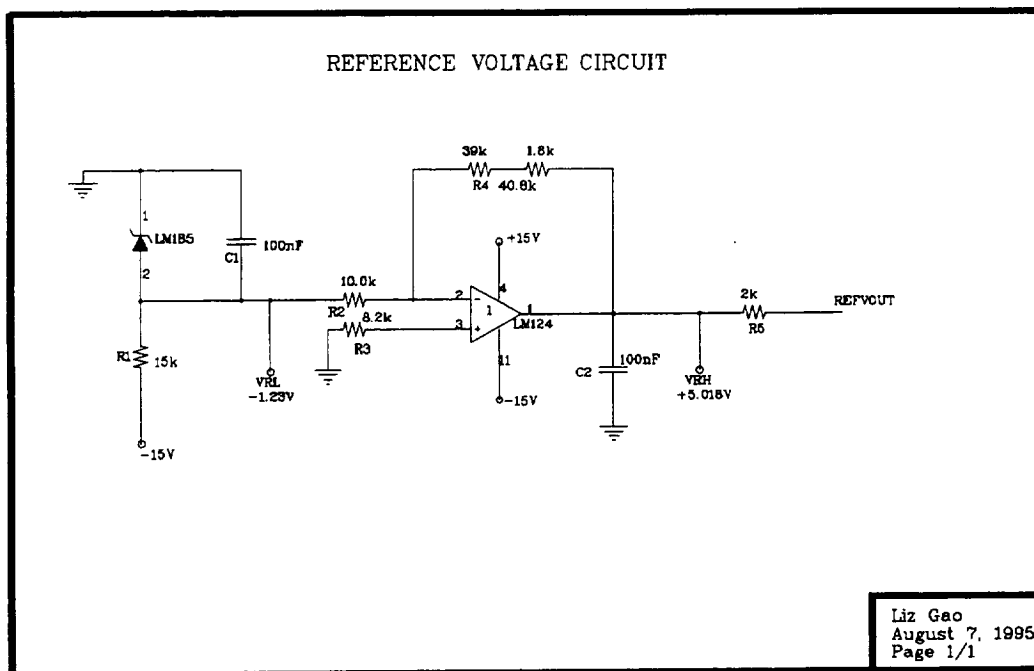


Figure 6-2 : Reference Voltage Circuit

With $R_2 = 10\text{ k}\Omega$ and $R_4 = 42\text{ k}\Omega$. Since the gain has been determined, the voltage reference high can be found by multiplying the -1.23 V level by the gain of the amplifier, which works out to be approximately $+5.17\text{ V}$.

The resistor R3 is present to minimize the offset current and was chosen to be 8.2 k Ω , which is the closest existing value to 42 k Ω || 10 k Ω . It is recommended that chip resistors be used in place of axial resistors wherever possible in order to conserve space on the printed circuit boards.

6.3.2 Internal Temperature

The internal payload air temperature sensor will be an Analog Devices AD590JH. It has an operating range from -55°C to 150°C . It is a two-terminal integrated circuit temperature transducer which produces an output current proportional to absolute temperature. The sensor is a current source with the current being independent of the voltage across the terminals, and dependent only on the temperature. For instance, changing the power supply from 5 V to 10 V results in only a $1\text{ }\mu\text{A}$ maximum current change, or 1°C equivalent error. For supply voltages between + 4 V and + 30 V the device acts as a high impedance ($> 10\text{ M}\Omega$), a constant current regulator passing $1\text{ }\mu\text{A/K}$. Laser trimming of the chip's thin film resistors was used to calibrate the device to $298.2\text{ }\mu\text{A}$ output at 298.2 K ($+ 25^{\circ}\text{C}$). It provides excellent rejection of supply voltage drift and ripple. In addition, power requirements are low, 1.5 mW at 5 V and 25°C . The AD590 may be used in any temperature sensing application below $+150^{\circ}\text{C}$.

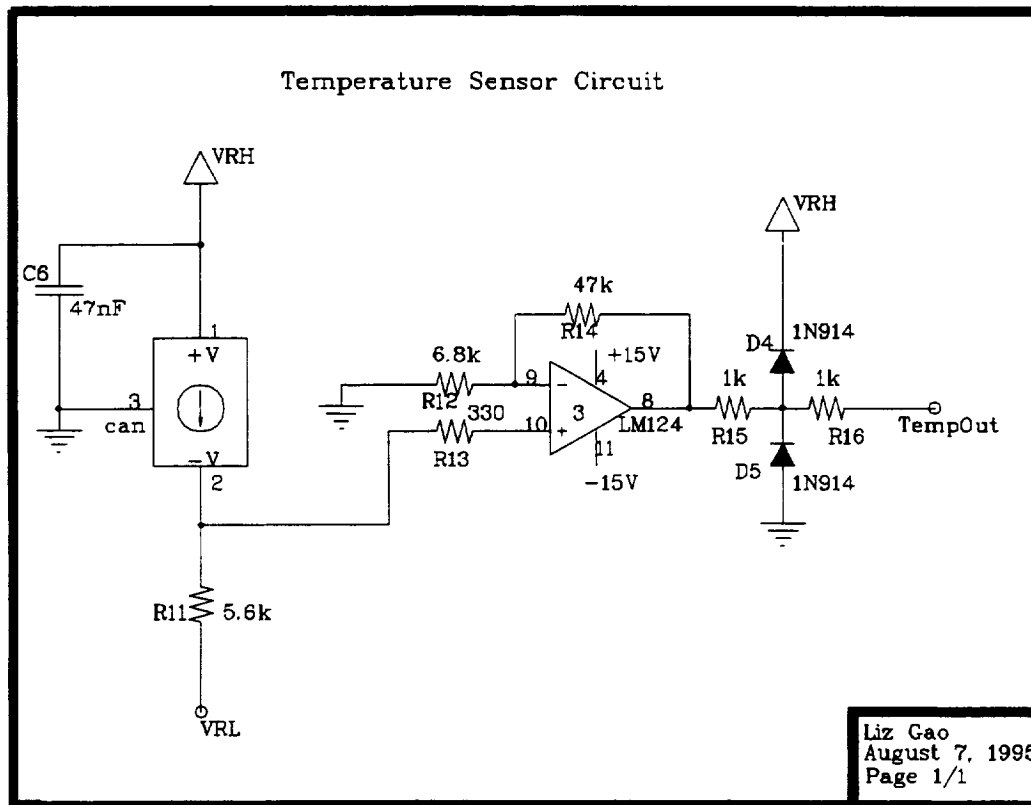


Figure 6-3 : Temperature Sensor Circuit

The current produced by the AD590 is linearly related to the temperature being measured. Therefore, for a temperature range of -55°C to 55°C the current ranges from $328.2\text{ }\mu\text{A}$ to $218.2\text{ }\mu\text{A}$. At $218.2\text{ }\mu\text{A}$, an output voltage of 0 V is desired as input to the amplifier. So in order to achieve this, the voltage drop over R11 must be 1.23 V . Therefore, R11 was chosen to be $5.6\text{ k}\Omega$. At 55°C , this circuit must supply a $+5\text{ V}$ level to the flight computer in order to maximize use of the available resolution. At this temperature the AD590 will push $328.2\text{ }\mu\text{A}$ through R11 producing a voltage level of 0.62 V on the non-inverting input of the amplifier. So, in order to produce the necessary $+5\text{ V}$ the amplifier needs to have a gain of 8.1 , and by setting R14 to $47\text{ k}\Omega$ and R12 to $6.8\text{ k}\Omega$ this goal can be attained.

In order to minimize offset currents R13 should be approximately $(R12 \parallel R14) - R11$, which works out to be about $330\text{ }\Omega$. Resistors 15 and 16 as well as the two diodes, D4 and D5, provide over and undervoltage protection for the flight computer.

6.3.3 Pressure

The pressure sensor measures the ambient pressure during flight. The pressure above $70,000\text{ feet}$ is approximately 0.65 psi . The pressure on the ground is about 14.5 psi . Therefore, it is unlikely the pressure will ever be greater than 14.5 psi .

The Motorola MPX2100AP pressure sensor was selected over other sensors, because it provides a highly accurate and linear voltage output that is directly proportional to

the applied pressure. It is temperature compensated over a temperature range of 0° C to + 85° C, with a large allowable error over the operating range of - 40° C to + 125° C.

The MPX2100AP pressure sensor has a range of 0 to 14.5 psi, and a nominal sensitivity, $\Delta V_{out}/\Delta P$, of about 0.4 mV/kPa at an excitation voltage of 10 V. Therefore the output is a differential voltage between the two terminals, and the excitation voltage inputs. It also has a nonzero offset of +/- 2 mV (that is +/- 2 mV output at 0 psi). Both the sensitivity and offset values will vary from one device to another. Now, air pressure follows a non-linear curve, but corrections in the software account for this. Figure 6-4 shows the circuit diagram for the pressure sensor.

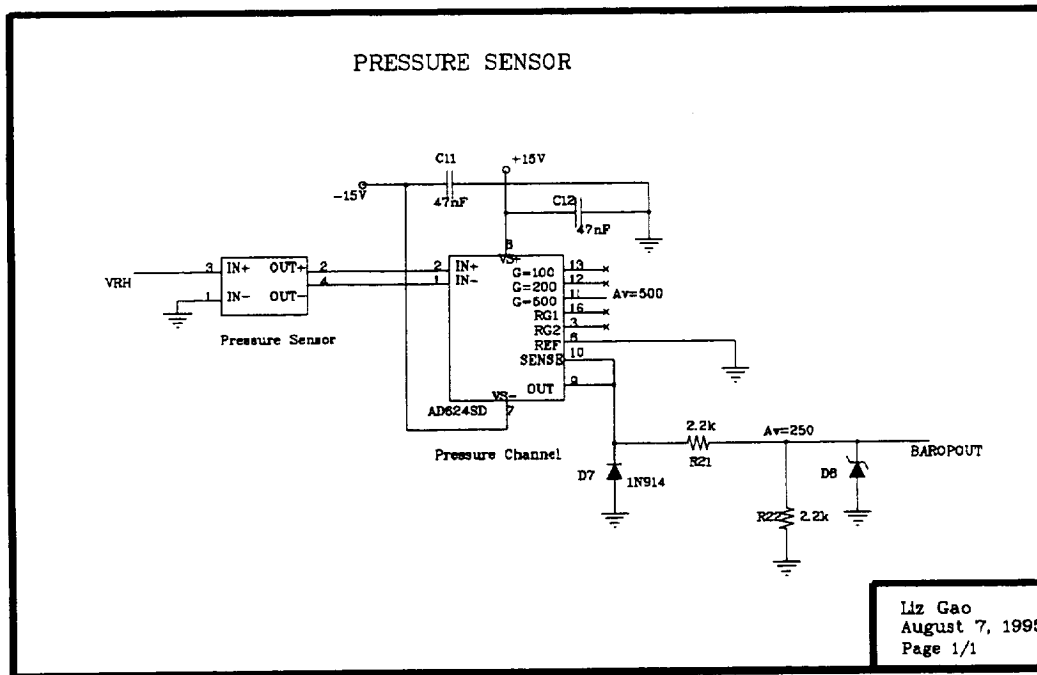


Figure 6-4 : Pressure Sensor

The AD624 is a high precision low noise instrumentation amplifier, which is used to amplify the signal from the pressure sensor. The AD624 has low noise high gain, a low gain temperature coefficient, and high linearity, which is ideal for use in high resolution data acquisition systems. The AD624 has programmable gains of 1, 100, 200, 500 and 1000 which are provided on the chip. Other gains are achieved by a single external resistor. The offset voltage, offset voltage drift, gain accuracy and gain temperature coefficients are guaranteed for all five preprogrammed gains.

The two above mentioned methods for setting the gain on the AD624 are 1) Connecting the terminals in one of several ways; 2) Using an external gain resistor. The external gain resistor method gives a gain that varies from device to device, over a range of +/- 20%.

If a full scaled output on the high reference voltage (VRH) at a pressure well above standard sea level air pressure (14.5 psi) is desired, the required gain is:

$$A_v = \frac{VRH}{V_{in}} = \frac{VRH}{Sensitivity \times P@sealevel} = 250$$

So, a gain of 500 was selected since it is a preprogrammed gain and a voltage divider (R21 and R22) was used on the output to cut the gain in half. The capacitors (C11 and C12) are simply decoupling capacitors, and D7 and D8 provide overvoltage and undervoltage protection for input to the flight computer.

6.3.4 Battery Voltage

The battery voltage is monitored to verify that the battery is properly charged and functioning normally. Figure 6-5 shows the detailed schematic of the battery voltage circuit.

To measure the battery voltage, a simple voltage divider and comparator were used. With an assumption of total battery voltage of 35 V, the resistive network was set to output about 5 V in order to provide a good logic level for the flight computer. If the voltage is below 15 V, the logic level will show zero. VRH is one input and battery's voltage is the other input. An op-amp, LM124 is used to amplify the voltage signal.

Let $R32 = 22 \text{ k}\Omega$, and $R33 = 44 \text{ k}\Omega$, the battery will be divided to one third of its original voltage.

$$\text{Divider1} := \frac{R32}{R32 + R33}$$

$$\text{Divider1} = 0.333$$

When the battery voltage is 35 V,

$$35 \cdot \text{Divider1} = 11.667 \quad \text{V}$$

The gain will be:

$$\text{Av4} := \frac{5}{35 \cdot \text{Divider1} - \text{VRH}}$$

which is 0.75. In order to have positive resistance for R35, the gain is increased too twice of its size. Then after the op-amp, a voltage divider is used to bring back the real gain. The new gain is 1.5, so the new equation is:

$$\text{Avb4} = \frac{R35}{R31} + 1$$

Let $R31 = 47 \text{ k}\Omega$, R35 is calculated to be $23.5 \text{ k}\Omega$. Then R34 equals to R31 parallels with R35 minus R32 parallels with R33, which is $1 \text{ k}\Omega$.

For the voltage divider, both R36 and R37 are $2.2 \text{ k}\Omega$, therefore the gain is reduced to the gain of 0.75 again.

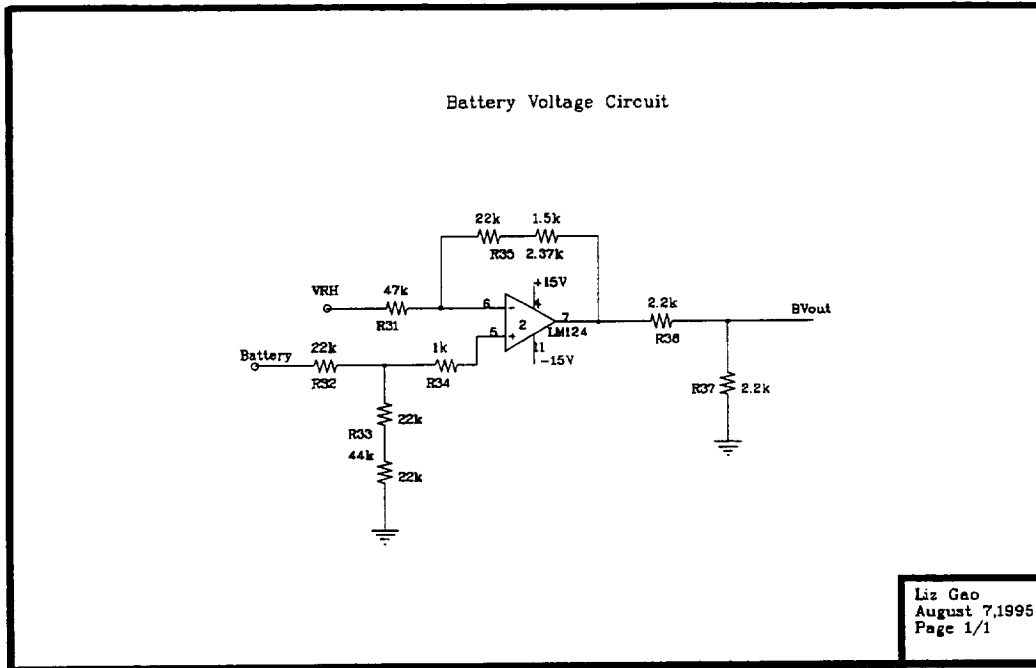


Figure 6-5 : Battery Voltage Circuit

6.3.5 Acceleration

The accelerometer will measure the motor thrust profile, and the vibration environment of the payload.

The ACH-04-08 accelerometer from Amp Inc. will measure acceleration in three axes, including one angular and two linear directions. The two linear axes are the Y and Z, and the rotation is about the Z axis. Figure 6-6 shows the three axes of the accelerometer.

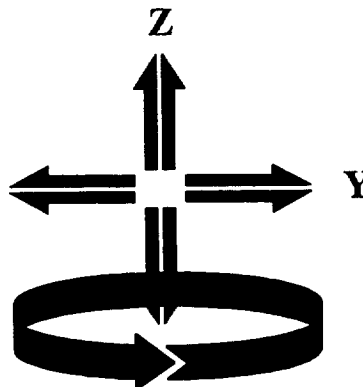


Figure 6-6 : Three Axes monitored by the Accelerometer

The dimensions of the accelerometer are 0.45 X 0.34 X 0.06 inches. The integrated electronics provide signal gain and processing capability that can be adjusted and configured by the user to meet the specific requirements of the application. Each sensor has a dedicated channel with adjustable gain, an adjustable comparator, and a

selectable output control to provide either a digital or analog signal. However, each chip only has one output. Since a three-axis accelerometer is required, three-chips would be needed.

6.3.6 Nose Cone Temperature

The nose cone temperature sensor measures the temperature of the nose cone during flight. The nose cone temperature data can help define the rocket's performance as well as provide design engineers with better information on the payload's operating environment.

The best thermocouple for high temperature is a type J Iron-Constantine thermocouple. Its measurement range spans 0°C - 700°C , depending on the model chosen. The XC-J-20 has a ceramic insulation, which will withstand a maximum temperature rating of 760°C . This model is more expensive and a little bit heavier than the others. If the HH-J-20 or HH-J-24 are chosen, the maximum temperature they can withstand is 704°C and use high temperature glass as insulation. These two are much less expensive and less weight. The J Iron-Constantine has an error of $\pm 2.2^{\circ}\text{C}$ or $\pm 0.75\%$ whichever is greater. Figure 6-7 shows the circuit schematic of the nose cone temperature.

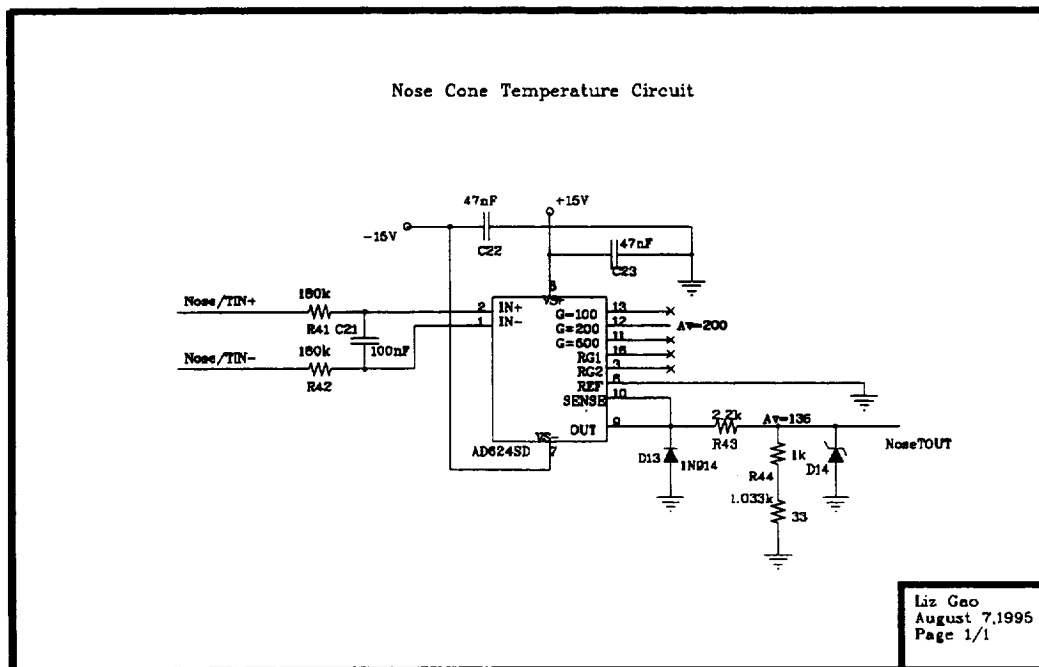


Figure 6-7 : Nose Cone Temperature Circuit

The maximum temperature is assumed to be 700°C . The sensitivity, $\Delta V_{\text{out}} / \Delta T$, of a Type J thermocouple is about $52.6 \mu\text{V}/^{\circ}\text{C}$. Therefore the differential voltage between the thermocouple output (V_{o1}) will be 37 mV.

The AD624SD is used as an instrumentation amplifier with a desired gain as shown below. However, a preprogrammed gain of 200 was selected and a voltage divider was used to reduce the gain to the desired setting.

$$Av6 = \frac{VRH}{Vol} = 136$$

R41 and R42 in combination with C21 act as a low pass filter to minimize any noise introduced into the system between the tip of the nose cone and the instrumentation circuitry. D13 and D14 are once again present to provide overvoltage and undervoltage protection for the flight computer's inputs.

6.3.7 Battery Temperature

The battery temperature sensor was chosen to be the same as the internal temperature sensor, the AD590JH. This sensor will be implemented in the same manner, the only difference will be the temperature range it is calibrated for. Figure 6-8 is a schematic of the sensors signal conditioning circuit.

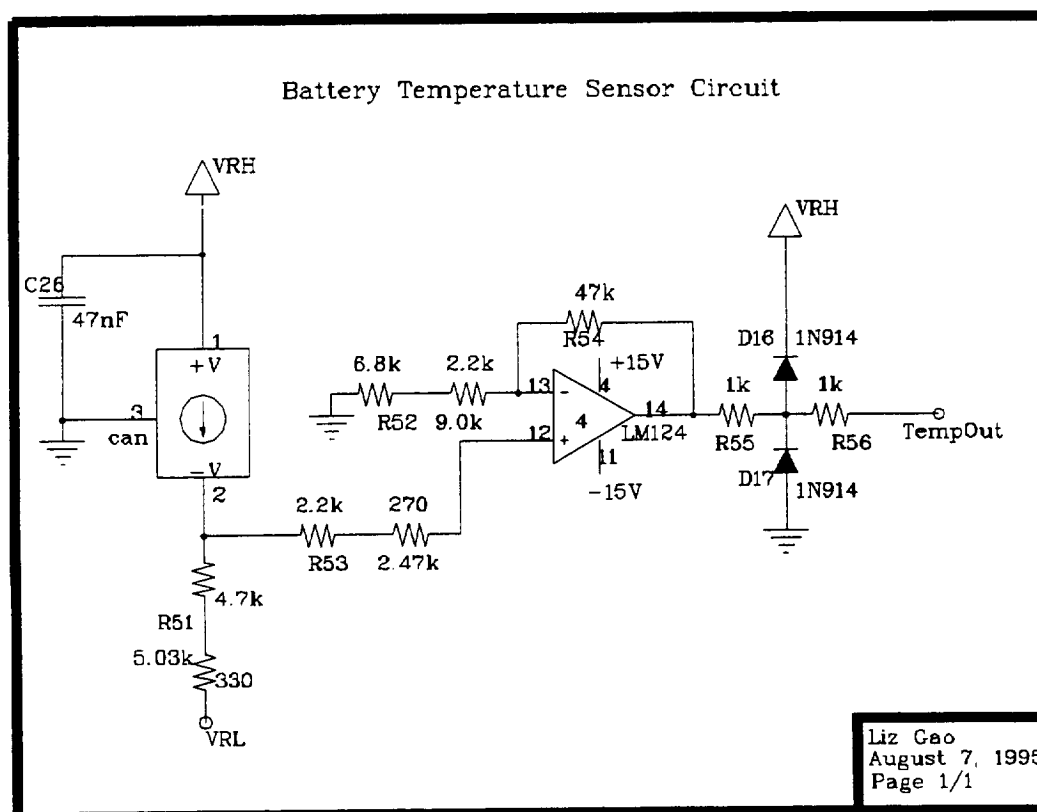


Figure 6-8 : Battery Temperature Sensor Circuit

According to the data sheets the selected lithium batteries were tested at 100° C for 30 days and experienced no venting or leakage while continuing to operate properly. Therefore, a range of - 30° C to 130° C (243.2 μ A - 403.2 μ A AD590 output current range) was selected for the battery temperature sensor.

At 243.2 μ A, an output voltage of 0 V is desired when the temperature is at -30° C. In order to achieve this, the voltage drop over R51 must be 1.23 V to account for the low reference voltage. Thus, R51 was chosen to be 5k Ω . The upper temperature range of 130° C will provide an output current of 403.2 μ A producing an input voltage to the

amplifier of 0.8 V, which corresponds to the maximum output for the transducer. Therefore, this value needs to be amplified to produce a logical 1 (+5 V), which means the amplifier should have a gain of 6.27. By letting $R54 = 47 \text{ k}\Omega$ and $R52 = 9 \text{ k}\Omega$ this goal is attained.

$R53$ is needed to minimize offset current and should have a value close to $(R52 \parallel R54) - R51$, which is about $2.47 \text{ k}\Omega$. $R55$ and $R56$ are two $1 \text{ k}\Omega$ resistors and are used in combination with the diodes $D16$ & $D17$ to provide overvoltage and undervoltage protection for the on-board flight computer.

6.3.8 Boom Angle Sensor

In the event the booms do not fully deploy the data collected by the thermosondes can still be salvages if the distance between the sensors is known. Therefore, the boom angle sensor would provide the information necessary to calculate this distance. Figure 6-9 is a schematic of the necessary circuitry for this sensor.

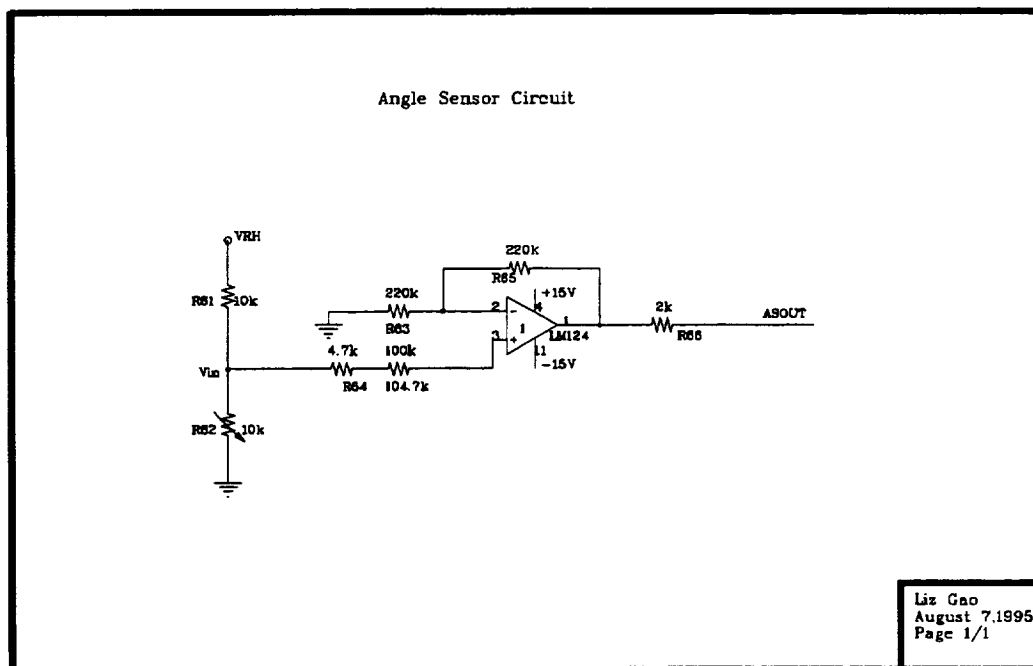


Figure 6-9 : Boom Angle Sensor Circuit

$R62$ is a $10 \text{ k}\Omega$ variable resistor, whose resistance would change as a function of the angle the booms make with the horizontal.

With $R61$ and $R62$ both $= 10 \text{ k}\Omega$ V_{in} to the amplifier is 2.5 V. Therefore, the gain of the op-amp must be 2 in order to provide an output signal of 5 V. This gain is easily obtained by allowing $R65$ and $R63$ to both be $220 \text{ k}\Omega$. Once again, the offset currents should be minimized. So, $R64$ was chosen to be $100 \text{ k}\Omega$ which is close to $(R65 \parallel R63) - R61$.

6.3.9 Digital Status Bits

The digital status bits are simple switches used to indicate the status of several on-board systems during flight. These systems include separation, parachute deployment. These switches are located on the housekeeping instrumentation board, and are implemented as follows.

Each status line is tied to the +5 volt bus through a 10 k Ω pull-up resistor. In addition, each line is tied to ground through a quick disconnect known as a Winchester connector. This implementation provides a low to the flight computer until the connection to ground is broken by a mechanical event in which case the on-board computer sees a high.

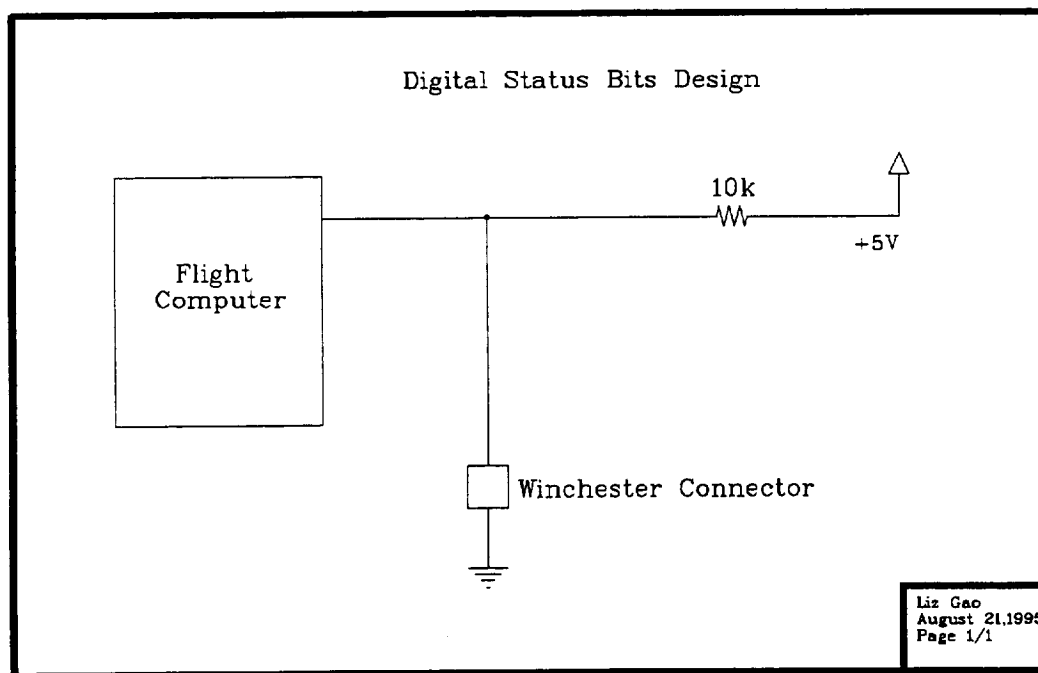


Figure 6-10 : Demonstration of Digital Status Bits

6.4 Flight Computer

The on-board computer system is comprised of three circuit boards: the main computer, external flash RAM, and an analog-to-digital converter. The flight computer samples and stores the analog data, such as temperature and pressure, as well as recording the digital data, such as the GPS packets. The flight computer organizes this data into pre-determined packet structures which are stored in the on-board flash RAM, and forwarded to the transmitter.

6.4.1 System Characteristics

The system selected was the embedded 386SX-25 IBM compatible. This system was selected due to its compact size and rigid construction. Table 6-7 provides a hardware description of this embedded PC.

Table 6-7 : Flight Computer System Characteristics

Type	Embedded IBM PC
Processor	386SX - 25 MHz
Memory	4 Mbytes on board parity checked DRAM
Operation	Standalone operation with 16-bit PC/104 Bus expansion connector on board.
Software development	Easy to do in any platform.
SSD	Supports on board bootable RAMDISK or ROMDISK in the 3 memory socket
Serial port	Two serial port; COM1 with RS-232/485 and COM2 with RS-232/422/485 support
Weight	350 gram
Power	+5V +/- 5% at 650 mA Max
Temperature	-40 - +85 degree Celsius
Operating system	MS-DOS, QNX or UNIX
Parallel port	One parallel port
Size	Small size 4.5"x 7.1"
Clock	Real time clock with battery backup
Humidity	5% - 95 %
Cost	\$ 795
Vendor	Win Systems, 715 Stadium Drive, Arlington Texas

6.4.2 386SX Processor

Below is the brief description of the 386SX processor.

(a) Execution unit:

Execution unit contains eight 32 bit general purpose registers which are used for both address calculation and data operation and a 64 bit barrel shifter which is used for speed shift , rotate , multiply and divide operations.

(b) Instruction Unit:

Instruction unit decodes the instruction op-codes and stores them in the decoded instruction queue for immediate use by execution unit.

(c) Memory Management Unit:

(i) Segmentation Unit:

The Segmentation unit allows the managing of the logical address space

(ii) Paging Unit:

The Paging unit which operates beneath and is transparent to the segmentation process to allow management of physical address space. It is useful for virtual memory , multitasking operating system.

6.4.3 Memory

The on-board data storage will require 10-12 Mbytes (not including accelerometer data), hence a minimum of 16 Mbytes of memory is required. The above mentioned memory system will fulfill this requirement. The environment in which this system will be operating dictates that static memory is a necessity, therefore the flash RAM described in Table 6-8 was selected.

Table 6-8 : Flash Memory Characteristics

Model	SDD-P-PCC
Maximum Capacity	64 MB
Type	Flash
Interface	PC/104
Power Requirements	5 VDC
Operating Temperature Range	-25° C to 75° C
Physical Dimensions	2.12" x 3.37" x 0.13"
Cost	\$ 275

In addition, each flash memory unit may be commanded through 10,000 store/erase cycles by software control.

6.4.4 Analog to Digital Converter

The analog data coming from the thermosondes and housekeeping instrumentation are converted to a digital signal by this A/D card. The AIM16-1/104 analog-digital converter chosen is described in Table 6-9.

The Analog AIM16-1/104 are 16-channel, 16 bit 100 kHz analog input boards that conform to the PC/104 standard. The AIM16-1/104 provides 16 bits of digital I/O, flexible triggering options, direct memory access (DMA), and interrupt operation. This board was designed specifically for embedded applications requiring high speed and high resolutions characteristics. The analog input multiplexer is software-configurable for up to 16 single ended or 8 differential channels, with an on-board programmable gain amplifier providing a bipolar or unipolar input, ranges 1.25V - 10V for the AIM16-1/104. The PGA, programmable "on the fly", drives a 16 bit, 100 kHz sampling A/D converter capable of 85 dB of spurious free dynamic range for the

AIM16-1/104. The data is first passed through a 256 X 16 bit FIFO before transferring to the host via programmed I/O or DMA in 16 bit format. The AIM16-1/104 also provides 16 digital I/O bits that can be programmed as inputs and/or outputs in 8-bit bytes. The use of an on-board DC-to-DC converter, powered from a single +5V supply, provides noise isolation from the system switching power supply.

Table 6-9 : Analog-to-Digital Converter Characteristics

Type	AIM 16/104 16 bit ,16 channel A/D
Resolution	16 bit
Throughput rate	100 kHz
Inputs	8 differential or 16 Single - ended inputs
Configuration	PC/AT Stack - Through
Power	+5 V @ 0.5 A
I/O lines	16 Digital
Dimensions	3.6" x 3.8"
Price	\$ 625.00
Vendor	Analogic Corporation, 360 Audubon Road, Wakefield, MA 01880-9863

6.4.5 Data Collected

Table 6-10 : Computer Data Rates

Instrumentation Data of 16 bit 1 kHz	2000 bytes/sec
Pressure	2 byte/sec
Temperature	1 byte/sec
Humidity	1 byte/sec
Digital status bits	1 byte/sec
GPS data	128 bytes/sec
Housekeeping (Internal pressure, temp, battery voltage of each 8 bit)	3 bytes/sec
Accelerometer (for 3 axis)	6000 bytes/sec
Overhead (Prefix, Postfix, Tag bytes, Checksum)	50 bytes
Total	8186 byte/sec

The data collected by the on-board flight computer is separated into four main categories: science, housekeeping instrumentation, digital status bits, and GPS. The science data consists of the measurements taken from the pressure, humidity, and absolute temperature sensors as well as the two thermosondes. The housekeeping instrumentation is a collection of standard sensors that monitor pressure, temperature, and acceleration, and is part of the standardized payload bus. The digital status bits simply indicate the status of various mechanical events throughout the course of the flight. Events such as, motor separation, skin separation, parachute deployment, and boom deployment. Table 6-10 shows the data rates required for sampling the data.

6.4.6 Data Format

The data received from the A/D converter is then organized into packets, stored in memory and forwarded to the transmitter. The packet size can be of any length depending upon the data size but the larger the packet size the more difficult error correction becomes.

The packet format has real-time data re-alignment and error correction capabilities. It has tag bytes inserted in the data in order to better identify the data when jumping into the middle of the data stream. The actual format for the science and acceleration data will be; prefix, data, checksum, and postfix. The packet format structure for the remainder of the data will be; prefix(10 bytes), GPS (128 bytes), tag bytes (2bytes), Digital Status Bits (1 byte), housekeeping instrumentation (7 bytes), postfix (10 bytes).

6.4.7 Data Collection and Transmission

The collection of data throughout the course of the flight is divided into two phases. This decision was based upon the limited usefulness of the vibration and science data as well as the enormous amount of on-board memory required to store the vibration data for the entire mission life. The first phase covers launch to boom deployment, and the second phase covers boom deployment to splash down. This way the acceleration data is only collected for a minimal amount of time, therefore conserving on-board memory, and the science data is only collected after the booms are deployed.

Phase (1) : Launch - Boom Deployment.

According to the information provided on the Viper V 12.001 UP the total ascent time is 250 sec or 4 min 9.6 sec. The data that will be collected during this time is shown in Table 6-11.

Table 6-11 : Data Collected During Phase One

Item	Data Rate	Duration	Total
DSB	1 byte		1 byte
Instrumentation	3 bytes/sec	250 sec	750 bytes
Acceleration	6000 bytes/sec	250 sec	1500000 bytes 1.5 Mb
GPS	128 bytes/sec	250 sec	32000 bytes
Total (T1) Data			1532751 bytes or 1.532751 Mb

Phase (2) : Boom Deployment - Splash Down.

Using preliminary numbers the estimated time for this portion of the mission is 1 hour and 45 minutes. Table 6-12 outlines the data that will be collected during this portion of the mission.

Table 6-12 : Data Collected During Phase Two

Item	Data rate	Duration	Total
Instrumentation	3 bytes/sec	6346.90 sec	19040.7 bytes
Thermosonde data	2000 bytes/sec	6346.90 sec	12693800 bytes or 12.69 Mb
Pressure, Humidity, and Temperature	4 bytes/sec	6346.90 sec	25387.6 bytes
Total (T2) Data			12738228 bytes or 12.738228 Mb

Hence the total memory required for the total flight time of approximately 110 minutes.

$$\text{Total}(T) = T(1) + T(2) = 1.53 + 12.73 = 14.26 \text{ Mb.}$$

This value includes the storage of the acceleration data. If acceleration data is not taken in account the total memory required would only be 12.76 Mb. Without the acceleration data a 16 Mb flash Ram card is sufficient for the mission, otherwise a higher capacity (64 Mb) memory card is available, and would be required. The data collected by the flight computer is to be forwarded to the transmitter during the course of the flight. This data is transmitted once per second to the ground station.

6.4.8 Architecture

The 386SX-25 embedded computer has a centralized architecture, which has point-to-point interfaces between processing units and possesses a single management computer, or central node. This architecture is often, referred to as a star, which does not allow the addition of nodes without affecting hardware and software on the main processor. When a few well defined systems need to interface with a single processor this architecture is effective and also reliable. A failure along one interface affects no other interfaces. However, the hub processor, through which all point to point traffic must pass, is a potential single point failure. Therefore the structure must be designed carefully to reduce or eliminate this risk. The centralized architecture usually requires a discrete or analog interface across either a serial or parallel bus with little protocol overhead.

Table 6-13 : On-board Computer Architecture

Candidate Architecture	Data Bus Standards	References
Centralized Architecture	RS 422, RS 232	Electronics Industry Standard

6.4.9 Serial Communications

Two independent, double buffered, full-duplex, serial asynchronous channels are implemented using the 16C452 Dual Asynchronous Communication Element. This device is a dual 8250A that offers software compatibility with PC type driver programs. They are mapped at COM1 and COM2 (3F8-3FF and 2F8-2FF hex), respectively. Independent control of transmit, receive, line status, and data set interrupts are provided on both channels. Each channel is setup to provide diagnostics such as loopback and echo mode on the data stream. The unit contains two independent on-chip software programmable baud rate generators which are selectable from 50 to 115,200 bits per second.

RS-232 interface levels are supported on both channels. The RS-232 drivers have an on-chip charge pump to generate the (plus and minus) voltages so that the computer board requires only +5 volts.

Table 6-14 : COM1 and COM2 Configuration Options

Configuration	COM1	COM2
1	RS-232	RS-232
2	RS-485	RS-232
3	RS-232	RS-485
4	RS-232	RS-422
5	RS-485	RS-485

RS-485 electrical levels can be supported on both COM1 and COM2. COM2 supports RS-422 if COM1 is configured as RS-232 only. An RS-422/485 configuration provides separate balanced transmit and receive signal pairs. For RS-485 multidrop lines, one signal pair can be used for "party line" network structures.

The SAT-386SX is designed to properly disable the serial data transmitter (located on the flight computer) upon reset to prevent potential lock-up problems caused by a transmitter stuck in the ON position. Both the RS-422/485 transmitter and receiver lines also permit user installable termination resistors for impedance matching and biasing.

Both serial channels are configured as Data Terminal Equipment (DTE) and wired to a 50 pin connector at the edge of the board

The CPU has a Multi-I/O connector on the COM1, COM2, LPT1, and keyboard. These four ports are combined into one 50 pin header at the top of the board. COM1 and COM2 are 9-pin male "D" connectors with strain relief. LPT1 is a 25-pin female "D" connector with strain relief.

Table 6-15 : COM1 and COM2 RS-232 Pin-Out

Pin	Flow	Signal
1	IN	Data Carrier Detect(DCD)
2	IN	Receive Data(RxD)
3	OUT	Transmit Data (TxD)
4	OUT	Data Terminal Ready(DTR)
5	---	Signal Ground(GND)
6	IN	Data Set Ready(DSR)
7	OUT	Request To Send(RTS)
8	IN	Clear To Send(CTS)
9	IN	Ring Indicator(RI)

6.4.10 Telemetry Format

The data received is stored in the flash memory and forwarded to the transmitter once per second. The format is as follows:

Table 6-16 : Telemetry Packet Format

Start Bit	Parity	Data Bit	Stop Bit
One	None	Eight	One

6.4.11 PC/104 Bus

The CPU is interfaced with the other peripheral cards like the A/D converter and the Flash memory card through a PC/104 expansion bus. The standard PC bus form factor (12.4" x 4.8") and its associated card cages and back planes are too bulky and expensive for most embedded control applications. A PC/104 was developed in response to the above requirements. It offers a complete architecture, hardware, S/F(Software) compatibility with the PC bus but in ultra compact (3.6"x 3.8") stackable modules. The advantage is, the cards can be arranged in a modular stack. This way it can withstand rugged conditions like the vibration inside the rocket and minimize the volume of space consumed. In addition, the PC/104 consumes little power.

6.4.12 Flight Computer Software Flowcharts

The main program executed by the flight computer will initialize its own hardware as well as the A/D converter and flash memory module. The on-board computer will then call its various interrupt service routines (ISRs), in order to collect the appropriate data. The following is a basic flowchart for the mechanical interrupt service routines that has been generated for the on-board computer system. This chart is not complete and is only intended to illustrate the underlying logic.

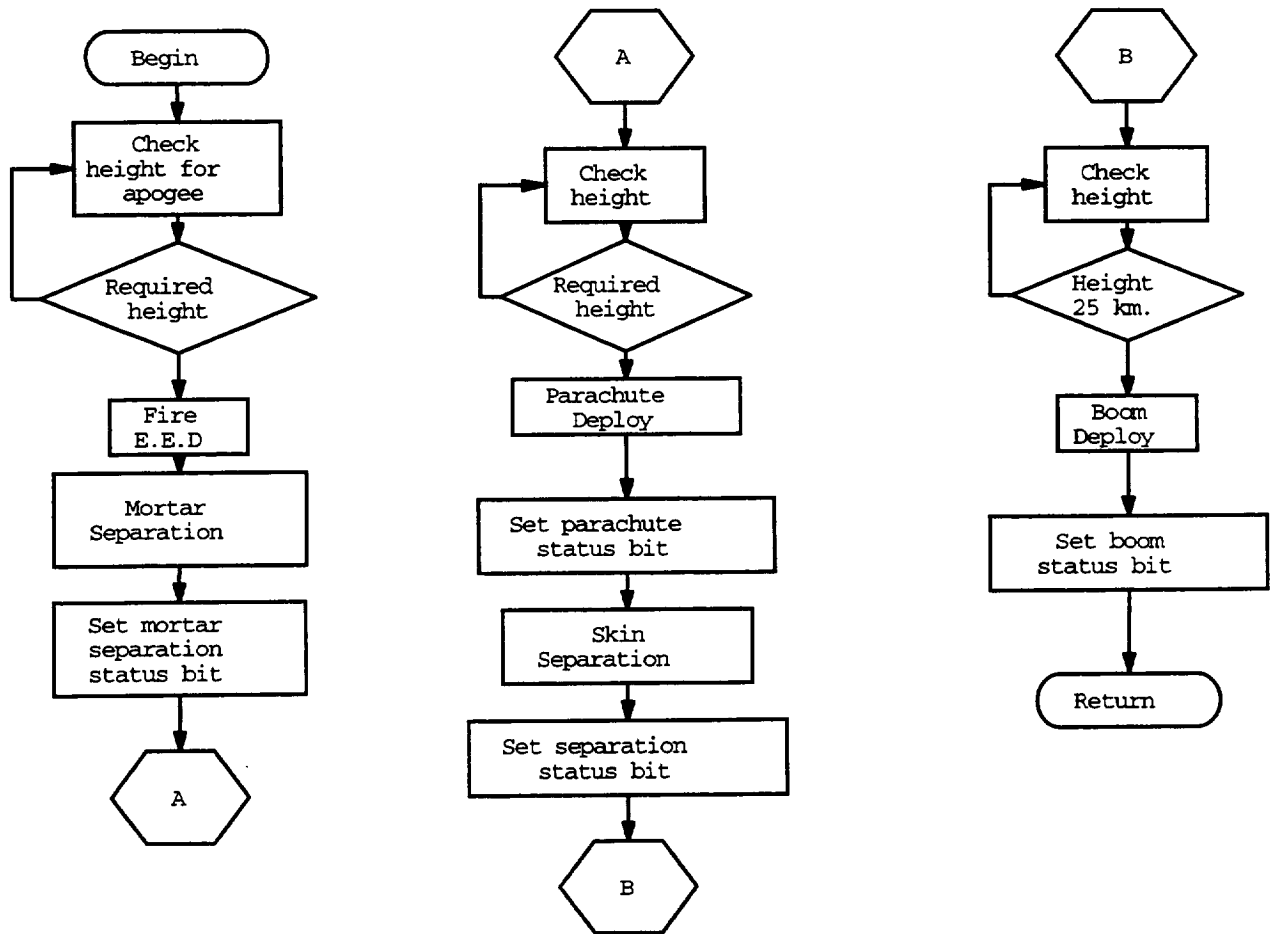


Figure 6-11 : Mechanical Interrupt Service Routines

6.5 On-Board Global Positioning System

A Motorola VP Oncore 8-channel GPS receiver module will be used in the rocket and on the ground. This unit can track 8 satellites simultaneously and has a position accuracy of 0.7 to 0.8 meters in the Differential Global Positioning System (DGPS) mode. The VP-8 operates on 5 V regulated DC with a power consumption of 1.1 Watts. This unit is capable of outputting the raw position data that is required to obtain the position accuracy stated above. This position accuracy will be available during post flight analysis as the RTCM-104 error correction data will be purchased for each flight and will be available the day after launch.

6.6 Telemetry System

6.6.1 Telemetry Transmitter

The transmitter that will be used for ARIM-1 is Aydin Vector's T-202SE S-band transmitter. The characteristics are shown in Table 6-17. This transmitter meets or

exceeds all requirements for this mission and can also be used in a standardized payload bus for later missions.

Table 6-17 : Transmitter Characteristics

Frequency	Input Voltage and Power	Modulation	Output Power	Environmental	Cost
2200-2300 MHz	28±4 Vdc 18.2 Watts	FM	2 Watts	-25°C + 70°C	\$3,000.00

Frequency: The 2200-2300 MHz S-Band was chosen because it is a designated frequency allocation for telemetry. Furthermore, the choice of S-band frequency facilitated the design of a conformal microstrip patch antenna with dimensions that were commensurate with the size of the rocket payload.

Voltage and Power: The input voltage required is 28±4 Vdc with a max current of 650 mA. The transmitter has reverse polarity protection as well as over-voltage protection.

Modulation type: - Frequency shift key (FSK) modulation was chosen for its immunity to noise and because receiving hardware is readily available. The standard input impedance into the modulator is 10 kΩ. The modulation signal frequency can range anywhere from DC to 500 kHz. This will easily accommodate the required data rate of 17.6 kbit/s. The frequency deviation will be ±1.125 MHz with a deviation sensitivity of ±500 kHz/V_{rms}. The deviation distortion will be 1% for ±500 kHz deviation.

Environmental specifications: The operating temperature range of the transmitter is from -25° C to +70° C. The transmitter will be able to withstand a steady vibration of 20 g in the frequency range of 20 to 2000 Hz on all 3 axis. The transmitter will also be able to withstand a shock load of 100g.

Mechanical specifications: The dimensions of the transmitter will be 3.50"×2.50"×1.34" with a weight of 0.45 kg. The power and modulator connectors are Bendix PT1H-8-4P which mates with Bendix PT06A-8-4S. The RF output connector is a TNC 7/16-28 THD which mates with TNC Male.

6.6.2 Link Budget

Signal Characteristics

The Signal characteristics of the transmitted signal are given in Table 6-18.

Table 6-18 : Signal Characteristics

Frequency	Power Output	RF Bandwidth	Modulation Type	Speed Channel	Receiver Characteristics
2.215 GHz	2 W	35.232 kHz	BFSK	17.616 kb/s	BFSK threshold: (C/N) = 0 dB

Since most systems do not use isotropic antennas, the transmitted power in a preferred direction with some gain G is replaced by the *effective isotropic radiated power* (EIRP) which is given by:

$$\text{EIRP} = P_{tx} * G$$

Where P_{tx} is the transmitted power and G is the gain of the antenna.

There are two possible cases:

- 1) $G_{tx} = 0\text{dB}$ When rocket is pointing sideways to ground station.
- 2) $G_{tx} = -6\text{dB}$ When rocket is pointing away from the ground station.

G_{tx} is the transmitted antenna gain with respect to an isotropic antenna.

The effective isotropic radiated power, EIRP is given by the following equation

$$\text{EIRP in dB} = P_{tx} - L_{tx} + G_{tx}$$

Where P_{tx} is the Power transmitted, L_{tx} is the Loss due to Transmission.

$$= 33.01 \text{ dBm} - 2\text{dB} + G_{tx} \text{ dB}$$

$$1) \text{EIRP} = 31.01\text{dBm}$$

$$2) \text{EIRP} = 25.01 \text{ dBm}$$

Space loss is the intensity of the transmitted power decreases with increasing distance. For the link budget, the normal $1/r^2$ power falloff with the wavelength of the radiation to form a dimensionless quantity called the space loss, L_s , which is given as:

$$L_s = 92.44 + 20\log D + 20\log F$$

where D is the distance in km and F is the frequency in GHz. For the case of ARIM-1 the space loss is:

$$L_s(100 \text{ km}) = -139.35 \text{ dB}$$

Received signal strength, in dB is given by:

$$P_{rx}(\text{dB}) = \text{EIRP} - L_s + G_{rx} - L_{rx}$$

where P_{rx} is the Power received and L_{rx} is the loss at the receiver, which for our case $L_{rx} = 1\text{dB}$.

$$1) P_{rx} = -109.34 \text{ dBm}$$

$$2) P_{rx} = -115.34 \text{ dBm}$$

Using the LNA with a gain of 30 dB the following received signal strength was calculated.

$$1) P_{rx} = -79.34 \text{ dBm}$$

$$2) P_{rx} = -85.34 \text{ dBm}$$

The Noise figure for the LNA is 1.5 dB. The noise figure for the receiver operating at a frequency of 2.215 GHz is about 12 dB.

System temperature:

$$T_i = (F_i - 1) * T_o$$

(5-28)

$$T_1 = (1.2589 - 1) * 290K = 75.088 K$$

$$T_2 = (1.4125 - 1) * 290K = 119.63 K$$

$$T_3 = (15.848 - 1) * 290K = 4306 K$$

$$T_{\text{effective}} = T_e = 75.088 + 1.2589 * 119.63 + 1.2589 * 4306 / 1000 = 231 K$$

$$T_s = T_{rx} + T_e = 290 + 231 = 521 K = 1.79655 * T_o$$

Signal to noise ratio (S/N) is a relative power of the signal to the noise in a channel, usually measured in decibels. The equation below provides the mathematical definition.

$$\text{Signal to noise ratio (S/N)} = P_{rx} / k * T_s * B_t$$

where k = Boltzman's constant, power received (P_{rx}) in Watts, $B_t = 35.232$ kHz for a bit rate of (R_b) = 17.616 kb/s and BPSK modulation, For this case, $P_{rx} = -109.344$ dBm = $1.163 * 10^{-14}$ W

$$1) (a) (S/N)_R = 1.163 * 10^{-14} / [4 * 10^{-21} * 1.79655 * B_t] = 16.61 \text{ dB}$$

$$2) (a) (S/N)_R = 10.61 \text{ dB}$$

The carrier-to-noise ratio(C/N) is given as:

$$C/N = EIRP + L_s + G_{rx} + 228.6 - 10\log(T_s) - 10\log(B_t)$$

$$1) (C/N) = 47.61 \text{ dB}$$

$$2) (C/N) = 41.61 \text{ dB}$$

The *bit error rate* (BER) is the usual criterion for evaluating the performance of a digital modulation system. The derivation of the probability of error in terms of the input SNR is derived in most digital communications. The results are presented below:

For BFSK and QFSK, the relationship between the signal strength, noise, and probability of error is given in terms of the complementary error function $Q(x)$ by

$$p_e = Q([2E_b/N_o]^{1/2})$$

where, $Q(x) \approx [(1 - 0.7/x^{1/2})/x(2\pi)^{1/2}] \exp(-x^{1/2}/2)$, and (E_b/N_o) or γ_b is the energy per bit to noise spectral density, which is given as:

$$E_b/N_o = EIRP + L_s + G_{rx} + 228.6 - 10*\log(T_s) - 10*\log(R_b)$$

where $R_b = 17,616$ b/s

- 1) $(E_b/N_o) = 50.61 \text{ dB}$
- 2) $(E_b/N_o) = 56.65 \text{ dB}$

In case of 56.65 dB the probability(p_e) is about 10^{-12} .

Fading is the intensity fluctuation of any or all components of a received radio signal due to changes in the characteristics of the propagation path. The fluctuation will be mainly from antenna pointing errors. Other errors are negligible, e.g., the margin from a rain attenuation term is less than -0.01 dB.

$(E_b/N_o) = (C/N) * (B_t/R_b)$. For the Microdyne-1400 receiver the minimum sensitive level in case of BFSK demodulation is $(C/N) = 0 \text{ dB}$. Therefore minimum $(E_b/N_o)[\text{dB}] = (C/N) + 10\log(B_t/R_b) = 0 + 10\log(2) = 3.01 \text{ dB}$

Fade margin(F_d) is mathematically defined as

$$F_d = (E_b/N_o)_{\text{available}} - (E_b/N_o)_{\text{required receiver characteristic}}$$

- 1) $F_d = 47.60 \text{ dB}$
- 2) $F_d = 41.60 \text{ dB}$

Safety factor(S_f) is mathematically defined as

$$S_f = P_{tx}[\text{dBW}] + G_{tx} + G_{rx} - (S/N) - B_f - L_s - L_1$$

where $(S/N) = 13 \text{ dB}$ in the case of PCM/FM, L_1 is the loss between receiving antenna and low noise amplifier (LNA), and $B_f = 10\log(k * T_s * B_t) = -156 \text{ dBW}$.

- 1) $S_f = 6.45 \text{ dB}$
- 2) $S_f = 0.45 \text{ dB}$

Table 6-19 : Receiving signal characteristics at 25 km for case1/case2

EIRP	31.01 dBm / 25.01 dBm
Space loss	-127.3 dBm
Rx signal strength (antenna output)	-97.3 dBm / -103.3 dBm
System temperature	521 K
S/N ratio	28.66 dBm / 22.66 dBm
C/N ratio	59.65 dBm / 53.65 dBm
E_b/N_o ratio	62.65 dBm / 56.65 dBm
Safety factor S_f	18.49 dB / 12.49 dB
Fade margin F_d	59.64 dBm / 53.64 dBm

6.6.3 Transmitting Antenna

The transmitting antenna is a wraparound S-band patch antenna with a 6 inch outer diameter, 0.5 dBi maximum gain, and an input impedance of 50Ω . This antenna is mounted on the outside of the inner nosecone and radiates through the outer nosecone on the ascent phase, but is open to the atmosphere after the payload's outer skin is disengaged.

7. Ground Station

7.1 Umbilical System

Communication with the rocket while it is on the launch pad will be done with the use of the umbilical cables that connect the blockhouse to the launcher. These cables use two 37 pin female cannon style plugs. One is at the launcher, the other one is in the block house. There are 5 channels labeled A through E. Any one of them can be used as long as the two cannon plugs connect in the same channel at the block house and the launcher. The rocket's battery voltage will be monitored with this system as well as the operation of the flight computer. The rocket's sequence board program will be down-loaded from a computer in the blockhouse via this system in order to compensate for temperature differences that may change the flight time to apogee just prior to launch.

7.2 Telemetry Receiver

A Microdyne 1400-MRA telemetry receiver will be used at the telemetry station. This unit operates in the frequency range of 1600-1750 MHz or 2200-2300 MHz when used with the model 14515 multi-band RF tuner. This receiver has a noise figure of 12 dB and will demodulate FM, PM, BPSK, and QPSK signals.

7.3 Low Noise Amplifier

A Mini-Circuits ZHL-1724HLN amplifier will be used as a preamplifier in the telemetry system. This amplifier will operate in the frequency range of 1700-2400 MHz and has a noise figure of 1.5 dB. The power gain for this amplifier is 30 dB and the maximum output power is 26 dBm.

7.4 Ground based GPS

The ground station will use a Motorola VP Oncore 8-channel GPS receiver module that is included in the VP evaluation kit. This unit can track 8 satellites simultaneously and has a position accuracy of 0.7 to 0.8 meters in the Differential Global Positioning System (DGPS) mode. The VP-8 operates on 5 Vdc regulated with a power consumption of 1.1 Watts. This unit is capable of outputting the raw position data that is required to obtain the position accuracy stated above. This unit will be used to calculate a DGPS position for the rocket during flight. The position from this system will not be as accurate as the position obtained during post-flight, but it will be available on a pseudo-real-time basis.

7.5 Ground Based Computers

The ground station will require two computer systems. One system will act strictly as an archival unit, while the other one will provide a graphical display of specific data in real time. A description of the computers need and the software tasks are provided below.

1) The archival system should be an IBM compatible system with the following minimum system specifications.

- Pentium Processor
- Memory 16 Mb
- Hard disk: minimum 500 Mb
- Multi I/O card
- Super VGA card and monitor

2) The graphic display terminal should be an IBM compatible system with the following minimum system specifications.

- 486 DX machine with 50 MHz
- Hard disk 250 Mb
- Multi I/O card
- Super VGA card and monitor
- Memory 8 MB

7.5.1 Ground Support Software

The Ground Station terminals will be using the following software packages:

Archival Software:

This software is mainly used to archive all of the data collected by the rocket during the entire flight. In addition, the archival software is also responsible for recording the data from the ground GPS.

Graphic Display Software:

This software's main purpose is to provide a graphical depiction of a majority of the data. In addition, this software package will receive the data packets from both GPS units and perform the differential technique.

7.5.2 Software Size and Throughput

The software size is measured in terms of memory and processing time in terms of throughput, usually expressed in millions of instructions per second (MIPS). The reason for estimating the size and throughput of on-board software is to determine how much computing power is needed to perform the mission. After we have established requirements for computer resources, we monitor the actual software requirements to make sure they don't exceed the hardware capability. The size estimate is also used to estimate cost.

The computer's capacity for throughput mainly depends on its clock speed and instruction mix. If there is only one instruction, a computer's throughput would be proportional to clock speed. If it has two instructions as given below:

- Instruction A requires 2 clock cycles
- Instruction B requires 7 clock cycles

The computer's throughput also depends on the instruction mix. The instruction mix is the proportion in which the software uses the instruction.

For example, if the software is 35% type A instruction and 65 % type B instruction, the throughput available with a 20 MHz clock is $(20 / \{0.35 * 2\} + (0.65 * 7)) = 3.80$ MIPS. If the instruction mix is reversed, i.e., 65% type A and 35% type B, the throughput available is 5.33 MIPS. So it can be seen that the throughput mainly is dependent on the software.

Previous missions have proved that early estimates of requirements are uncertain at best. In addition, changes in software are easier than in hardware during late stages of spacecraft development. Spare memory and throughput is also required at launch to correct anomalies or to increase performance after system calibration. Thus, we need to establish reserve capacity when initially defining requirements. Refer to

Figure 7-1 at the end of this section. So in ARIM-1 the instrumentation is sampling data at 1000 samples/sec with 16-bit resolution. The storage required for one hour of data is approximately:

$$1000 \text{ samples/sec} * 2 \text{ bytes} * 3600 \text{ sec} = 7.2 \text{ Mb}$$

Similarly other sources like housekeeping instrumentation, pressure, temperature, humidity, and the digital status bits will be sampled at 1 sample/sec at 1 byte which comes to approximately 1-2 Mb. So a minimum of 10 Mb of permanent memory is required for this mission.

7.5.3 Data Analysis

The ground station archival computer will be receiving two kinds of data.

- High speed data from the rocket
- slow speed data (128 bytes/sec packet) from the ground GPS

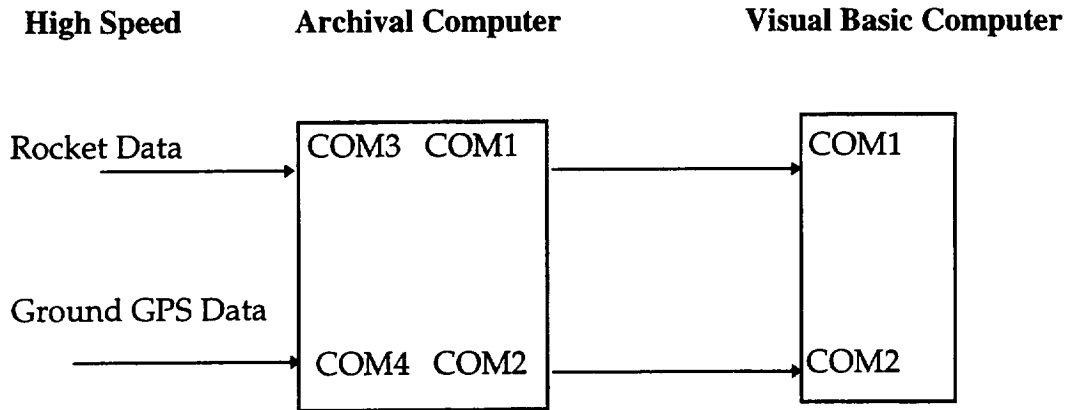


Figure 7-1 : Ground based Computer Configuration

The archival computer, which has an Intel Pentium processor, will require a high speed multi I/O card in order to accept data from the rocket. So the data from the rocket and the ground GPS will be input to the Pentium through the COM3 and COM4 ports which are the serial ports of the high speed I/O card. The Visual Basic Computer will not be able to accept and display all the high speed data instantly. In addition, it is imperative that the ground-based GPS data must be synchronized in time with the on-board GPS data to perform accurate differential GPS measurements. This is complicated by inherent delays within this data collection system. The rocket's collection and transmission of the data, the receivers demodulation, and the insertion of the archival computer all have associated time delays. Among these delays the one associated with the archival computer is the only one that can most easily be adjusted. Therefore, the archival computer will be responsible for assuring the coalition in time the two GPS packets.

8. Testing Plans

ARIM-1 will be subjected to three levels of testing. The design verification tests are intended to verify that each module does indeed function for the task it was designed. The integration test will then combine all the modules in order to verify the proper operation of the entire system. Finally, the environmental test will confirm that the payload will operate in the environment that it will be subjected to during the flight.

8.1 Design Verification Tests

The DVT test plan is intended to demonstrate that each of the electrical subsystem modules operates as designed.

8.1.1 Battery Module Test.

Description

This is a standalone functional test of the battery pack.

Success Criterion

The battery pack must supply 40 W for two hours.

Test Procedure

1. Fully charge battery pack. (Not applicable for primary non rechargeable batteries.)
2. Attach 20 W, 50 W load resistor to battery pack.
3. Measure battery terminal voltage.
4. Battery voltage must stay above 27 V for two hours.

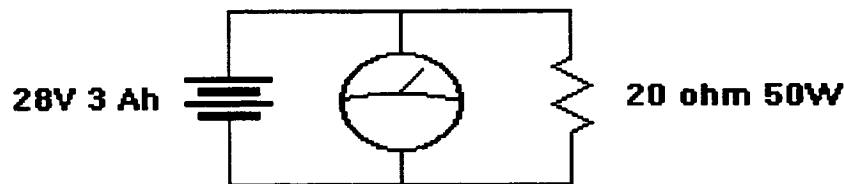


Figure 8-1 : Battery Test Setup

Note: This is a destructive test if the batteries used are primary non-rechargeable.

8.1.2 Power Regulator Module Test

Description

This is a standalone functional test of the power regulator circuitry.

Success Criterion

Regulator output voltage must not drop below 95% of the nominal value. For example, if a +5V power supply is specified to deliver 400 mA, the voltage must not drop below 4.75V with a 440 mA load.

Test Procedure

1. Attach regulator board to 28V 2A power supply.
2. Attach a load resistor scaled to draw 110% of rated current to each regulator circuit.
3. Measure output voltage from each regulator circuit.

Note: Reference the power supply specification for nominal voltage and current ratings for each regulator circuit.

Note: All regulator outputs should be loaded tested simultaneously to test for inter-circuit effects.

8.1.3 EED Driver Module Test

Description

This is a standalone test of the EED driver circuits.

Success Criterion

Each EED circuit must deliver the recommended firing current for the particular EED. The duration of the firing pulse must exceed the minimum required value by a factor of five. For example, an EED driver for the Horex model 2900 Linear Actuator must deliver 5 A for 35 ms.

Test Procedure

1. Attach regulator board to 28V 2A power supply.
2. Attach EED driver board to regulator board.
3. Attach EED equivalent circuit load to EED driver output.
4. Attach digital storage oscilloscope across EED equivalent circuit load.
5. Activate charge circuit and allow capacitor banks to fully charge.
6. Trigger the EED driver circuit.
7. Observe the oscilloscope display.
8. Repeat test for each EED driver circuit.

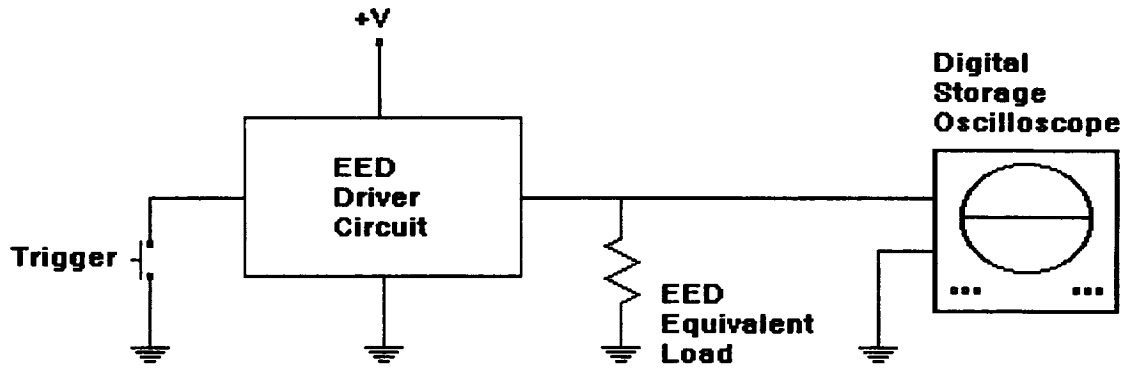


Figure 8-2 : EED Driver Test Setup

Note: Reference the particular EED data sheets for firing voltage, current, and time ratings.

8.1.4 Instrumentation Module Test

Description

This is a standalone functional test of the science analog data conditioning circuitry.

Success criteria

Each signal conditioner output must remain within the range of 0 to 5V over the entire operating input range.

8.1.5 Flight Computer Module Test

Description

This is a standalone functional test of the flight computer hardware and software.

Success criteria

1. Each analog input must be represented correctly in the telemetry data stream.
2. Each digital input must be represented correctly in the telemetry data stream.
3. GPS data must be represented correctly in the telemetry data stream.
4. Each actuator output must be activated at the proper time.

Test Procedure

1. Attach the flight computer with loaded flight software to a 5V 1A power supply.
2. Patch the telemetry serial port output to a ground station computer with telemetry analysis program loaded and running.
3. Attach LED indicators to actuator outputs.
4. Attach potentiometers to analog telemetry inputs.
5. Attach switches to digital telemetry inputs.
6. Attach GPS receiver module to serial telemetry input.
7. Power on the flight computer.
8. Stimulate each telemetry input and verify it is updated correctly in the telemetry data stream.
9. Observe LED indicators to verify proper actuator sequencing.

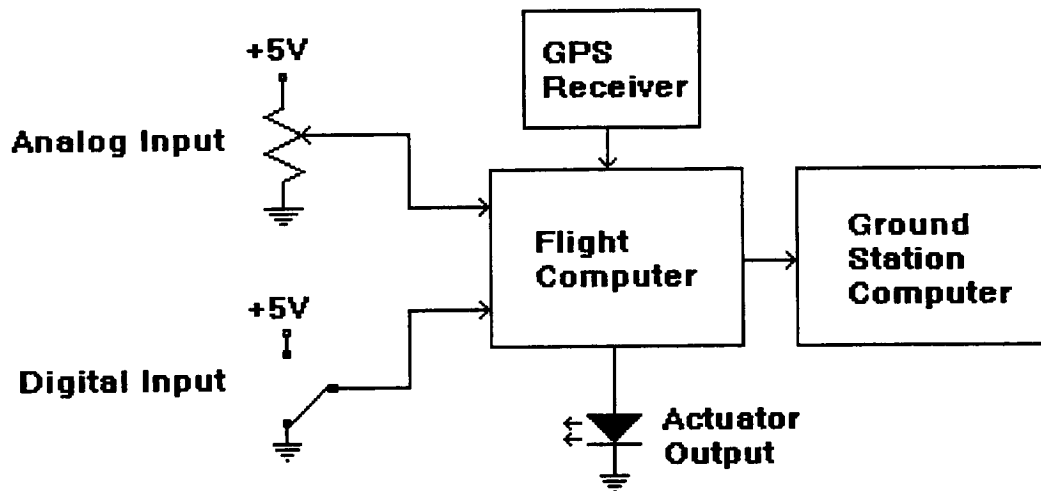


Figure 8-3 : Flight Computer Test Setup

8.1.6 Transmitter Module Test

Description

This is a standalone test of the telemetry transmitter.

Success Criterion

The transmitter must deliver 1 W at 2.3 GHz with +/- 1.5 MHz deviation at TTL input levels.

Test Procedure

1. Attach transmitter to 28V 2A power supply.
2. Attach power meter and dummy load to transmitter output.
3. Connect transmitter data input to ground.
4. Measure output power and frequency
5. Connect transmitter data input to +5V.
6. Measure output power and frequency.

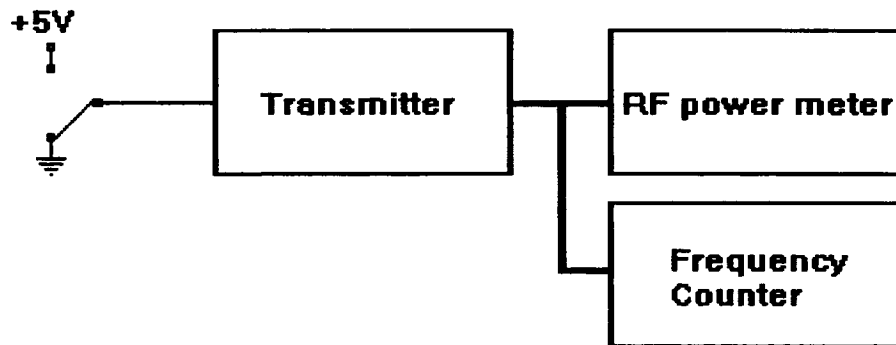


Figure 8-4 : Transmitter Test Setup

8.1.7 Receiver Subsystem Test

Description

This is a standalone functional test of the receiver subsystem. It is not practicable to test the low noise preamplifier, receiver and demodulator independently so they are tested together.

Success Criterion

Receiver subsystem must deliver byte error rate of less than one byte per ten thousand at a received signal level of -111 dBm at the input of the low noise preamplifier.

Test Procedure

1. Connect a computer running a 128 kbps serial data pattern generator based on a random number generator to the modulation input of an FM signal generator.
2. Adjust the signal generator to a center frequency of 2.2 GHz and frequency shift of 1.5 MHz. Adjust the output signal level to -111 dBm. Additional external attenuation may be necessary.
3. Connect the signal generator output to the input of the low noise preamplifier of the receiver subsystem.
4. Connect the baseband TTL output of the receiver subsystem to the input of a second computer running a data analyzer program based on the same random number generator as the first computer.

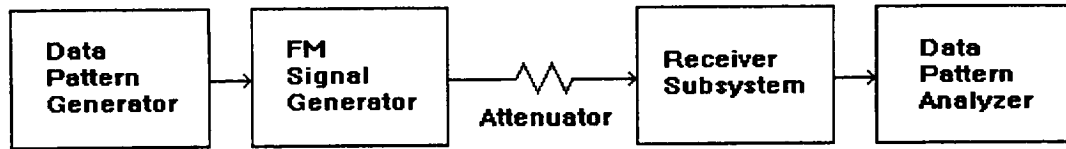


Figure 8-5 : Receiver Subsystem Test Setup

8.2 Environmental Test Plan

The environmental test plan will prove that the payload electronics will operate correctly in the space-flight environment. Hostile conditions in that environment include temperature, pressure, moisture, and radio frequency interference.

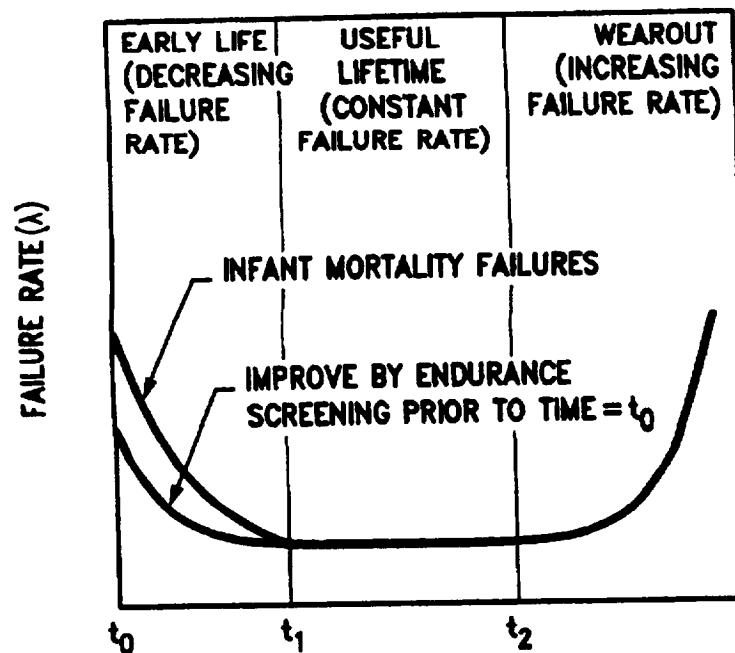


Figure 8-6 : Component Failures over Time

An important part of the environmental test is burn-in. Burn-in attempts to ameliorate a phenomenon known as infant mortality. The diagram in Figure 8-6 is a plot of failure probability over time and illustrates this.

The burn-in test seeks to operate all of the payload electronics past the infant-mortality zone. This minimizes the chances of an in-flight failure.

8.2.1 Temperature Cycle Test

Description

This test subjects the payload electronics to the extreme limits of operating temperature. It also subjects the payload electronics to thermal expansion stress in

order to break any marginal solder joints or components before the actual mission flight.

Success Criterion

Payload electronics must operate correctly for the duration of the test.

Test Procedure

1. Attach payload assembly to a 28V 2A power supply.
2. Attach 50 ohm dummy load to transmitter.
3. Place receiving sense antenna near the transmitter dummy load.
4. Attach receiving sense antenna to ground station receiver.
5. Attach ground station receiver to ground station computer.
6. Start ground station computer telemetry monitor program.
7. Turn on payload electronics.
8. Chill payload assembly to -45 °C.
9. Heat payload assembly to 65 °C.
10. Repeat steps 8 and 9 for at least 72 hours.

8.2.2 RFI Susceptibility Test

Description

This test proves that the payload is not adversely affected by its own transmitters.

Success Criterion

The GPS receiver and flight computer must operate correctly with all on-board transmitters keyed.

Test Procedure

1. Hang the payload in a fashion similar to the under-parachute data collection configuration.
2. Place receiving sense antenna near the transmitter dummy load.
3. Attach receiving sense antenna to ground station receiver.
4. Attach ground station receiver to ground station computer.
5. Start ground station computer telemetry monitor program.
6. Turn on payload electronics.
7. Verify correct telemetry, especially GPS data.
8. Key the auxiliary transmitters (FAA transponder, Radar transponder, and recovery beacons) one at a time and verify correct telemetry.

8.3 Integration Test Plan

Description

This procedure successively adds electronic subsystem modules together and verifies the whole system functions correctly.

Success Criteria

The whole system must function correctly.

Test Procedure

1. Measure output voltage of battery module. Must be 28V +/- 10%.
2. Attach the umbilical box to the umbilical module.
3. Attach the umbilical module to the battery module.
4. Verify that the main power bus can be turned on and off from the umbilical box.
5. Attach power regulator module to umbilical module switched +28V output.
6. Turn main power on via the umbilical box.
7. Measure output voltages of power regulator module. Each output must be +/- 5% of nominal value.
8. Attach GPS antenna to GPS receiver module.
9. Attach GPS receiver module to power regulator module.
10. Measure +5V regulator output voltage again. It must be +5V +/- 5%.
11. Probe GPS time mark pulse output and serial data outputs with an oscilloscope to verify the GPS receiver is operating.
12. Attach flight computer assembly (stack of three PC/104 boards) to the power regulator module.
13. Measure +5V regulator output voltage again. It must be +5V +/- 5%.
14. Probe flight computer serial data output with an oscilloscope to verify the flight computer is operating.
15. Attach GPS time mark pulse output and serial data output to the flight computer board.
16. Temporarily patch the flight computer serial data output to the archive computer. Verify that telemetry data is being received correctly by the archive computer.
17. Attach instrumentation board to the power regulator.
18. Measure output voltages of power regulator module again. Each output must be +/- 5% of nominal value.
19. Attach sensors to the instrumentation board.
20. Measure instrumentation board output voltages. Each output must be within the range 0 to 5V. Exercise each sensor and verify that the output voltage remains within the range 0 to 5V.
21. Attach instrumentation board outputs to A/D board inputs.
22. Exercise each sensor and verify that its value is updated correctly in the telemetry data stream.

23. Attach EED equivalent circuit loads to the outputs of the EED driver module.
24. Attach the EED driver module to the power regulator board and umbilical board.
25. Trigger the capacitor charge circuit and verify the capacitor charge level with a voltmeter.
26. Trigger the capacitor discharge circuit and verify the capacitor charge level with a voltmeter.
27. Turn off main power from the umbilical box.
28. Attach the EED driver module to the flight computer.
29. Attach jumper wires to the lanyard switch, and separation switch inputs.
30. Turn main power on from the umbilical box.
31. Verify the flight computer is sending telemetry data include GPS data.
32. Trigger the capacitor charge circuit.
33. Observe the timing sequence of the EED outputs to verify the sequence logic is operating correctly.
34. Observe the telemetry data to verify that the telemetry mode changes correctly.

9. Mission Implementation

In order to implement a project of this magnitude first requires an enormous amount of planing, scheduling, and an assessment of available resources. The first step taken in planning this project was to develop a management structure to lead the implementation team. Next, a logical block diagram and Work Breakdown Schedule (WBS) was generated to outline the course of the project. From this an implementation schedule was constructed to identify milestones. Finally, a cost estimate was generated.

9.1 Managerial Overview

ARIM-1 will be implemented by the Alaska Student Rocket Program and therefore be using students to provide more detailed designs and undertake the fabrication of the vehicle. This offers students the opportunity to gain hands on experience with real word engineering problems. However, students only attend college on an average of four years and are typically not involved with the program for more than three. In addition, the rocket is not intended to be completed for two years. This means several students will graduate during the implementation of ARIM-1. Therefore, it is imperative to continually enlist new students and bring them up to speed prior to the loss of a key member, in order to minimize any disturbance in the project during transitions. There is also a handful of program members that consist of faculty and staff which handle aspects of program funding, and aid in the perpetuation of the program.

The personnel structure in Figure 9-1 was generated based upon the logistical tasks in need of the most attention and the small amount of stipend hours available. The organizational chart below depicts the personnel structure that will be used for the implementation of ARIM-1.

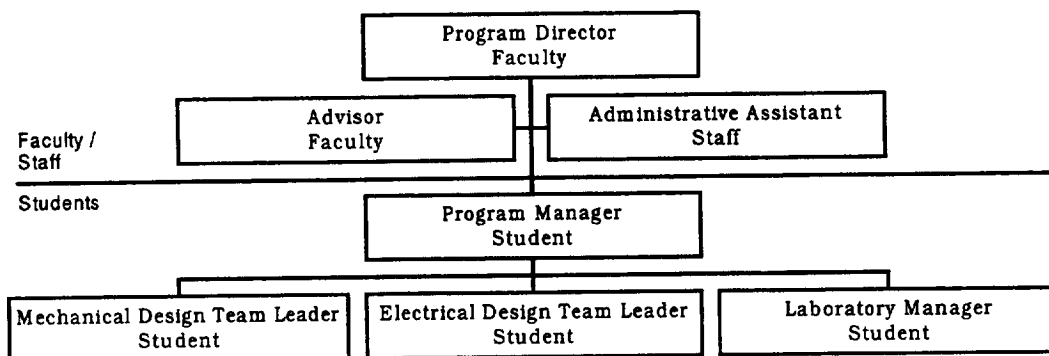


Figure 9-1 : Personnel Structure

The organizational chart in Figure 9-1 shows both faculty and student positions. The faculty perform a lot of administrative tasks and keep the program operating over the years. This is necessary because of the high turnover rate of students. It is not unusual for a student to only be with the

project for a total of one year or even one semester. The student positions in the chart above are all funded and consume the logistical tasks necessary to keep the program running smoothly. Obviously, the program will require more than four students to complete the project. Therefore, the program is still heavily depended upon volunteer labor. However, past experience dictates that the logistical tasks should be covered first because it is easier to find volunteers for the technical tasks in need of attention. Job descriptions for the four student positions listed in Figure 9-1 are shown below.

Project Manager:

- ◆ Track the status of all aspects of the project; monitor completion of all action items; shift project resources as needed to insure that project is completed in a timely fashion.
- ◆ Prepare comprehensive schedule for project and update weekly and post in SRP lab.
- ◆ Coordinate weekly meetings; prepare and distribute agenda for each meeting.
- ◆ Prepare a comprehensive budget for the project; monitor all purchase orders that are submitted; prepare a weekly status report of all expenditures to date and compare with budget.
- ◆ Maintain a list of design team members and project assignments; maintain a list of outstanding projects available for assignment to new design team members.
- ◆ Delegate an editor for each technical document who will be responsible for coordinating the assembly and technical accuracy and orderly presentation prior to submission for publication.
- ◆ Coordinate, or delegate the coordination, of range and flight safety plans with Poker Flat Research Range
- ◆ Coordinate all systems-level tests of payload

Mechanical Design Team Leader:

- ◆ Coordinate usage of SOE machine shop by SRP on a non-interference basis
- ◆ Provide or delegate training on mechanical fabrication techniques to new team members.
- ◆ Conduct walk-through of all mechanical subsystems, including review of mechanical drawing and fabrication techniques, prior to fabrication.
- ◆ Provide quality assurance of all mechanical fabrication
- ◆ Approve results of testing for each completed component

Electrical Design Team Leader:

- ◆ Coordinate timely return of any equipment borrowed for EE department.
- ◆ Provide or delegate training on electrical fabrication techniques to new team members.
- ◆ Conduct walk-through of all electrical subsystems, including review of schematic drawing and PCB layout, prior to fabrication
- ◆ Provide quality assurance of all electrical fabrication
- ◆ Approve results of testing for each completed component.

Laboratory Manager:

- ◆ Insure lab remains neat and orderly at all times
- ◆ Maintain critical supplies of frequently used commodities
- ◆ Maintain inventory of equipment
- ◆ Maintain file of Material Safety Data Sheets
- ◆ Maintain library and database of technical information
- ◆ Maintain archive of ASRP documents

Basically, it is the responsibility of the four students above to assure the project operates smoothly from the assignment of labor to the working conditions of the lab.

9.2 Logical Project Breakdown

Producing a schedule to actually implement this project can be broken down into three parts. One, produce a logical block diagram which provides a graphic depiction of the tasks to be completed. Two, produce a Work Breakdown Schedule (WBS) from the block diagram, which identifies the individual tasks. Three, use the WBS to generate a Gantt chart by identifying tasks that can be completed in parallel and assigning a time duration to all of them.

A logical block diagram is just as explained above, a breakdown of major tasks to be completed in order to finalize the project. The logical block diagram shown in Figure 9-2 was developed for ARIM-1.

STUDENT ROCKET PROJECT III

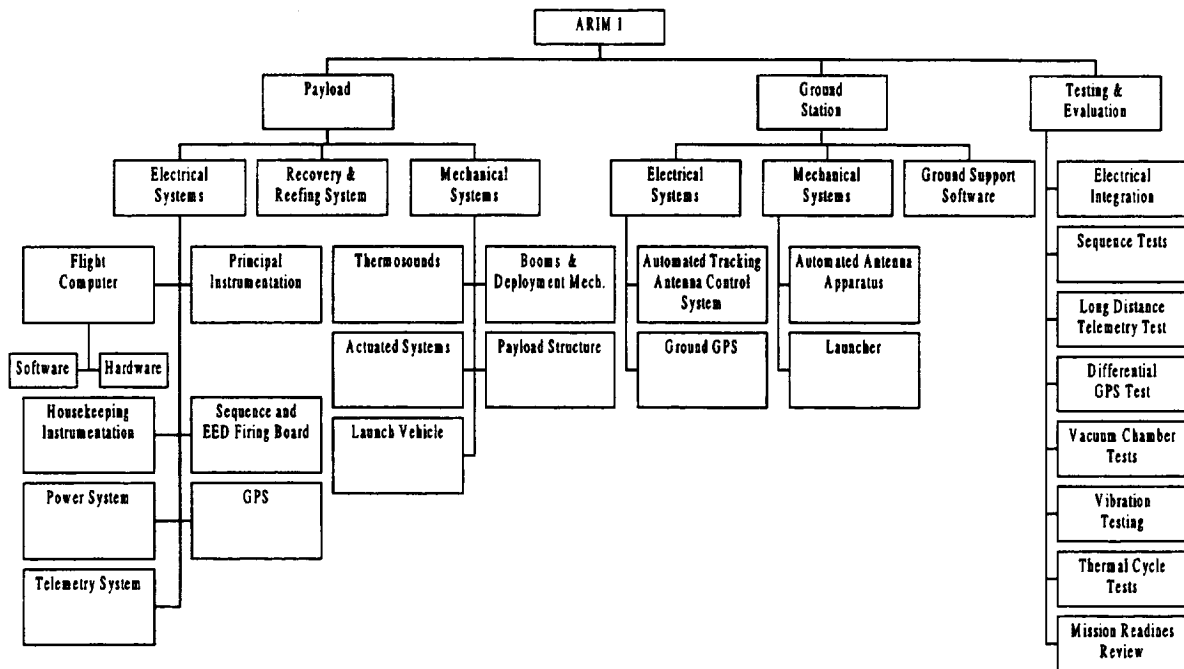


Figure 9-2 : Logical Block Diagram for ARIM-1

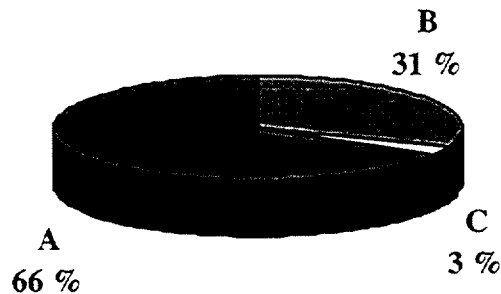
The Work Breakdown Schedule serves two purposes. The first is to subdivide the logical blocks from the diagram in Figure 9-2 into individual tasks. The second is to provide a level of responsibility to the members of the ARIM-1 implementation team. However, the second purpose is a function of time due to the high turnover rate of students. Therefore, it is impossible to assign any responsibility without prior knowledge of the available human resources. Furthermore, the work breakdown schedule will be a growing document and intended to be altered to reflect the actual tasks performed throughout the course of the project.

As stated above the Gantt chart then identifies which of these tasks can be completed in parallel and assigns a time duration, start date, and completion date to each of them. This then provides a timeline for the entire project. It is typical for a Gantt chart to provide a graphical depiction of the project over time. However this type of representation consumes an enormous amount of space. Therefore, only a preliminary list of tasks to be completed with man hour estimations has been included in appendix B of this report.

9.3 Estimated Cost Analysis

Similar to the work breakdown schedule the cost analysis is difficult to know at the beginning of the project. However, price quotes were gathered and man hour estimations based on previous experience were made. From this information an Estimated Cost Analysis (ECA) was generated for the project. This ECA is in appendix B which is attached to the end of this report. However, the pie chart below

provides a graphical depiction of the project's cost breakdown. It is intended that an itemized budget be maintained throughout the entire course of the project.



A. Student Labor - \$74,000
B. Parts and Supplies - \$37,200
C. Contracted Labor - \$3,200
Total Project Cost - \$114,400

Figure 9-3 : Project Cost Analysis.

It is obvious, from the figure above that the costs of student labor is by far the largest. This emphasizes the need to minimize student labor by purchasing an off the shelf item whenever possible vs. fabricating it in the lab. In addition, the parts and supplies costs do not include any infrastructure costs such as new computers and other equipment.

9.4 Mission Success Criteria

9.4.1 Comprehensive

The complete success of the science mission requires that all of the following items are accomplished.

- The proper operation of the differential temperature sensors.
- Successful deployment of the temperature sensor support booms.
- Parachute deployment and stabilization near 82,000 feet is needed for high-altitude data acquisition. Achieving a parachute descent rate of 5 m/s or less from 48,000 feet (15 Km) to touch-down.
- Proper operation of the absolute temperature, pressure and humidity sensors.
- Proper operation of the transmitter.
- Proper operation of the on-board storage system.

9.4.2 Minimum

Valid science data may be obtained in the event of a component failure, however, the resulting data may have different parameters than the designed data. For example, if a partial failure of the main parachute occurs then the descent rate may be greater than 5 m/s resulting in a degraded altitude resolution. The following list contains the minimum conditions for data (possibly degraded data) collection.

- Proper operation of the differential temperature sensors and the boom deployment system.
- Operation of either the on-board data recovery system or the transmitter.
- If the transmitter fails then recovery of the pay load is essential.
- A partial failure of the parachute may not cause a complete mission failure providing that the resulting descent rate is not excessive (say < 15 m/s).

REFERENCES

1. Allnutt, J. A., Satellite-to-Ground Radiowave Propagation, BPCC Wheatons Ltd, Exeter, UK, 1989.
2. Cadet, Daniel, "Energy Dissipation Within Intermittent Clear Air Turbulence Patches", Laboratoire de Meteorologie Dynamique, Ecole Polytechnique, 91120 Poaaisau, France, 1977.
3. Good, R. F., Brown, J. H., Quesada, A. F., Watkins, B. J. and Laariot, G. B., "Intercomparison of Cn2 Profile Measurement Techniques", Aeronomy Division, Air Forde Geophysics Laboratory, Hanscom AFB, MA 01731, 1982.
4. Hills, Robert S., "Research, Design and Development Study to Measure Atmospheric Optical Turbulence", Tri-Con Associates, Inc., Cambridge, Massachutts, 1982.
5. Perry, A. E., Hot Wire Anemometry, Oxford University Press, New York, 1982.
6. Bradshaw, P., An Introduction to Turbulence and its Measurement, Pergamon Press Inc., New York, 1971.
7. McGee, Thomas D., Principles and Methods of Temperature Measurement, John Wiley and Sons, New York, 1988.
8. Regan, Frank C., Jr., "Technical Support for Optical Turbulence Research", Systems Integration Engineering, Inc., Lexington, MA, 1988.
9. Watkins, B.J., and Wand, R.H., "Observations of Clear Air Turbulence and Winds With the Millstone Hill RADAR", Journal of Geophysical Research, vol.86, number C10, pages 9605 to 9614, October 20, 1961.

Appendix A



Recovery System Supplements

References

1. J. Cockrell. "The Aerodynamics of Parachutes," AGARDograph No. 295, available from National Technical Information Service (NTIS), 5285 Port Royal Road, Springfield, Virginia 22161.
2. F. Doherr, "Parachute Trajectory Simulation and Analysis", University of Minnesota 1990 Parachute Systems Technology Short Course. (Includes source code for five computer programs in pascal, basic, and fortran. (1)-"2DOFGAMA", (2)-"2DOFTIME", (3)-"SNATCH", (4)-"OSCILxxx", and (5)-"SIXDSIM". These are 2, 3, and 6 degree of freedom trajectory analysis programs for a parachute recovery system).
3. Ewing, E. G., Bixby, H. W. and Knacke, T. W., Recovery Systems Design Guide, AFFDL-TR-78-151, December 1978.
4. L. Garrad. "Application of Inflation Theories to Preliminary Opening Forces and Stress Analysis." Paper presented at the University of Minnesota-CCG lecture on parachute systems technology, Munich-Oberpfaffenhofen, June 1987.
5. W. Higgins. "Recovery System Preliminary Design. A Simplified Approach to Determining Drogue Chute Staging, Timing, and Altitude requirements" AIAA Paper, March 1979. (AIAA 79-0446).
6. Industrial Solid Propulsion, Inc. Viper V Sounding Rocket Motor Technical Data. Las Vegas, Nevada. 1995.
7. W. Johnson. "Evolution of the Recovery System for High Altitude Sounding Rockets," Journal of Spacecraft and Rockets, Vol. 6, No. 4, April 1969, pp. 489-491.
8. W. Johnson. "A Recovery System for the Sandia Hawk Series of Sounding Rockets," AIAA Paper No. SC-65-470(RR), November 1965.
9. F. Jorgenson and D. J. Cockrell. "Aerodynamics and Performance of Cruciform Parachutes," AIAA Paper, October 1981, (AIAA 81-1919).
10. C. Maydew & C. W. Peterson. Design and Testing of High-Performance Parachutes. AGARDograph 319, (available from National Technical Information Service NTIS), 5285 Port Royal Road, Springfield, Virginia 22161, November 1991, 289 pages.
11. Meyer. "An Introduction to Deployable Recovery Systems." Sandia Report No. (85-1180), August 1985, 33 pages.
12. Naval Air Development Center. AN/SSQ-41, "Two Stage Parachute System," by E. Reed, III. Johnsville, Pa., NADC, October 1972, (NADC-72-174-VT).
13. Naval Ordnance Laboratory. Effects of Canopy Geometry on the Infinite Mass Opening Shock of a cross Parachute With a W/L Ratio of 0.264, by W.P. Ludtke. NOL, July 1973. (NOL TR 73-157).

14. NASA. "Sounding Rocket User's Handbook" Goddard Space Flight Center, Wallops Flight Facility, September 1988.
15. NOAA, NASA, and U.S. Air Force. Standard Atmosphere, 1976. U.S. Government Printing Office, Washington, D. C., October 1976.
16. Naval Ordnance Laboratory. "Effects of Canopy Geometry on the Spinning Characteristics of a Cross parachute with a W/L Ratio of 0.264", by W. P. Ludtke. NOL, June 1972. (NOL TR72-145).
17. Naval Ordnance Laboratory. "Effects of Canopy Geometry on the Infinite Mass Opening Shock of a Cross Parachute With a W/L Ratio of 0.264," by W. P. Ludtke. NOL, July 1973. (NOL TR 81-81-41).
18. Naval Surface Warfare Center. "Effect of Canopy Geometry and Cloth Permeability on Drag Coefficient of a Cross Parachute in the Fully Open and Reefed Condition for a W/L Ratio of 0.3," by W. P. Ludtke. NSWC, February 1982. (NSWC TR 81-441).
19. Naval Surface Weapons Center. "Notes on a Theoretical Parachute Opening Force Analysis Applied to a General Trajectory", by W. P. Ludtke, NSWC, May 1988. (NSWC TR 88-6).
20. B. Pepper. "Rocket and Parachute System Design and Performance for Project Twinkle." Sandia Report No. SC-DR-68-766, November 1968.
21. B. Pepper. "Development of a Parachute Recovery System for a Reentry Nose Cone (NRV)." Sandia Report No. 75-0564, September 1977.
22. B. Pepper. "Parachute/Flotation Bag Recovery System for a Large RV Nose Cone." Sandia Report No. 79-1800, March 1980.
23. B. Pepper. "Development of the Parachute Recovery System for the LBRV-2 Reentry Vehicle." AIAA Paper, April 1984, (AIAA 84-0802).
24. Poker Flat. "Range User's Handbook", 1989.
25. F. Poynter. The Parachute Manual, Vol. 1. Published 1978 by Para Publishing, P.O. Box 4232, Santa Barbara, California 91340-4232.
26. F. Poynter. The Parachute Manual Vol. II. "Published 1992 by Para Publishing, P.O. Box 4232, Santa Barbara, California 91340-4232.
27. Rogers. ALT - Version 4.05, Rocket Performance Software. Rogers Aeroscience, P.O. Box 10065, Lancaster, California 92534, 1991.
28. Shen & D. J. Cockrell. "Aerodynamic Characteristics of Flow Around Cross Parachutes in Steady Motion." AIAA Paper 86-2458-CP. 9th Aerodynamic Decelerator Conference, Albuquerque, New Mexico, 1986.
29. Naval Surface Warfare Center. "Wind Tunnel Measurements of the Variations of Suspension Line Forces in a Cross Parachute," by W. P. Ludtke. NSWC, May 1990. (NSWC TR 89-36).
30. L. Thomas. Calculating Parachute Descent Rates for High Power Rocket Recovery Applications. Published 1990 by Paratech Parachutes, 139 Kelsan Way, Fairbanks, Alaska 99709.
31. L. Thomas. Sounding Rocket Parachute Recovery System Packing Manual. 1995 by Paratech Parachutes, 139 Kelsan Way, Fairbanks, Alaska 99709. To be published.
32. W. Siaw. "Recovery System Design For Ausroc III", Department of Aerospace Engineering, Royal Melbourne Institute (R.M.I.T), Melbourne,

- Australia, 1992. (Includes pascal computer program source code for descent profile of a payload recovery system).
33. D. Sundberg, "New Solution Method for Steady-State Canopy Structural Loads." *Journal of Aircraft*, Vol. 25, No. 11, November 1988, pp. 1045-1051. AIAA Paper 86-2489.
 34. Tong. "Payload Vehicle Aerodynamic Re-Entry Analysis," *Journal of Spacecraft and Rockets*, Vol. 29, No. 5, September/October 1992, pp. 641-645.
 35. UAF. "Viper V Flight Requirements Plan," Project ARIM-1, University of Alaska Fairbanks, Fairbanks, Alaska 1995.
 36. E. Widdows. Packing and Installation Instructions for Sandia Laboratories/NASA/DFVLR Rocket Payload Parachute Recovery System (PN TI19328-000), Sandia Laboratories, SLA-73-0997, April 1974.

Symbols

A	Area (ft ²)
CD	Drag coefficient
C _x	Opening force coefficient
(CD _s) _o	Parachute drag area relative to canopy surface area (S _o)
(CD _s) _o	Parachute drag area projected (inflated) (ft ²)
(CD _s) _R	Parachute drag area reefed (ft ²)
D	Drag, diameter
D _B	Diameter of forebody
D _F	Design factor
D _O	Nominal parachute diameter (ft)
D _P	Projected parachute diameter when inflated (ft)
e _s	Gore width at canopy skirt (ft)
F _x	Maximum parachute opening force (lb.)
F _s	Parachute snatch force (lb.)
G	Load factor = (a/g)
g	Acceleration of gravity = [32.17 ft/sec ² at sea level]
K _f	Dimensionless canopy filling time parameter
le	Suspension line length
M	Mach number (speed of sound in air) = [1,116.45 ft/sec at sea level]
m	Vehicle mass = (Weight(W) / 32.17) [slugs]
n	Canopy filling constant
N _G	Number of canopy gores
N _{SL}	Number of suspension lines
p	Atmospheric pressure (lb./ft ²) = [2,116.22 at sea level]
q	Dynamic pressure of the atmosphere = (1/2) ρ v ² [lb./ft ²]
ρ	Atmospheric density in mass units (slugs/ft ³) = [0.00237689 at sea level]
σ	Atmospheric density ratio
S _F	Safety factor
S _g	Area of canopy gore (ft ²)
S _O	Parachute canopy surface area (ft ²)
s _f	Parachute canopy filling distance (ft)
t _f	Parachute canopy filling time (sec)
V	Volume (in ³ or ft ³)
v _e	Equilibrium velocity achieved for terminal rate of descent (ft/sec)
v _∞	Sea-level rate of descent (ft/sec)
v _s	Velocity at parachute line stretch (ft/sec)
W _P	Parachute weight (lb.)
X ₁	Parachute opening-force-reduction factor

Ballistic Free Fall Table

Table C1 : Table of terminal descent values for payload reentry velocity with a drag coefficient of 0.83, a surface area of 5 ft², and a reentry weight of 52 pounds.

Altitude (ft)	Altitude (km)	Velocity (ft/sec)	Velocity (mph)	Velocity (mps)	Mach No.	Time (sec)
126,751	38.63	1,630.44	1,111.64	496.96	1.578	0.46
126,000	38.40	1,594.01	1,086.79	485.85	1.545	0.62
125,000	38.10	1,558.26	1,062.42	474.96	1.513	0.63
124,000	37.80	1,523.25	1,038.55	464.29	1.482	0.65
123,000	37.49	1,488.84	1,015.09	453.80	1.451	0.66
122,000	37.19	1,455.12	992.10	443.52	1.421	0.68
121,000	36.88	1,422.02	969.53	433.43	1.391	0.70
120,000	36.58	1,389.57	947.41	423.54	1.361	0.71
119,000	36.27	1,357.79	925.74	413.86	1.333	0.73
118,000	35.97	1,326.60	904.47	404.35	1.304	0.75
117,000	35.66	1,296.01	883.62	395.02	1.279	0.76
116,000	35.36	1,265.99	863.16	385.88	1.249	0.78
115,000	35.05	1,236.61	843.12	376.92	1.222	0.80
114,000	34.75	1,207.77	823.46	368.13	1.196	0.82
113,000	34.44	1,179.52	804.20	359.52	1.170	0.84
112,000	34.14	1,151.84	785.32	351.08	1.145	0.86
111,000	33.83	1,124.67	766.80	342.80	1.120	0.88
110,000	33.53	1,098.07	748.67	334.69	1.095	0.90
109,000	33.22	1,072.00	730.89	326.75	1.071	0.92
108,000	32.92	1,046.46	713.48	318.96	1.047	0.94
107,000	32.61	1,021.44	696.42	311.33	1.024	0.97
106,000	32.31	996.91	679.69	303.86	1.002	0.99
105,000	32.00	973.49	663.73	296.72	0.979	1.02
104,000	31.70	951.19	648.52	289.92	0.957	1.04
103,000	31.39	929.27	633.58	283.24	0.936	1.06
102,000	31.09	907.86	618.98	276.72	0.915	1.09
101,000	30.78	886.92	604.70	270.33	0.894	1.11
100,000	30.48	866.44	590.74	264.09	0.874	1.14
99,000	30.18	846.41	577.08	257.98	0.855	1.17
98,000	29.87	826.79	563.71	252.01	0.836	1.20
97,000	29.57	807.63	550.64	246.17	0.817	1.22
96,000	29.26	788.86	537.84	240.44	0.798	1.25
95,000	28.96	770.51	525.34	234.85	0.780	1.28
94,000	28.65	752.56	513.10	229.38	0.763	1.31
93,000	28.35	735.01	501.13	224.03	0.745	1.34
92,000	28.04	717.84	489.42	218.80	0.728	1.38
91,000	27.74	701.04	477.97	213.68	0.712	1.41
90,000	27.43	684.62	466.77	208.67	0.696	1.44
89,000	27.13	668.56	455.83	203.78	0.680	1.48
88,000	26.82	652.85	445.12	198.99	0.664	1.51
87,000	26.52	637.49	434.64	194.31	0.649	1.55
86,000	26.21	622.47	424.40	189.73	0.634	1.59
	Free Fall Distance = 40,751 ft. (12.42 km.)				Total Time	
	(Free Fall From 126,751 Ft. to 86,000 Ft.)					
		(Weight = 52 lb.)			(sec)	42.64
		(CD = 0.83)			(min)	0.711
		(So = 5.03 sq. ft.)			(hr)	0.012

Guide Surface Drogue Chute

Table C2 : Table of terminal descent values of 6 foot diameter guide surface drogue chute with a drag coefficient of 0.34 and a recovery weight of 49 pounds.

Altitude (ft)	Altitude (km)	Velocity (ft/sec)	Velocity (mph)	Velocity (mps)	Velocity (ft/min)	Mach No.	Time (sec)
100,000	30.48	554.31	378.04	168.95	33,258.66	0.559	
98,000	29.87	528.95	360.74	161.22	31,736.94	0.535	
96,000	29.26	504.68	344.19	153.83	30,280.74	0.511	
94,000	28.65	481.46	328.35	146.75	28,887.45	0.488	
92,000	28.04	459.24	313.20	139.98	27,554.58	0.466	
90,000	27.43	437.99	298.71	133.50	26,279.58	0.445	
88,000	26.82	417.67	284.85	127.31	25,060.18	0.425	
86,000	26.21	398.23	271.60	121.38	23,894.04	0.406	6.80
84,000	25.60	379.65	258.92	115.72	22,779.01	0.387	3.35
82,000	24.99	361.88	246.80	110.30	21,713.00	0.370	
80,000	24.38	344.90	235.22	105.13	20,693.96	0.353	
78,000	23.77	328.67	224.15	100.18	19,719.97	0.337	
76,000	23.16	313.15	213.57	95.45	18,789.18	0.321	
74,000	22.56	284.17	193.80	86.61	17,049.98	0.292	
72,000	21.95	277.32	189.13	84.53	16,639.40	0.285	
70,000	21.34	270.64	184.57	82.49	16,238.19	0.279	
68,000	20.73	257.71	175.76	78.55	15,462.84	0.266	
66,000	20.12	245.37	167.34	74.79	14,722.35	0.253	
64,000	19.51	233.90	159.52	71.29	14,033.94	0.242	
62,000	18.90	222.99	152.08	67.97	13,379.23	0.230	
60,000	18.29	212.58	144.98	64.80	12,754.95	0.215	
58,000	17.68	202.66	138.22	61.77	12,159.72	0.205	
56,000	17.07	193.20	131.76	58.89	11,592.12	0.195	
54,000	16.46	184.18	125.61	56.14	11,050.94	0.186	
52,000	15.85	175.58	119.75	53.52	10,534.92	0.177	
50,000	15.24	167.38	114.15	51.02	10,042.91	0.169	
48,000	14.63	159.56	108.82	48.63	9,573.78	0.161	
46,000	14.02	152.11	103.74	46.36	9,126.49	0.154	
44,000	13.41	145.00	98.89	44.20	8,700.01	0.146	
42,000	12.80	138.22	94.27	42.13	8,293.38	0.139	
40,000	12.19	131.76	89.86	40.16	7,905.70	0.133	
38,000	11.58	125.60	85.66	38.28	7,536.06	0.127	
36,000	10.97	119.81	81.71	36.52	7,188.63	0.012	
34,000	10.36	115.30	78.63	35.14	6,917.91	0.118	
32,000	9.75	111.03	75.72	33.84	6,661.87	0.113	
30,000	9.14	106.99	72.97	32.61	6,419.48	0.108	
28,000	8.53	103.16	70.36	31.44	6,189.78	0.103	
26,000	7.92	99.53	67.88	30.34	5,971.92	0.098	
24,000	7.32	96.09	65.53	29.29	5,765.12	0.094	
22,000	6.71	92.81	63.30	28.29	5,568.65	0.090	
20,000	6.10	89.70	61.17	27.34	5,381.82	0.087	
18,000	5.49	86.73	59.15	26.44	5,204.03	0.083	
16,000	4.88	83.91	57.23	25.58	5,034.71	0.080	
14,000	4.27	81.22	55.39	24.76	4,873.33	0.077	
12,000	3.66	86.31	58.86	26.31	5,178.65	0.081	
10,000	3.05	83.62	57.03	25.49	5,017.45	0.078	
8,000	2.44	81.06	55.28	24.71	4,863.50	0.075	
6,000	1.83	71.64	48.86	21.83	4,298.13	0.066	
4,000	1.22	69.50	47.40	21.18	4,169.89	0.063	
2,000	0.61	67.71	46.18	20.64	4,062.43	0.061	
0	0.00	65.49	44.67	19.96	3,929.68	0.059	
Free Fall Distance = 2,938 Ft. (0.90 km)							Total Time
(Weight = 49 lb.) (Cd = 0.34 / So = 28.27 sq. ft.)							(sec) 10.15
							(min) 0.169
Free Fall Distance From: 86,000 Ft. to 83,062 Ft.							(hr) 0.003

33 Ft. Main Cross Parachute Descent Table

Table C3 : Table of performance values for terminal descent of 33 foot diameter main parachute with a drag coefficient of 0.85 and a recovery weight of 31 pounds.

Altitude (ft)	Altitude (km)	Velocity (ft/sec)	Velocity (mph)	Velocity (mps)	Velocity (ft/min)	Mach No.	Time (sec)
82,000	24.99	39.36	26.84	12.00	2361.51	0.040	0.00
80,000	24.38	38.88	26.51	11.85	2332.63	0.039	51.13
78,000	23.77	37.51	25.58	11.43	2250.68	0.038	52.36
76,000	23.16	34.06	23.23	10.38	2043.51	0.035	55.89
74,000	22.56	30.91	21.08	9.42	1854.36	0.031	61.57
72,000	21.95	30.16	20.57	9.19	1809.70	0.031	65.50
70,000	21.34	29.43	20.07	8.97	1766.07	0.030	67.12
68,000	20.73	28.03	19.12	8.54	1681.74	0.028	69.61
66,000	20.12	26.69	18.20	8.14	1601.50	0.027	73.10
64,000	19.51	25.44	17.35	7.75	1526.33	0.026	76.73
62,000	18.90	24.25	16.54	7.39	1455.13	0.025	80.50
60,000	18.29	23.12	15.77	7.05	1387.23	0.023	84.44
58,000	17.68	22.04	15.03	6.72	1322.49	0.022	88.57
56,000	17.07	21.01	14.33	6.40	1260.76	0.021	92.91
54,000	16.46	20.03	13.66	6.11	1201.90	0.020	97.46
52,000	15.85	19.10	13.03	5.82	1146.06	0.019	102.22
50,000	15.24	18.20	12.42	5.55	1092.27	0.018	107.22
48,000	14.63	17.35	11.84	5.29	1041.25	0.018	112.49
46,000	14.02	16.54	11.28	5.04	992.60	0.017	118.00
44,000	13.41	15.77	10.76	4.81	946.21	0.016	123.79
42,000	12.80	15.03	10.25	4.58	901.99	0.015	129.86
40,000	12.19	14.33	9.77	4.37	859.82	0.015	136.22
38,000	11.58	13.66	9.32	4.16	819.62	0.014	142.90
36,000	10.97	13.03	8.89	3.97	781.84	0.013	149.86
34,000	10.36	12.54	8.55	3.82	752.39	0.013	156.43
32,000	9.75	12.08	8.24	3.68	724.55	0.012	162.50
30,000	9.14	11.64	7.94	3.55	698.18	0.012	168.69
28,000	8.53	11.22	7.65	3.42	673.20	0.011	175.01
26,000	7.92	10.83	7.38	3.30	649.51	0.011	181.45
24,000	7.32	10.45	7.13	3.19	627.02	0.011	188.01
22,000	6.71	10.09	6.88	3.08	605.65	0.010	194.70
20,000	6.10	9.76	6.65	2.97	585.33	0.010	201.52
18,000	5.49	9.43	6.43	2.88	565.99	0.010	208.46
16,000	4.88	9.13	6.22	2.78	547.58	0.009	215.52
14,000	4.27	8.83	6.02	2.69	530.02	0.009	222.72
12,000	3.66	8.55	5.83	2.61	513.28	0.009	230.04
10,000	3.05	8.29	5.65	2.53	497.31	0.008	237.48
8,000	2.44	8.03	5.48	2.45	482.05	0.008	245.06
6,000	1.83	7.79	5.31	2.37	467.47	0.008	252.76
4,000	1.22	7.56	5.15	2.30	453.52	0.008	260.59
2,000	0.61	7.34	5.00	2.24	440.17	0.007	268.55
0	0.00	7.12	4.86	2.17	427.39	0.007	276.64
(Free Fall Distance = 82,000 ft.)							Total Time:
(Weight = 31 lb.)							(sec) 5,985.56
(CD = 0.85)							(min) 99.76
(So = 604.8 sq. ft.)							(hr) 1.66

1976 U.S. Standard Atmosphere Table

Table D1 : U.S. Standard Atmosphere Table of values used for input to determine parachute descent rates, parachute drag areas, atmospheric dynamic pressure, and payload reentry velocities.

Altitude (ft)	Altitude (km)	Air Press (psf)	Density - ρ (slugs/ft ³)	Density Ratio (ρ/ρ_0) (1/ ρ/ρ_0) ^{0.5}	Temperature (C)	Temperature (F)	Speed-Sound (ft/sec)
200,000	60.96	402.29-2	.434943-7	6.6791+1	-28.767	-19.781	1,028.17
198,000	60.35	437.25	.469519	6.4285	-27.092	-16.766	1,031.68
196,000	59.74	474.99	.506580	6.1889	-25.417	-13.751	1,035.19
194,000	59.13	515.71	.546317	5.9596	-23.741	-10.734	1,038.67
192,000	58.52	559.61	.588869	5.7402	-22.066	-7.719	1,042.15
190,000	57.91	606.94-2	.634428-7	5.5303+1	-20.390	-4.702	1,045.62
188,000	57.30	657.92	.683188	5.3293	-18.713	-1.683	1,049.10
186,000	56.69	712.81	.735344	5.1368	-17.037	1.333	1,052.55
184,000	56.08	771.89	.791109	5.4171	-15.360	4.352	1,055.99
182,000	55.47	835.46	.850715	4.7758	-13.682	7.372	1,059.40
180,000	54.86	903.80-2	.914397-2	4.6065+1	-12.005	10.391	1,062.82
178,000	54.25	977.27	.982425	4.4441	-10.327	13.411	1,066.26
176,000	53.64	1056.20	1.05501	4.2885	-8.649	16.432	1,069.64
174,000	53.04	1140.95	1.13249	4.1392	-6.970	19.454	1,072.95
172,000	52.43	1231.92	1.21513	3.9960	-5.291	22.476	1,076.40
170,000	51.82	1329.54-2	1.30324-6	3.8586+1	-3.612	25.498	1,079.78
168,000	51.21	1434.26	1.40012	3.7227	-2.500	27.500	1,082.01
166,000	50.60	1547.10	1.51025	3.5844	-2.500	27.500	1,082.01
164,000	49.99	1668.82	1.62910	3.4511	-2.500	27.500	1,082.01
162,000	49.38	1800.16	1.75731	3.3229	-2.500	27.500	1,082.01
160,000	48.77	1941.87-2	1.89564-6	3.1993+1	-2.500	27.500	1,082.01
158,000	48.16	2094.77	2.04491	3.0804	-2.500	27.500	1,082.01
156,000	47.55	2259.55	2.20595	2.9658	-2.500	27.500	1,082.01
154,000	46.94	2437.91	2.38990	2.8494	-3.634	25.459	1,079.74
152,000	46.33	2631.51	2.59596	2.7339	-5.316	22.431	1,076.36
150,000	45.72	2841.61-2	2.82104-6	2.6226+1	-6.998	19.404	1,072.99
148,000	45.11	3070.30	3.06746	2.5151	-8.681	16.374	1,069.57
146,000	44.50	3319.04	3.33716	2.4113	-10.364	13.345	1,066.16
144,000	43.89	3589.92	3.63267	2.3111	-12.048	10.314	1,062.75
142,000	43.28	3884.61	3.95632	2.2145	-13.731	7.284	1,059.30
140,000	42.67	4206.09-2	4.31159-6	2.1214+1	-15.415	4.253	1,055.86
138,000	42.06	4556.27	4.70160	2.0315	-17.100	1.220	1,052.45
136,000	41.45	4938.47	5.12963	1.9449	-18.784	-1.811	1,048.94
134,000	40.84	5355.54	5.59997	1.8614	-20.469	-4.844	1,045.46
132,000	40.23	5811.25	6.11726	1.7810	-22.155	-7.879	1,041.98
130,000	39.62	6309.36-2	6.68635-6	1.7035+1	-23.840	-10.912	1,038.47
128,000	39.01	6853.83	7.31288	1.6289	-25.526	-13.947	1,034.96
126,000	38.40	7449.68	8.00325	1.5571	-27.212	-16.982	1,031.42
124,000	37.80	8102.34	8.76425	1.4879	-28.899	-20.018	1,027.87
122,000	37.19	8817.23	9.60402	1.4214	-30.586	-23.055	1,024.33
120,000	36.58	9601.04-2	1.05311-5	1.3574+1	-32.273	-26.091	1,020.76
118,000	35.97	1046.11	1.15552	1.2958	-33.961	-29.130	1,017.18
116,000	35.36	1140.57	1.25426	1.2337	-35.649	-32.168	1,013.59
114,000	34.75	1244.29	1.37073	1.1798	-37.337	-35.207	1,009.98
112,000	34.14	1358.31	1.49767	1.1251	-39.025	-38.245	1,006.36
110,000	33.53	1483.75-2	1.63598-4	1.0726+1	-40.714	-41.285	1,002.72
108,000	32.92	1621.85	1.77480	1.0222+1	-42.403	-44.325	999.07
106,000	32.31	1773.99	1.92654	9.7380	-44.093	-47.367	995.41
104,000	31.70	1941.48	2.09360	9.2911	-44.958	-48.924	993.53
102,000	31.09	2125.36	2.27238	8.8864	-45.562	-50.012	992.21
100,000	30.48	2327.25-2	2.4631	8.4631	-46.166	-51.099	990.90

1976 U.S. Standard Atmosphere Table Continued

Altitude (ft)	Altitude (km)	Air Press (psf)	Density - ρ (slugs/ft ³)	Density Ratio (ρ/ρ_0) ($1/\rho/\rho_0$) ^{0.5}	Temperature (C)	Temperature (F)	Speed-Sound (ft/sec)
98,000	29.87	2548.98	0.364413	8.0762	-46.769	-52.184	989.58
96,000	29.26	2792.56	0.400305	7.7059	-47.192	-52.946	988.26
94,000	28.65	3060.20	0.439851	7.3513	-47.977	-54.359	986.93
92,000	28.04	3354.42	0.483433	7.0121	-48.582	-55.448	985.61
90,000	27.43	3766.88-2	.531480-4	6.6876	-49.186	-56.535	984.28
88,000	26.82	4033.60	0.584461	6.3771	-49.790	-57.622	982.95
86,000	26.21	4424.91	0.642902	6.0805	-50.395	-58.711	981.62
84,000	25.60	4855.49	0.707382	5.7968	-51.000	-59.800	980.29
82,000	24.99	5329.42	0.778546	5.5255	-51.604	-60.887	978.95
80,000	24.38	5851.20-2	0.857110	5.2659	-42.209	-43.976	977.62
78,000	23.77	6425.82	.943868-4	5.0183	-52.814	-63.065	976.28
76,000	23.16	7058.82	0.103970	4.7813	-53.419	-64.154	974.93
74,000	22.56	8525.13	0.126263	4.5550	-54.025	-65.245	973.59
72,000	21.95	8938.59	0.132571	4.3388	-54.630	-66.334	972.24
70,000	21.34	9372.76-2	.139203-3	4.1322	-55.236	-67.425	970.90
68,000	20.73	1030.76	0.153513	3.9348	-55.841	-68.514	969.55
66,000	20.12	1133.88	0.169344	3.7464	-56.447	-69.605	968.20
64,000	19.51	1247.55	0.186365	3.5713	-56.500	-69.700	968.08
62,000	18.90	1372.63	0.205051	3.4046	-56.500	-69.700	968.08
60,000	18.29	1510.28-1	.225613-3	3.2458	-56.500	-69.700	968.08
58,000	17.68	1661.76	0.248243	3.0943	-56.500	-69.700	968.08
56,000	17.07	1828.47	0.273148	2.9499	-56.500	-69.700	968.08
54,000	16.46	2011.95	0.300556	2.8121	-56.500	-69.700	968.08
52,000	15.85	2213.67	0.330721	2.6809	-56.500	-69.700	968.08
50,000	15.24	2436.11-1	.363919-3	2.5556	-56.500	-69.700	968.08
48,000	14.63	2680.70	0.400458	2.4363	-56.500	-69.700	968.08
46,000	14.02	2949.90	0.440673	2.3224	-56.500	-69.700	968.08
44,000	13.41	3246.20	0.484936	2.2139	-56.500	-69.700	968.08
42,000	12.80	3572.33	0.533655	2.1105	-56.500	-69.700	968.08
40,000	12.19	3931.29-1	.587278-3	2.0118	-56.500	-69.700	968.08
38,000	11.58	4326.40	0.646302	1.9177	-56.500	-69.700	968.08
36,000	10.97	4761.28	0.710284	1.8293	-56.200	-69.160	968.75
34,000	10.36	5234.80	0.766963	1.7604	-52.251	-62.052	977.52
32,000	9.75	5745.85	0.82705	1.6953	-48.301	-54.942	986.22
30,000	9.14	6269.69-1	.890686-2	1.6336	-44.351	-47.832	994.85
28,000	8.53	6889.64	0.958016	1.5751	-40.399	-40.718	1,003.40
26,000	7.92	7527.14	0.102919	1.5197	-36.447	-33.605	1,011.89
24,000	7.32	8211.72	0.110435	1.4671	-32.494	-26.489	1,020.30
22,000	6.71	8946.02	0.118365	1.4171	-28.541	-19.374	1,028.65
20,000	6.10	9732.75-1	.126726-2	1.3695	-24.586	-12.255	1,036.93
18,000	5.49	1057.48	0.135533	1.3243	-20.631	-5.136	1,045.15
16,000	4.88	1147.50	0.144802	1.2812	-16.675	1.985	1,053.30
14,000	4.27	1243.65	0.154551	1.2401	-12.718	9.108	1,061.40
12,000	3.66	1346.65	0.164796	1.2010	-8.761	16.230	1,069.43
10,000	3.05	1455.60+0	.175555-2	1.1636	-4.803	23.355	1,077.40
9,000	2.74	1512.93	0.181133	1.1455	-2.823	26.919	1,081.37
8,000	2.44	1572.07	0.186845	1.1279	-0.844	30.481	1,085.32
7,000	2.13	1633.08	0.192695	1.1106	1.136	34.045	1,089.26
6,000	1.83	1696.00	0.198685	1.0938	3.116	37.609	1,093.19
5,000	1.52	1760.87	0.204817	1.0773	5.096	41.173	1,097.10
4,000	1.22	1827.75	0.211093	1.0611	7.077	44.739	1,100.99
3,000	0.91	1896.69	0.217516	1.0453	9.057	48.303	1,104.88
2,000	0.61	1976.69	0.224088	1.0299	11.038	51.868	1,108.75
1,000	0.30	2040.86	0.230812	1.0148	13.019	55.434	1,112.60
0	0.00	2116.22+0	.237689-2	1.0000	15.000	59.000	1,116.45

Parachute Types


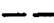

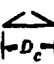





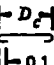

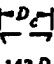






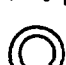


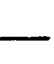
TYPE	CONSTRUCTED SHAPE		$\frac{D_c}{D_o}$	INFLATED SHAPE $\frac{D_p}{D_o}$	DRAG COEF C_{D_o} RANGE	OPENING FORCE COEF C_X (INF MASS)	AVERAGE ANGLE OF OSCILLATION, DEGREES	GENERAL APPLICATION
	PLAN	PROFILE						
FLAT CIRCULAR			1.00	0.87 TO 0.70	0.75 TO 0.80	~1.7	±10 TO ±40	DESCENT, OBSOLETE
CONICAL			0.93 TO 0.95	0.70	0.75 TO 0.80	~1.8	±10 TO ±30	DESCENT, M < 0.5
BICONICAL			0.90 TO 0.95	0.70	0.75 TO 0.92	~1.8	±10 TO ±30	DESCENT, M < 0.5
TRICONICAL POLYCONICAL			0.90 TO 0.95	0.70	0.80 TO 0.96	~1.8	±10 TO ±20	DESCENT, M < 0.5
EXTENDED SKIRT 10% FLAT			0.86	0.86 TO 0.70	0.78 TO 0.87	~1.4	±10 TO ±15	DESCENT, M < 0.5
EXTENDED SKIRT 14.3% FULL			0.81 TO 0.85	0.66 TO 0.70	0.75 TO 0.90	~1.4	±10 TO ±15	DESCENT, M < 0.5
HEMISPHERICAL			0.71	0.86	0.82 TO 0.77	~1.6	±10 TO ±15	DESCENT, M < 0.5, OBSOLETE
GUIDE SURFACE (RIBBED)			0.83	0.82	0.28 TO 0.42	~1.2	0 TO ±2	STABILIZATION, DROGUE, 0.1 < M < 1.5
GUIDE SURFACE (RIBLESS)			0.86	0.83	0.30 TO 0.34	~1.4	0 TO ±3	PILOT, DROGUE, 0.1 < M < 1.5
ANNULAR			1.04	0.94	0.85 TO 0.95	~1.4	<±6	DESCENT, M < 0.5
CROSS			1.15 TO 1.19	0.66 TO 0.72	0.60 TO 0.85	1.1 TO 1.2	0 TO ±3	DESCENT, DECELERATION

Figure E1 : Parachute Performance parameters and specifications for parachute performance. Use values in this table to find parameters.

Parachute Reduction Factor (X_1) and Opening Force Coefficient (C_x) Graphs

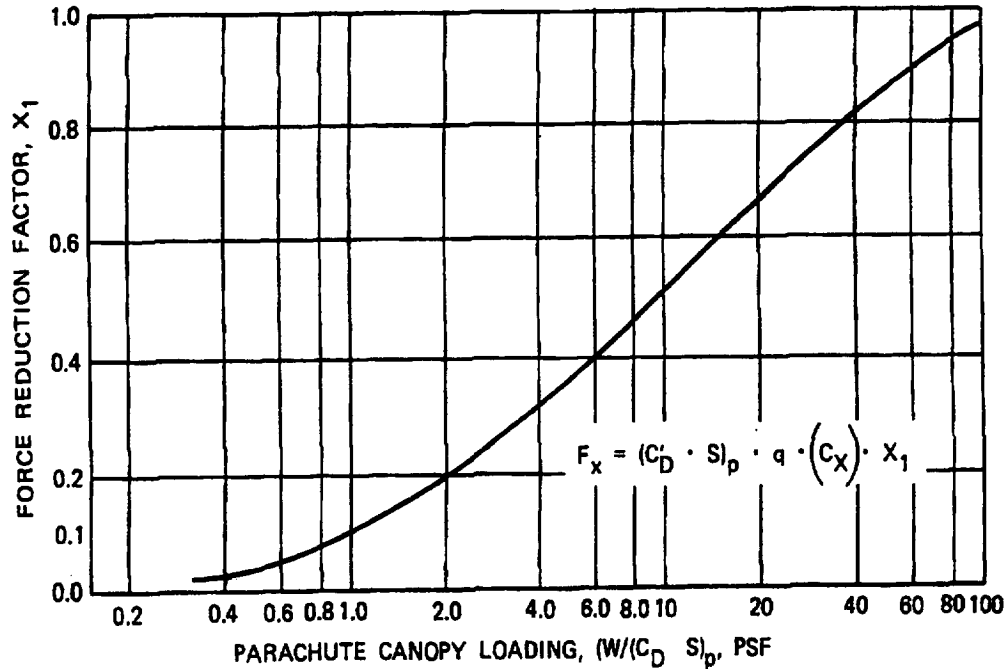


Figure F1 : Parachute opening force coefficient (C_x) as a function of canopy loading for all parachutes. Values are used to determine the parachute opening force (F_x) using the equation inset on graph. Use for unreefed parachutes with low canopy loading.

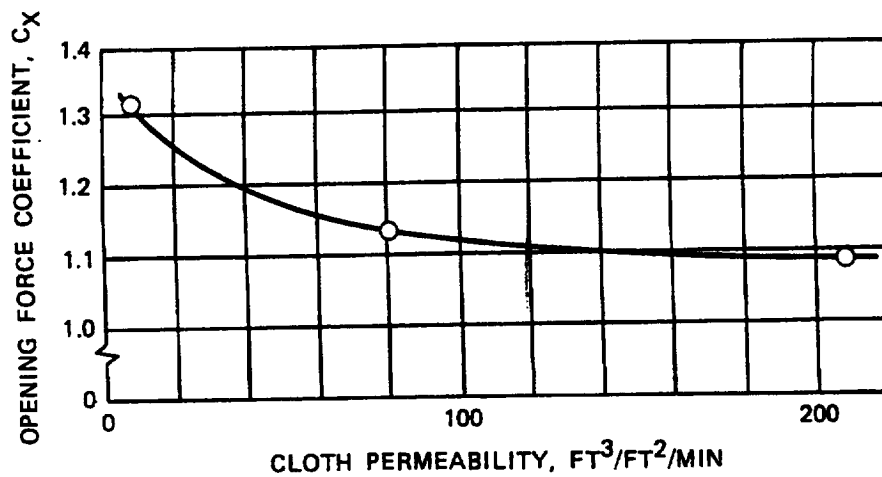


Figure F2 : Parachute opening force coefficient as a function of canopy fabric permeability for cross type parachutes.

Parachute Opening Force Factor (X1) Graph

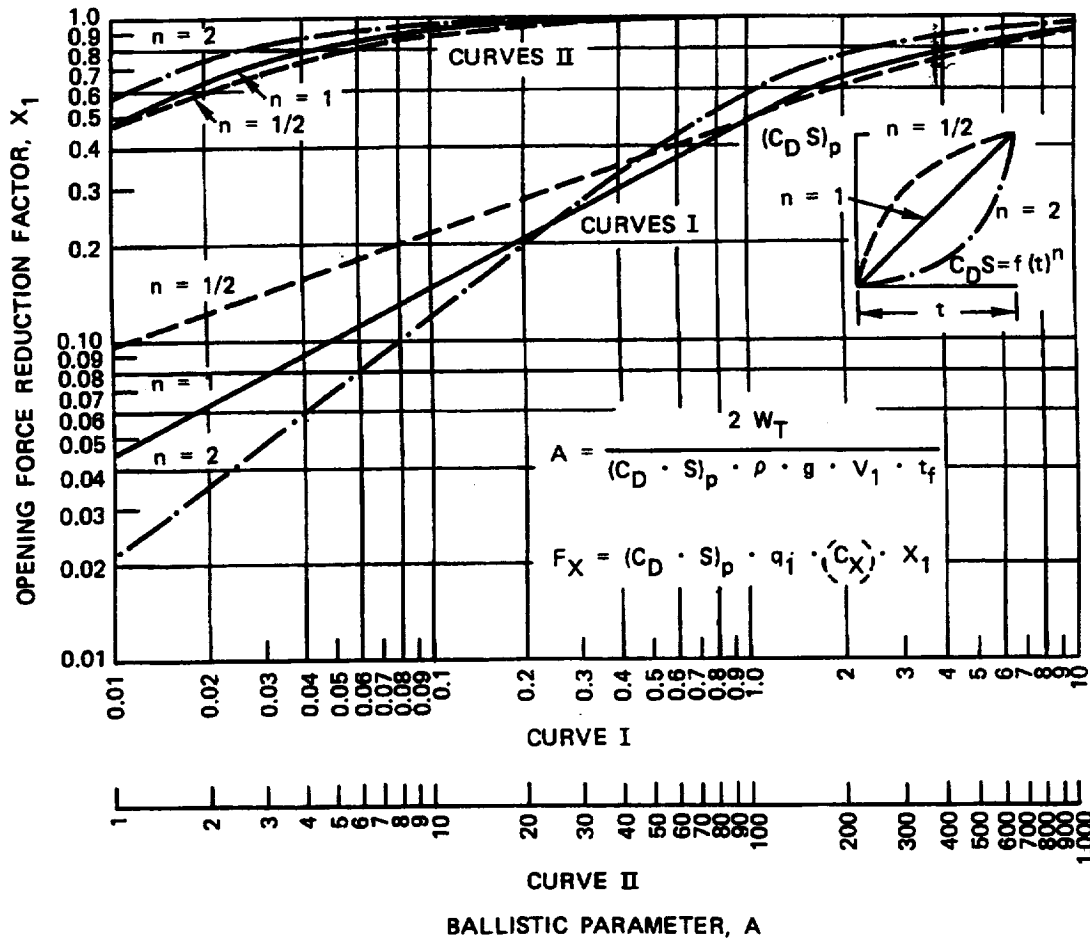


Figure F3: Ballistic parameter as a function of parachute opening force reduction factor (X_1). First, the ballistic parameter (A) is calculated from the inset on the graph above. The value obtained for (A) is used on the graph above to obtain a value for the force reduction factor (X_1). This value is then put into the equation above, to solve for the parachute opening force (F_X). Calculating parachute opening forces in this way is known as the Pflanztz Method, which is more accurate than the canopy loading method used in figure F1.

Use $n = 1/2$ for reefed parachutes

Use $n = 1$ for ribbon and ringslot parachutes

Use $n = 2$ for solid cloth, flat circular, conical, extended skirt, and triconical chutes

Parachute Performance Parameters Formulas

1. Parachute Descent Rate:

$$V_e = [(C_D) (W) / (C_D) (\rho) (S_o)]^{1/2}$$

Where:

- V_e = Equilibrium velocity (descent rate in ft/sec)
- W = Weight of payload and parachute
- C_D = Parachute drag coefficient
- ρ = Mass density of atmosphere at given altitude (slugs/ft³)
- S_o = Parachute surface area in ft² = $(\pi * D_o^2)$

2. Dynamic Pressure:

$$q = (\rho / 2) v^2 = v^2 / x \quad (\text{Where: } x = v/x = [(\text{ft/sec}) / 841.40])(q = \text{lb./ft}^2)$$

3. Canopy Inflation Time:

A. Solid flat circular (guide surface drogue):

$$t_i = (n) (D_o) / v^{0.85}$$

where: $n = 4.0$ for standard porosity canopies
 $n = 2.5$ for low porosity canopies

B. Cross parachute:

$$t_i = (CD_s)_p (n) / v^{0.9}$$

where: $n = 8.7$ for medium range velocity of about (150 to 500 ft/sec)

4. Parachute Opening Force (Canopy Loading Method):

$$F_x = (CD_s)_p (q) (C_x) (X_1) \quad (\text{Use only for low load canopies})$$

Where: (Refer to figure E1)

- F_x = Opening force (lb.)
- $(CD_s)_p$ = Drag area of full open parachute (ft²)
- q = Dynamic pressure of atmosphere at line stretch (lb./ft²)
- C_x = **Opening force coefficient at infinite mass**
(no velocity decay) (*Don't use at low canopy loading*)
- X_1 = Force reduction factor (unknown quantity)

5. Parachute Opening Force (Pflantz Method):

$$F_x = (CD_s)_p (q) (C_x) (X_1)$$

Where: (Refer to figure E3)

A. First calculate parachute velocity decay during inflation:

$$V_1 = V_o / 1 + [(CD_s)_p (\rho) (g) (t_f) V_o] / 2 (W)]$$

Where:

- V_o = Velocity at beginning of deceleration
- $(CD_s)_p$ = Drag area of full open parachute (ft²)
- ρ = Mass density of atmosphere at given altitude (slugs/ft³)
- g = Gravitational acceleration (32.17 ft/sec²)
- t_f = Canopy filling time (sec)
- W = Weight of suspended payload
(includes parachute weight)

B. Second, calculate the ballistic parameter (A):

$$A = 2 (W_t / (CD_s)_p (\rho) (g) (v_1) (t_i) \quad \text{Where:}$$

A = Ballistic parameter (dimensionless)
 W_t = System weight (lb.)
 $(CD_s)_p$ = Parachute drag area reefed, or full open (ft²)
 g = Gravitational acceleration (32.17 ft/sec²)
 v_1 = Velocity at line stretch or start of disreef (ft/sec)
 ρ = Dynamic pressure of atmosphere at line stretch (lb./ft²)
 t_i = Canopy inflation time (sec)

With the ballistic parameter value, refer to figure E3.

Find the value for the force reduction factor (X_1) from the graph

Use $n = 1$ for ribbon and ringslot parachutes

Use $n = 2$ for solid cloth, flat circular, conical, extended skirt, and triconical chutes

Use $n = 1/2$ for reefed parachutes

6. Steady State Parachute Force:

$$F_s = (q_s) (CD) (S_o) = \text{lbs.}$$

7. Maximum Parachute Opening Force:

$$F_{MAX} = (F_s) (X_1) = \text{lbs.}$$

8 . Parachute Average Relative Filling Distances: (In canopy diameters)

<u>Parachute Type</u>	<u>Dia. (ft)</u>	<u>Total Porosity</u>	<u>Mach No.</u>	<u>Filling distance</u>
<i>Ribless Guide</i>	9.8	60	0.36	4.75
<i>Surface</i>	-	-	0.51	4.0
	-	-	0.65	3.5
	-	-	1.10	6.0
<i>Cross</i>	30.0	-	<0.2	10.0
	-	-	1.4	18.0

Appendix B



Mission Implementation Supplements

ARIM-1 Task List

1. Payload Electrical Systems			
Program Flight Computer Software	64		
Update Ground Support Software	64		
Modify Recorder Software	22		
Construct Science Payload	71		
Construct Housekeeping Instrumentation	49		
Construct Battery Pack	14		
Construct Power Regulator	49		
Build Sequence and EED Firing Board	45		
Purchase and Test Transmitter	14		
Construct Transmitting Antenna	21		
Verify Tx Antenna in Nose Cone	6		
Study ASRP Microdyne Receiver	11		
Study ASRP S-Band Tracking Antenna	11		
Verify Telemetry System Operation	11		
Acquire and test GPS units	7		
Integrate Ground GPS	7		
Integrate GPS into Rocket Payload	14		
Electrical Integration	55		
2. Payload Mechanical System			
Construct Thermosondes	26		
Construct Boom Assembly	23		
Construct Battery Box	10		
Mount Boom Assembly to Battery Box	6		
Cast Umbilical Block	5		
Construct Umbilical Tube	14		
Purchase Antenna Section	5		
Retrofit Antenna Section	17		
Purchase Nose Cone	5		
Retrofit Nose Cone	17		
Construct Longeron & Deck Assembly	45		
Construct Outer skin on Deck Assembly	15		
Adapt Deck Assembly to CKT. Boards	23		
Mate Deck Assembly to Battery Box	3		
Mount and Pot Battery Pack	5		
Verify Operation of Booms in Airflow	28		
Construct Payload Tube	21		
Construct Pressure Plenum	14		
Drill Static Port Holes	14		
Mount Pressure Plenum	14		

Mount Telemetry Antenna	6		
Construct Motor Coupling Section	41		
3. Recovery and Reefing System			
Construct Drogue Chute	46		
Construct Drogue Bag	11		
Construct Main Chute	60		
Construct Main Bag	16		
Pack Drogue Chute	14		
Pack Main Chute	14		
Construct Chute Canister	20		
Construct Reefing System	17		
Integrate Reefing System into Canister	9		
Mount Canister in Payload Tube	7		
4. Ground Station			
Tracking Antenna Tripod	25		
Obtain Launch Vehicle	107		
Construct Launcher	25		
5. Poker Flat Relations			
Finalize Flight Safety Plan	21		
Contact Poker Flat about Launch	5		
6. Testing & Evaluation			
Sequence Testing	14		
Long Distance TX Testing	21		
Differential GPS Testing	21		
Vacuum Chamber Testing	13		
Vibration Testing	13		
Thermal Cycle Testing	14		
Accuated Device Testing	7		
Mission Readiness Review	11		
7. Management			
Purchasing	Recurring		
Update Work Breakdown Schedule	Recurring		
Resource Allocation	Recurring		
Update Cost Analysis	Recurring		
Public Relations	Recurring		

Estimated Cost Analysis

Item	Price		Student Hours
	Parts	Contracted Labor	
Mechanical Systems			
Outer Payload Tube	\$200.00	\$1325.00	18
Inner Payload Tube	\$125.00	\$0.00	120
Longeron and Deck Assembly	\$150.00	\$500.00	320
Battery Box	\$125.00	\$0.00	80
Antenna Section	\$100.00	\$65.00	136
Nose Cone	\$125.00	\$90.00	136
Outer Shell Sep. Mechanism	\$125.00	\$100.00	200
Booms	\$125.00	\$500.00	184
Boom Deployment Mechanism	\$90.00	\$0.00	40
thermosondes	\$65.00	\$100.00	208
Umbilical Block	\$35.00	\$90.00	40
Umbilical Tube	\$75.00	\$360.00	112
Pressure Plenum	\$50.00	\$0.00	336
Drogue Parachute	\$193.62	\$0.00	368
Main Parachute	\$506.77	\$0.00	480
Drogue Reefing System	\$128.24	\$0.00	68
Main Reefing System	\$297.26	\$0.00	68
Parachute Rigging Supplies	\$110.50	\$0.00	0
System Reefing Supplies	\$1,625.50	\$0.00	0
Parachute Canister	\$425.00	\$0.00	160
Motor Coupling Section	\$250.00	\$0.00	328
Viper 5 Motor and Fin Assembly	\$20,000.00	\$0.00	160
Tracking Antenna Assembly	\$350.00	\$0.00	200
Umbilical Box	\$45.00	\$0.00	112
Launcher	\$180.00	\$0.00	200

Electrical Systems			
Batteries	\$80.00	\$0.00	112
Power Regulator	\$400.00	\$0.00	392
Flight Computer - SAT-386 SX - 25 - 2M	\$795.00	\$0.00	128
PCM Flash RAM 10MB	\$460.00	\$0.00	10
A/D Converter Card	\$300.00	\$0.00	10
Flight GPS	\$700.00	\$0.00	84
Flight GPS Antenna	\$64.00	\$0.00	0
Ground GPS	\$1,200.00	\$0.00	140
Housekeeping Instrumentation	\$400.00	\$0.00	392
Principal Instrumentation	\$450.00	\$0.00	568
Sequence and EED firing Board	\$400.00	\$0.00	360
Telemetry Transmitter	\$3000.00	\$0.00	112
Telemetry Antenna	\$2,000.00	\$0.00	216
Ground Based Antenna Tracking System	\$1,200.00	\$0.00	168
Umbilical Box Electronics	\$250.00	\$0.00	160

Manpower			
These Figures are based on a crew of five working 10 hours a week during the semester and 40 hours a week during the summer.			
3 Semesters at \$1,400 per Student	\$21,000.00	Production Hours	
2 Summers at \$5,300 per Student	\$53,000.00	6926	

Totals			
Sub Totals:	Parts	Contracted Labor	Student Labor
	\$37,200.89	\$3,130.00	\$74,000.00
Total Project Cost:	<u>\$114,330.89</u>		

—

[illegible]